UNIVERSITY OF SOUTHAMPTON

FACULTY OF ENGINEERING AND PHYSICAL SCIENCES

Optoelectronics Research Centre

Fabrication of structured GLS-Se glass preforms for fibre drawing

by

Fernando Alberto Guzman Cruz

A thesis submitted for the degree of Doctor of Philosophy

November 2020

UNIVERSITY OF SOUTHAMPTON

Abstract

FACULTY OF ENGINEERING AND PHYSICAL SCIENCES
Optoelectronics Research Centre

Doctor of Philosophy

by Fernando Alberto Guzman Cruz

Gallium lanthanum sulfide (GLS) with the addition of selenium (Se) glasses, have been proven as a reliable medium to transmit light in the range from the visible to the longwave infrared (LWIR). This family of chalcogenide glasses offer a broad transparency window depending on the composition. Their optical, mechanical and thermal properties have been exploited in their bulk form. Increasing interest in chalcogenide photonics research includes sensing for the civil, medical and military areas, as the molecular fingerprint region is within the GLS-Se glass transmission window. These application areas exploit the GLS-Se characteristics in an optical fibre geometry. The aim of this work was to explore the feasibility of obtaining glass rods and structured preforms from GLS-Se glass that could be drawn into optical fibres. For this, the extrusion process is explored by emphasizing the need to maintain the desirable glass characteristics throughout the entire process, from the glass melting to the fibre drawing. For this purpose, each step was studied and defined to maximise the exploitation of the equipment and the materials involved. For the first time it is shown that GLS-Se glasses can be extruded with a minimum alteration of their optical, thermal and mechanical properties. The amorphous phase was maintained, and corroborated by refractive index measurements, Raman spectroscopy and XRD. Several challenges were arisen during this work, using each of them to fully complete and develop a methodology to be able to obtain optical fibres. Further work might include reducing the losses of the optical fibres using this process.

Contents

List of Figures

List of Tables

Declaration of Authorship

I, FERNANDO ALBERTO GUZMAN CRUZ, declare that this thesis titled, 'FABRICATION OF STRUCTURED GLS-SE GLASS PREFORMS FOR FIBRE DRAWING' and the work presented in it are my own. I confirm that:

- This work was done wholly or mainly while in candidature for a research degree at this University.
- Where any part of this thesis has previously been submitted for a degree or any other qualification at this University or any other institution, this has been clearly stated.
- Where I have consulted the published work of others, this is always clearly attributed.
- Where I have quoted from the work of others, the source is always given. With the exception of such quotations, this thesis is entirely my own work.
- I have acknowledged all main sources of help.
- Where the thesis is based on work done by myself jointly with others, I have made clear exactly what was done by others and what I have contributed myself.
- Parts of this work have been published as:

- Morgan, Katrina, Zeimpekis, Ioannis, Huang, Chung-Che, Feng, Zhuo, Craig, Christopher, Weatherby, Edwin, Aspiotis, Nikolaos, Alzaidy, Ghadah, Abdulrahman, Ravagli, Andrea, Moog, Bruno, Jean, **Guzman Cruz, Fernando, Alberto**, Lewis, Adam, Henry, Delaney, Matthew and Hewak, Daniel (2019) *"Chalcogenide materials and applications: from bulk to 2D (Invited Talk)"*. Electronic Materials and Applications 2019 (EMA 2019), Orlando, United States. 23 - 25 Jan 2019. 1 pp.

- **Guzman Cruz, Fernando, Alberto**, Ravagli, Andrea, Craig, Christopher, Moog, Bruno, Jean and Hewak, Daniel (2019) *"Fabrication of structured GLS-Se glass preforms by extrusion for fibre drawing"*. OSA Frontiers in Optics Laser Science APS/DLS, Washington, United States. 15 - 19 Sep 2019. 2 pp. (doi.org/10.1364/FIO.2019.JW4A.11).

- Ravagli, Andrea, Moog, Bruno Jean, **Guzman Cruz, Fernando Alberto**, Craig, Christopher, Kar, Ajoy, Mackenzie, Mark, Morris, James and Hewak, Daniel (2018) *"Chalcogenide materials: Novel compositions and new applications"*. Advanced Architectures in Photonics 2018, Cambridge, United Kingdom. 02 - 05 Sep 2018.

- **Guzman Cruz, Fernando, Alberto**, Ravagli, Andrea, Craig, Christopher, Moog, Bruno, Jean and Hewak, Daniel (2018) *"Chalcogenide optical fibres based on gallium lanthanum sulphide-Se for passive and active applications"*. São Paulo School of Advanced Science on Frontiers in Lasers and their Applications, São Paulo, Brazil. 16 - 27 Jul 2018.

- Ravagli, A., Boetti, N.G., **Guzman Cruz, F.A.**, Alzaidy, G.A., Pugliese, D., Milanese, D. and Hewak, D.W. (2018) *"Structural and spectral characterisation of Er3+ and Nd3+ doped Ga-La-S-Se glasses"*. RSC Advances, 8 (48), 27556-27564. (doi:10.1039/c8ra04795b).

- Donko, Andrei, Laszlo, Núñez-Velázquez, Martin, Barua, Pranabesh, **Guzman Cruz, Fernando, Alberto**, Ismaeel, Rand, Lee, Timothy, Sahu, Jayanta, Beresna, Martynas and Brambilla, Gilberto (2017) *"Femtosecond inscription and thermal testing of Bragg gratings in high concentration (40 mol%) Germania-doped optical fibre"*. Optics Express, 25 (26), 32879-32886. (doi:10.1364/OE.25.032879).

Signed: _____

Date: _____

Acknowledgements

I would like to thank Prof. Dan Hewak, as without his guidance these years would have been tougher, for your technical support and moreover for always listening and helping me every time I was in trouble. Thanks for giving me another chance to continue this path to obtain a PhD when I was about to quit and for trusting my work. I also want to personally thank Chris Craig and Bruno Moog, for putting up with me and all my stress during these years. Big thanks to each and every member of the Novel Glass Group, for your advice, help and nice times. Thanks to CONACYT for the scholarship and to the University of Southampton students' funds for the extra money to cover my expenses.

I want to name and thank each one of my friends that have never left me and have always supported me even from the distance. Thanks for making time to listen to me, the memories, letting me cry and definitely for all the good times we have laughed. Thanks to Norberto Ramirez, Vinicius Ormenesse, Luis Herrera, Ana Soares, Andrea Ravagli, Gabriela Romero, Soonki Hong, Krzysztof Herdzik, Cristal de Oliveira, Moises Morales, Jhair Baldarrago, Lucas Faria, Alyssa Browne, Toby Jackson and Israel Figueroa. Each one of you directly and/or indirectly have impulsed me to keep going and have set an example in how to be every day a better person. Raquel Costa, without you my world would not be the same, I love you infinite and will always do, thanks for everything.

Now, a big thanks and eternal gratitude to my family: Julieta Cruz, Fernando Guzman and Paloma Guzman. I know our family has not been perfect and we have made a lot of mistakes, but you also have never let me down whenever I really needed to be rescued even at the expense of your own mental and physical health. To Hermenegildo Cruz, Fernando Guzman and Susana Salazar, I miss you every day but your sole memory makes me keep going. To Herlinda Mejia, for raising me up when I was a kid. Finally to all my aunts, uncles and cousins that have always helped me, and treated me like a kid and brother of themselves.

My time in the UK has not been a bed of roses, but I am definitely convinced these years have been a time to grow up personally and to obtain maturity. I will always be grateful with the people here that have allowed me to try and fail, without judging, in my search of becoming a better version of myself. Thanks, this PhD goes to you all.

"You cannot hope to build a better world without improving the individuals. To that end, each of us must work for our own improvement."

Marie Curie

Abbreviations

IR	Infra Red
GLS	Gallium Lanthanum Sulphide
MWIR	Mid Wavelength Infra Red
LWIR	Long Wavelength Infra Red
Ga	Gallium
La	Lanthanum
S	Sulphide
Se	Selenium
T_g	Transition temperature
T_x	Crystallization temperature
T_c	Peak crystallization temperature
T_m	Melting temperature
T_f	Fictive temperature
RE	Rare earth
Er	Erbium
Nd	Neodymium
Pr	Praseodymium
Dy	Dysprosium
Tb	Terbium
LRO	Long Range Order
SRO	Short Range Order
Ga_2S_3	Gallium Sulphide
La_2S_3	Lanthanum Sulphide
Ga_2Se_3	Gallium Selenide

LO	Longitudinal Optical
TO	Transverse Optical
WAT	Weak Absorption Tail
SMF	Single Mode Fibre
MMF	Multi Mode Fibre
SiO_2	Silicon Oxide
AsSe	Arsenic Selenide
DTA	Differential Thermal Analysis
TMA	Thermomechanical Analysis
TTT	Time Temperature Transformation

Chapter 1

Introduction

1.1 A short review of "modern" optical fibres

On May 27th, 1879 Dr Otto Schott wrote a letter to Professor Dr Abbe with some exciting news: "I recently produced a glass..." [7], this short letter contained an inherent excitation that can be perceived in each word. Dr Schott was certain that his achievement could mean the start of a new phase in the production of glasses with unique optical properties, a breakthrough event which occurred after the 93rd trial melt. After moving to Jena in 1884 the Glastecnsisches Laborarorium Schott und Genossen was established, with the help of Ernst Abbe, Carl and Roderick Zeiss. This team work obtained its success in 1886, a year that is considered the start if the age of glass science [8] as the publication of 44 optical glasses was listed in the first ever catalogue, and since then a now renowned glass industry has grown remarkably.

To be honest no one knows what was in their mind, I do not believe they thought those tenths of failures and increasingly number of achievements would mean a new era in materials science, technology and engineering. What we can know is that their first steps they did back in 1884, lead them to start understanding and predicting glass behaviour through the assimilation of its properties and the characteristics of its components [9, 10]. The team in Jena started a revolution in glass, scientific and industrial applications as long as further optical properties were extensively studied and the knowledge started to spread [11].

FIGURE 1.1: Otto Schott, Ernst Abbe and Carl Zeiss

Their constant work and experiments motivated them to overcome technical difficulties such as thermal shock, mechanical, and chemical durability. One of the glasses they introduced to the world was borosilicate glasses containing up to 15% of boric oxide, which lead to a very low coefficient of thermal expansion, good stability against thermal shock, both strong needs at that time for the gas lamps and lanterns [8, 12, 13]. As history has showed us, once someone shows the path the others start to follow, maybe not necessarily as followers but as competitors. Therefore, on the other side of the world Corning Research Laboratory, established in 1908, invented NONEX (non-expansion glass) that resisted sudden changes in temperature [14], this new glass showed that these combinations produced materials that could be used for applications that needed to apply heat (i.e. glassware for laboratories) [15], the counterpart for this glass was the traces of lead, potentially toxic if consumed. This latter concern pushed researchers to develop a lead-free chemical and heat resistant glass: PYREX [16] which we all know from any possible laboratory we have worked at. Up to here the battle for novel compositions was based in producing new combinations under the premise of the study of glass network former, network modifiers and in some way glass doping [17].

This short review from 1879 until 1915, as a full review could be a thesis itself, shows us how a group of great minds understood the importance of the development of glass manufacturing and the need to enhance desired properties to further manipulate the types of material for multiple purposes.

If optics is the field of interest for glass then the engineered material could be called Optical Glass, where the manufacturing and improvement is directed to enhance

the properties of the material to manipulate light and exploit its advantages. To highlight some properties such as: transparency, refractive index, dispersion, etc. the chemical compositions need to be tailored, the melting processes and thermal behaviours need to be understand [18] and modified depending on the purpose of the optical material.

Before the term "fiber optics" was introduced [19] the use of glass to transmit light and specifically in the shape of thin transparent filaments was explored and proved for the first time in 1930 with relatively success as increasing applications, such as medical, benefited from the abilitiy to guide images through a material that could be flexible to avoid discomfort on patients but reliable enough to obtain a picture [20]. This first attempts to guide light through an optical glass fibre did not consider light leakage, they were unclad fibres, but further experiments showed that total internal reflection phenomenon, in other words: no light leakage, would only be possible if the surrounding material of the main light guide was from a material with a lower refractive index [21], and by doing so light was kept guided through the main glass fibre. After discovering that optical fibres needed to be coated with a glass composition with lower refractive index the next steps were to develop trustworthy methods to draw fibres with a cladding; techniques which were successfully obtained and subsequently exploited since 1957 [22]. One of the, now essential, characteristics of the optical fibres that had not been taken into consideration was the light absorption by the material per se, in 1965 the best fibres had attenuations of at least 1000 dB per km [23], therefore the next problem to be attacked was obtaining purer glass to reduce the losses through the length [24]. This brought into sight development and improvement in the techniques to process raw materials in order to decrease the impurities and therefore enhance the optical quality of the glasses and decrease the loses over the transmission windows [25]. Although all these experiments and people working together towards the obtention of reliable, functional and high-quality optical materials and optical fibres showed the path of research for the materials science industry, the applications of these improvements were implemented towards the communications industry, and the material selected was silica, which despite the fact that it is a trusted material it has its own disadvantages such as high melting point [26], high phonon energy [27], opacity at wavelengths above 2 μm [28], difficulty for rare earth (RE) doping [29], amongst others.

To overcome all these points the further study, development and use of multicomponent optical materials needed to be explored [30], particularly for the feasibility to obtain optical fibres exploiting their mechanical, chemical and optical characteristics for applications from the visible to the IR region [31].

The optical material described and used in this work belongs to the family of chalcogenide glasses, and particularly to the family of gallium lanthanum sulphide (GLS) based glasses. It is important to emphasize that the path to developing new techniques to fabricate novel materials, understanding their inherent properties and explaining their behaviour is not a straight-forward route. As explained by Hecht, "Materials science if often empirical, specialists make measurements first, then try to explain them" [23].

1.2 Chalcogenide glasses for IR applications

Chalcogenide glasses are amorphous solid materials constituted of chalcogens (III-V group elements of the periodic table) bonded covalently with glass network forming elements [32]. These glasses due to their own nature possess desired properties for the IR window transmission and IR applications, such as high density, polarizability and refractive index [4]. In the Novel Glass Group led by Professor Dan Hewak, a new family of chalcogenides glasses have been developed over the years. GLS glasses have demonstrated their reliability by maintaining a wide transmission window ranging from 420 nm to 10 μm (as shown in previous works) [1]. An aspect to consider explaining the reason why chalcogenide glasses are a reliable medium to transmit the longer wavelengths than 2 μm is due to the low phonon energy of the bonds that composes the glass network, which make this glass an ideal candidate for active and passive fibres and amplifiers for the MWIR and LWIR [33]. Efforts have been made to produce chalcogenide glasses that can extend the IR transmission window, being successful to fabricate a selenium modified GLS (GLS-Se) glass that can transmit up to 15 μm [34], though these glasses are still in a bulk glass form. A point to remark is that the addition of Se to the GLS matrix has also broadened the distance between T_g and T_x, giving exciting promises for a better thermal stability [5].

1.3 IR Optical Fibre Fabrication

Optical fibres that transmit beyond 2 μm are defined as IR fibres, and they started to be fabricated in the second half of the 60's from chalcogenide glasses [3]. The first fibres to be fabricated were from arsenic trisulfide (As_2S_3) in 1965 but losses were high and the material too brittle [35]. This first attempt opened the search for other chalcogenide compositions and means to fabricate multicomponent based glasses optical fibres. Different techniques started to be explored [31] in the aims of reliability, reproducibility and feasibility. The disadvantage of chalcogenide glass optical fibres is that the methods used for their fabrication are not as straight forward as for silica [36]. Particular attention is needed to process the raw materials prior to forming a glass, then shape the glass compositions into a glass rod and finally perform which is then drawn to fabricate an optical fibre [3].

As stated in the previous paragraph once the raw materials are prepared, according to compositions, and a glass is obtained the next step is how to turn it into a glass rod (preform), and the chosen technique will depend strongly on the thermal characteristics of the chalcogenide glass [37]. For chalcogenide glasses several approaches have been explored and developed throughout the years such as: rod-in-tube technique [38], double crucible technique [39], in situ melt to produce rods with cladding [40], core-suction technique, extrusion [41] and co-extrusion [42], just to name some, to produce unstructured and structured preforms.

In this overview we can already imply, that to obtain reliable optical fibre fabrication from chalcogenide-based glasses, a well determined process had to be already available to obtain reliable bulk glass samples that can be further processed to obtain preforms and fibres, and that the processes steps involved should not affect the original properties of the glass, as in the final product, we want to exploit each and every one of the characteristics of the well-studied family of chalcogenide glasses once it is drawn into an optical fibre.

1.4 Research Objectives

The aim of this research is to develop a reliable and repeatable process of chalcogenide optical fibres fabrication with a GL-Se composition, as it has a higher transparency than the best composition of GLS in the LWIR. Previous studies

have proved that GLS-Se has a good thermal stability that justifies that fibres can be produced [5]. The potential of the glass as a fibre has being predicted [43] but still not achieved. My objective is to produce chalcogenide fibres starting from the well-known melt quenching glass technique, developing preforms and finally obtaining fibres. It might sound simple, but we depend on the standardization of a fibre fabrication process to move forward to more complex research objectives such as chalcogenide fibre sensors, lasers and/or amplifiers.

1.5 Report Structure

The following thesis comprises 8 chapters. Below is a summary of each chapter.

Chapter 2: The basics of chalcogenides GLS-Se glasses fabrication, outlining their optical properties and thermal characteristics, introducing the suitability for the chalcogenide glass for fibre fabrication.

Chapter 3: The description of extrusion process as it is a reliable but still relatively un-explored mechanism for the production of GLS-Se preforms that could be drawn into fibres. Unlike oxide glass chalcogenide glasses cannot be casted into shapes thus extrusion seems to be an answer to manipulate these glasses without changing their optical properties.

Chapter 4: An overview in optical fibre fabrication, fibre drawing tower for soft glass at the Optoelectronics research Centre, and basic principles of optical fibre principles for GLS-Se compositions.

Chapter 5: Glass melting technique to suit the extrusion process, from the raw materials to the preparation of glass billets, including an explanation of each action taken for successful melts.

Chapter 6: The description of extrusion and co-extrusion with the GLS-Se based glasses is detailed, from failed attempts to successful glass rods and structured preforms, including the steps and logic that was followed to overcome the challenges.

Chapter 7: Optical fibre fabrication for GLS-Se glass rod and structured preforms after extrusion, the initial considerations, actual process and results, including

preparations, measurements and complete description in how to reproduce the best results up to date.

Chapter 8: Final remarks and future work.

Chapter 2

Chalcogenide Glasses

2.1 Introduction

The word chalcogenide comes from the joining of two words: one of Greek origin "khalkós" which means ore and the other from Latin-Greek origin "genēs" which means formation, so we can state that the word chalcogenide means through all the different possible combinations: "$oreformer$" [44] in our case specifically: glass former. Chalcogenide glasses are composed of and based on one or more chalcogen elements from group VI of the periodic table other than oxygen [45], making them fall in to three categories depending on the base element: sulphide (S), selenide (Se) or telluride (Te) [46] and are formed by the addition of other elements that are network formers such as As, Ge, Sb and in this work, with Ga and La [47].

One of the properties of these glasses, amongst others, is their low phonon energy [3] that make them suitably transparent from the visible up to the infrared region, [48], and interesting as host for rare earth (RE) ions [33]. In this work the research path to produce novel transparent optical glasses with is focused on: a) the election of powdered ultra-pure raw materials, that need to maintain their high purity during the glass production [49], b) adequate fabrication process in accordance with the raw materials of election and c) optical characterization and devices. Depending on the composition, application and post processing, there are different manufacturing techniques that can be explored, applied and improved such as: sealed ampoules [50], CVD [51], melt-quench [52], to name a few.

In this work we are going to concentrate our effort to study, understand and apply all the benefits of chalcogenide glasses, specially the family of GLS based glasses with the novel composition through the addition of Se. As stated in previous studies the GLS and GLS-Se compositions are reliable in terms of manufacture, post processing, and applications [53], it is our interest to maintain each one of the characteristics of the bulk glass in the processed glass.

To be successful in the processing of bulk glass samples, there should be an understanding of their structure, fabrication conditions, thermal properties and optical characteristics. These define our background and allow us to establish the foundation for further experiments, based on the nature that every glass is unique and will behave differently. As part of this work we therefore look at the balance between the results to be obtained and the initial conditions of fabrication. Most of the materials science knowledge comes in the shape of a delicate mix between reading, imagining, trying, failing and having enough data for feedback until success comes.

2.2 Glass melting for GLS-Se compositions

As stated in the past sections, material purity is the essential requirement of the manufacturing process with the goal to obtain a reliable glass, either for scientific or industrial reasons. Ultra-pure and consistent quality glass will mean that the experiments can be repeated if the glass melting process is uniform and stable [52]. Therefore, the impurities of the raw materials are of big concern for the glass melting process, it brings considerable effort to obtain trustworthy raw materials that will produce transparent glass without impurities that could contribute to the loss in transmission [54]. By eliminating impurities in the raw materials the possibility of losses by scattering are also eliminated, as said impurities could act as nucleation sites that could promote nucleation [55] or contribute to refractive index fluctuations which will also induce scattering. In simple words: the process needs to be controllable and reproducible through the uses of high purity raw materials.

To further understand the importance of the purification and use of raw materials IR glass experts have invested enormous quantities of efforts and resources to demonstrate that the very first step for a world changing application starts with

the basic requirements, high quality raw materials and the elimination of impurities [53, 56, 57].

Chalcogenide GLS-Se based glasses are produced by a melt quench process, which can be described as a straight forward process, as once the composition is decided the raw materials are mixed together and put inside a furnace in a purged environment at an optimized temperature to make the different components melt together as the fluxes of one component incorporates the other, provided the viscosities are low enough to produce a full mix without the need of stirring or a rocking furnace [52].

In this work the raw materials in the form of powders of Ga_2S_3, La_2S_3 and Ga_2Se_3 were firstly homogenized on a rolling mixer for 1 hour, Figs. 2.1 and 2.2, and then transferred to a carbon crucible. Many chalcogenides are made within sealed systems, where the sealed ampoules are made of silica but for La_2S_3 compounds there is a reaction with silica so to avoid any reactive impurities carbon crucibles are preferred [58]. The crucibles then are placed inside a horizontal silica tube furnace. During the melt and quenching processes, the furnace is purged with a steady argon flow. The temperature was then ramped up at a rate of 10 °C/min reaching a temperature of 350 °C, here the temperature was maintained for 3 hours to foment the elimination of volatile oxides of Se and S contained in the mixture, these oxides loses could represent up to 2% of the average loss in mass. After this step the temperature was ramped up again with the same rate of 10 °C/min until a temperature of 1150 °C was reached. These melting conditions were kept for 21 hours. Subsequently the temperature was abruptly decreased by removing the crucibles from the furnace and increasing the argon purge flow, Fig. 2.3 [1, 4, 5, 34, 52] until the melt cooled to room temperature The samples then were annealed at 490 °C (a temperature below T_g) for 48 hours to release any possible internal stress in the glasses [4, 5].

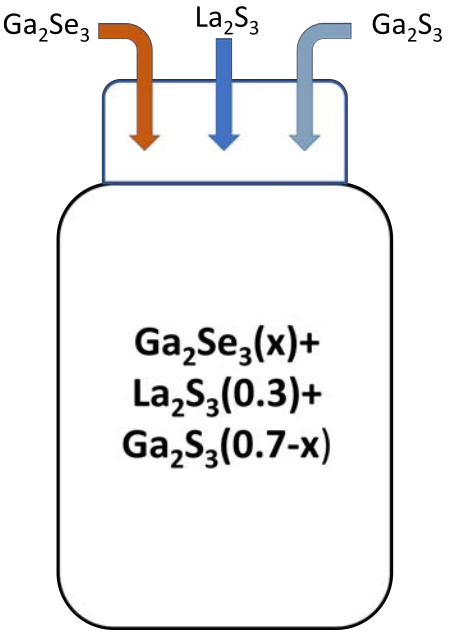

FIGURE 2.1: Batching of the raw materials mixture for glass melting

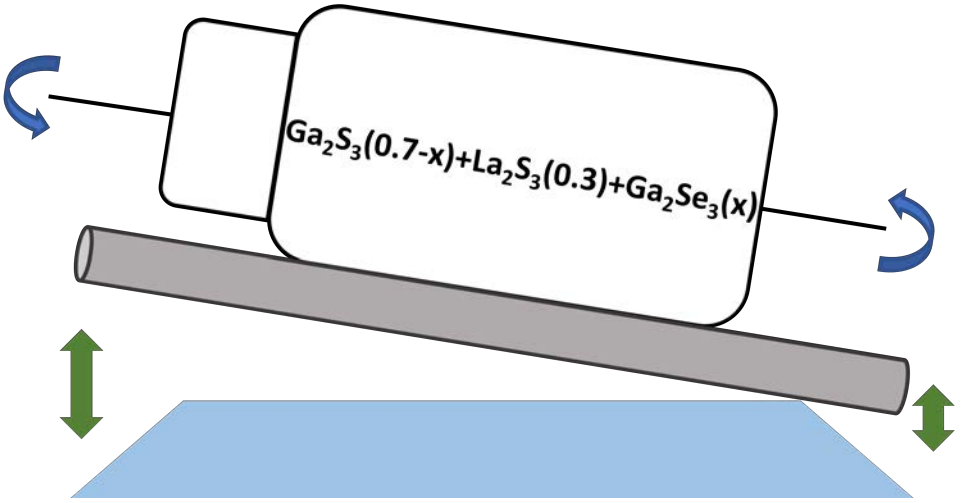

FIGURE 2.2: Roller mixing of the batch for 1 hour

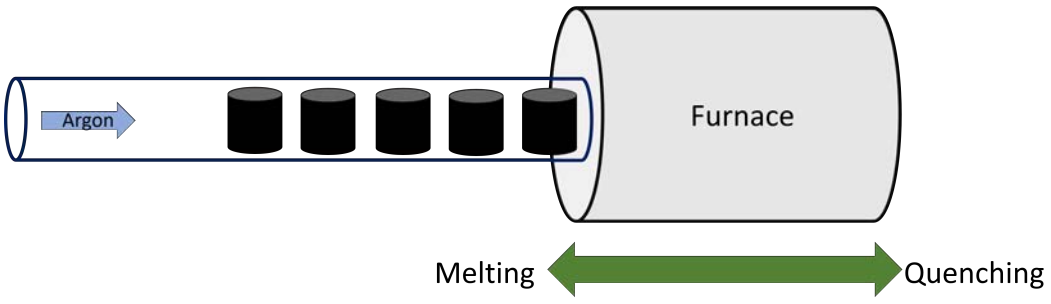

FIGURE 2.3: Carbon crucibles in a horizontal furnace for melting and quenching the glass

2.3 Transformation from melt to glass

The melt-quenching process as described in the previous section consists of two steps: a) to raise the temperature of the furnace sufficiently enough promote an homogeneous melt of the raw materials and b) then quenching it to abruptly to decrease the temperature from the melting temperature (T_m) to below the glass transition (T_g) temperature, this will promote a transition from a liquid state to a quasi-solid state, also identified as a supercooled liquid [59]. What is important during the quenching step is to obtain an amorphous phase of the material, so we can obtain a transparent glass [60]. For this to occur we need a specific cooling rate, which depends on composition. The reason to establish a critical cooling rate is simple; avoid crystallization.

If the quenching is fast enough the atoms of the glass will not have enough time to arrange themselves into a crystalline lattice [61]. The atomic movement will be restricted by the change in viscosity as a function of the temperature; as the temperature drops the viscosity increases the objective is to reach a temperature low enough to reach a viscosity higher than $10^{12}\ Pa \cdot s$ [62]. At this point the glass will be below its T_g, a temperature where the molecules would have frozen, meaning that they will maintain the arrangement established by the quenching process.

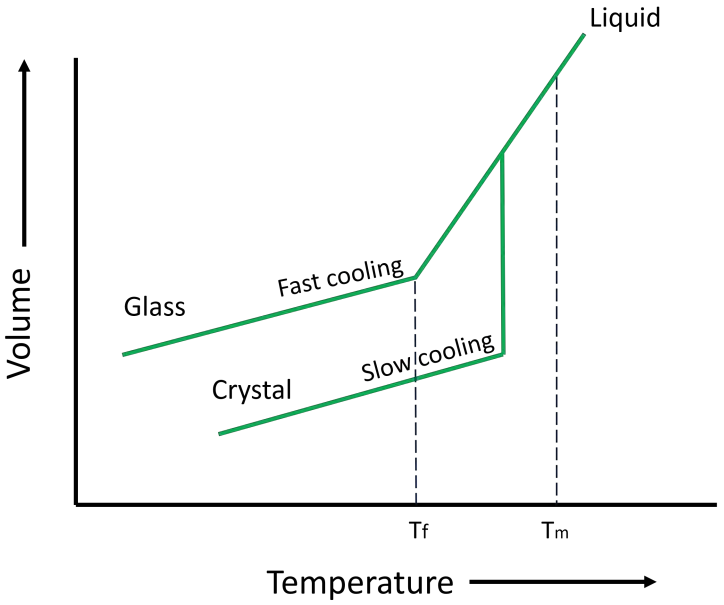

FIGURE 2.4: Glass forming curve, showing final phase depending on the cooling rate

Fig. 2.4 shows conceptually that during the quenching process the volume of the melt starts to decrease with reducing temperature. If the cooling rate is optimal for a glass formation the volume will reduce slowly up to its T_g where it cannot suffer from any more volume alterations. If the melt has a lower cooling rate, the volume and molecules would have more time to start reducing and arranging, respectively, into a crystalline phase. Here the volume is smaller compared to the amorphous phase, this can be explained as any molecule tends to move to a lower energy state, meaning a lower enthalpy, therefore by having more time in the cooling process each molecule would arrange into a crystalline lattice occupying less volume [63].

To demonstrate the ability of a composition to form a glass from its liquid state the critical cooling rate parameter for glass formation can be estimated, as shown in equation 2.1 where R_c is the critical cooling rate, α is the cooling rate, T_L is the temperature of the liquid state, T_x is the onset of crystallization temperature and d is a specific constant for the glass [64]. Understanding that a low R_c means that the liquid to form a glass has a strong forming ability.

$$\ln \alpha = \ln R_c + \frac{d}{(T_L - T_x)^2} \tag{2.1}$$

Equation 2.1 Critical cooling rate for glass formation [64]

It has been demonstrated that for glass networks with only two elements complete substitution of S for Se or Te (heavier chalcogens) the glass formation ability decreases. On the other hand, multi component networks benefit from the addition of heavier ions as the number of possible bondings is reduced, decreasing also the tendency to crystallize [65, 66].

Once the glass is formed after quenching, it is important to understand that the material might experience mechanical weakness from being brittle as internal stresses arise throughout the process. To mechanically strengthen glass an annealing process can be used. This latter step might also increase the transparency of the glass, eliminate photodarkening and be a medium to enhance its properties as density could change while the glass goes through structural relaxations, meaning changes in either the atoms position or the chemical environment around them [32, 67, 68]. Also, to understand the importance of the annealing

step it is important to acknowledge that the configuration of the element's atoms, when the amorphous phase is reached, have a phase called fictive temperature (T_f) that favors the internal stresses to remain within the glass structure [69, 70]. Where this T_f is the temperature within the glass formation region at which the cooling curve obtained during the melt-quenching departs from the equilibrium contraction curve of the supercooled liquid. The T_f indicates the extent of the configurational volume frozen into the glass at T_g and the T_f of a glass could usefully be a performance indicator of glass properties below T_g (i.e. density) [121].

2.4 Chalcogenide glass structure

Super cooled liquids are a state of matter identified by strong interactions between their particles (i.e. molecules, atoms). They can be found in a disordered state (non-crystalline). A non-crystalline solid lacks periodicity in its constituent particles, it can also be called amorphous or glassy. Crystals possess a long range order (LRO) in their structure, in amorphous phase a SRO exists [48, 71], a continuous random short range order (SRO) is considered an optimal non-crystalline [72]. One of the simplest chalcogenide glasses are the sulphide glasses [1] like GLS glass, that has been widely investigated, produced and improved for novel compositions and applications

The GLS glass family started to be investigated in 1976 [73] and later it was proven that this glass network could also be used as a base for other glass modifiers [74]. GLS has proved its value as it presents low toxicity, high strength, wide transmission window (Fig.2.6), thermal stability, high solubility of RE ions, low thermal expansion, low phonon energy and high laser damage threshold [1, 75]. The characteristic orange colour of this family of glasses is due to the 2.6eV bandgap that corresponds to a 475 nm wavelength [56]. In Fig. 2.6 it is showed that the composition 45:55 is in the limit of its glass forming range, the 3 and 4.7 μm absorption peaks correspond to O-H and Ce^{3+} ion respectively. This latter ion was inherently contained within the La_2S_3 and was confirmed by glow mass spectroscopy of the raw materials [1].

In GLS glasses Ga atoms in the glass exist in tetrahedral networks of GaS_4. The Ga and S environment in crystalline Ga_2S_3 is such that two of the three S are

linked to three Ga atoms and the third S atom is linked to two Ga atoms. The bonds that link two of the three S atoms consist of two covalent bonds and a third dative bond, while the third sulphur atom linked to two Ga atoms represents the bridging atom. The addition of La_2S_3 brings in an additional S^{2-} anion that results in modification of the dative bond of the trigonally coordinated S atom. The dative bond is broken and the S^{2-} anion provided by the modifying RE sulphide helps in restoring and maintaining the tetrahedral environment of GaS_4, at the same time creating a negative site for the La^{3+} cation [48, 52].

As mentioned before the GLS glass network has the potential to accept more elements to further tailor its properties. Also with the goal of reducing the crystallization tendency a new structural modified family of glasses was introduced in 2017 [4]. Further studies confirmed that this addition of Ga_2Se_3 (Fig. 2.5) extends the transmission window to longer wavelengths, and their thermal and mechanical properties remain robust, making it a suitable glass to be considered for optical fibres for passive [5] and active applications [6].

Understanding the characteristics of bulk samples defines the compositions that are more suitable for fibre fabrication as seen in the following chapters and would guide the steps in the fabrication process with the main task to maintain the bulk glass properties, while exploiting the favourable properties in an optical fibre geometry.

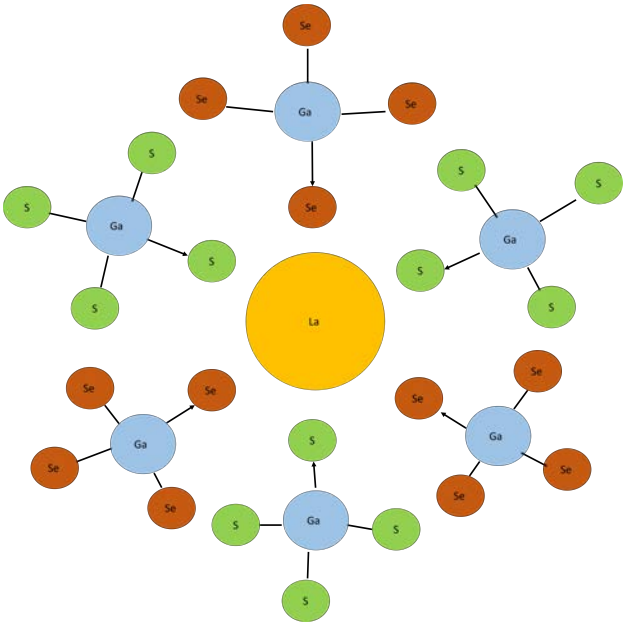

FIGURE 2.5: Schematic of the molecular structure of GLS-Se, where the La shows ionic bonds with the S and Se, and the Ga presents one dative bond

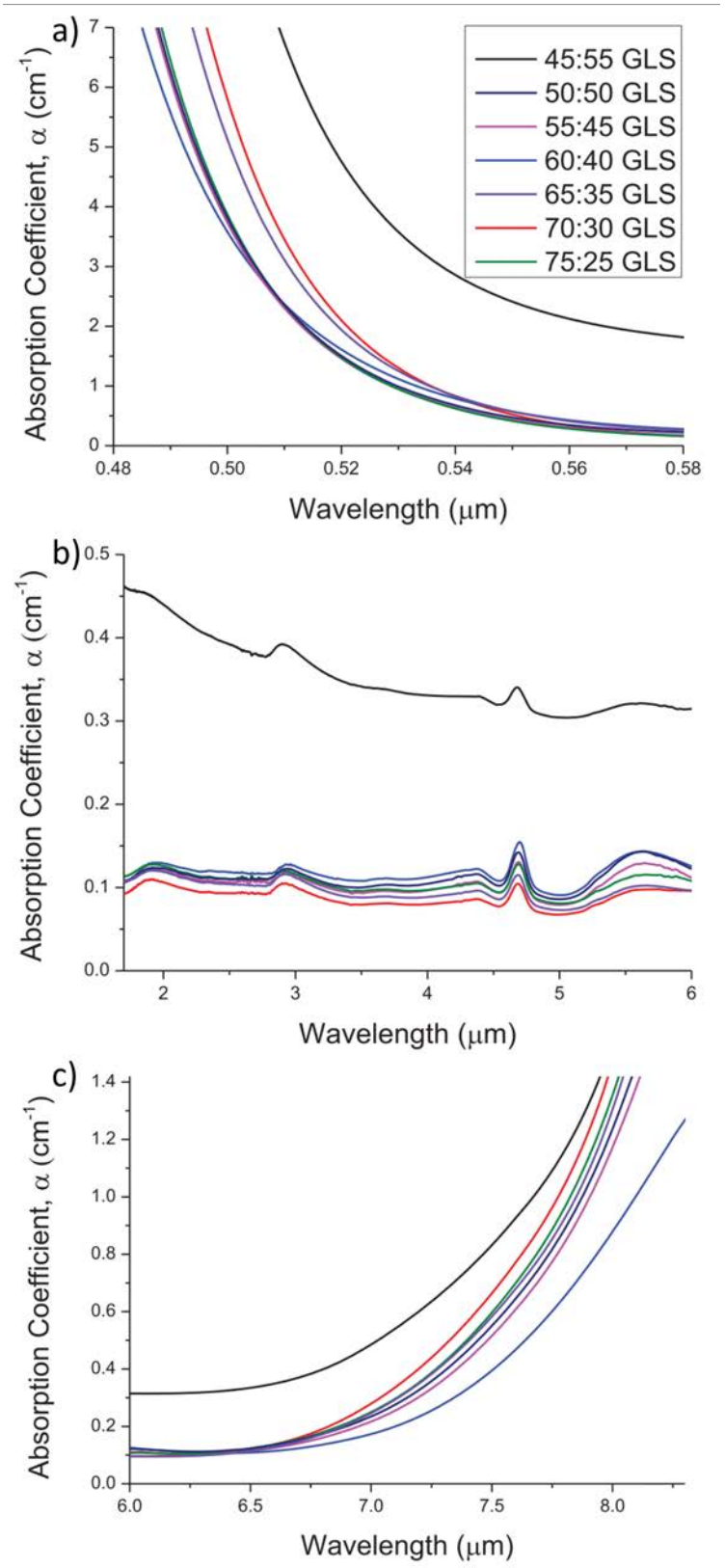

FIGURE 2.6: Optical transmission of GLS glasses fabricated by the Novel Glass Group at the Optoelectronics Research Centre, showing the a) electronic absorption edge, b) near-infrared losses and c) multiphonon absorption edge [1]

2.5 Thermal properties

Chalcogenide glasses are low temperature glasses. As the atomic mass of the chalcogen increases, the value of T_g decreases [3]. A low value in the transition temperature means that glass moulding is relatively easy, therefore fabricating optical components with chalcogenide elements would extend the applications of this family of glasses (e.g. thermal imaging) [46]. Thermal stability of the GLS-Se glasses has been estimated using the Weinberg parameter (K_W) [5] equation 2.2 which relates the gap between T_g and T_x with T_m.

$$K_W = \frac{T_x - T_g}{T_m} \tag{2.2}$$

Equation 2.2 Weinberg parameter for thermal stability [76]

The larger the span between T_g and T_x the better and more desired for fibre drawing as crystallization could be avoided during the process [34] GLS-Se glasses have shown a larger Weinberg parameter, and this can be explained due to the lower melting point of Ga_2Se_3 [5].

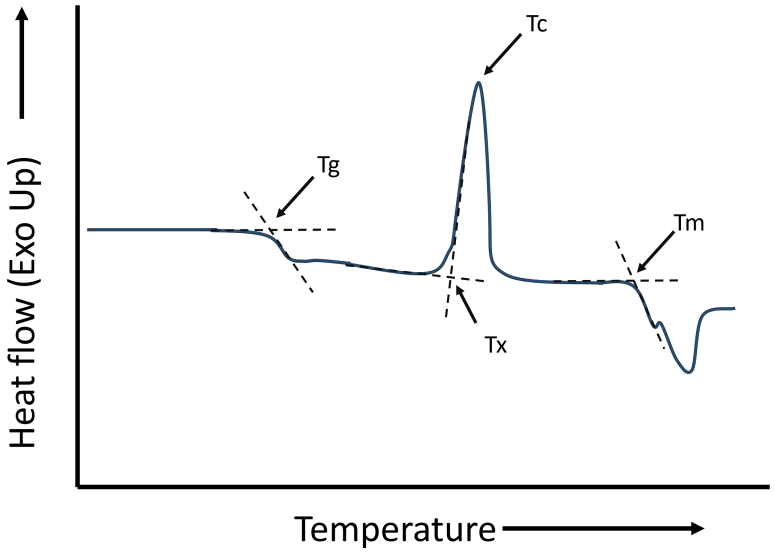

FIGURE 2.7: Differential thermal analysis (DTA) for a glass composition showing the heat flow behavior at each characteristic temperature, where T_g = glass transition temperature, T_x = crystallization temperature, T_c= crystallization peak temperature and T_m = melting temperature

To determine the Weinberg parameter, and therefore define the thermal stability of a glass, a thermal analysis for example through a DTA needs to be performed [77], Fig. 2.7. To do this, a sample of the glass after annealing is placed in an alumina crucible and the temperature is increased at a ramping rate of 10 °C/min from room temperature to 950 °C, as to preserve the conditions of the melting process. In the following chapters it is shown that ramping rate modifies the position of each of the characteristic temperatures.

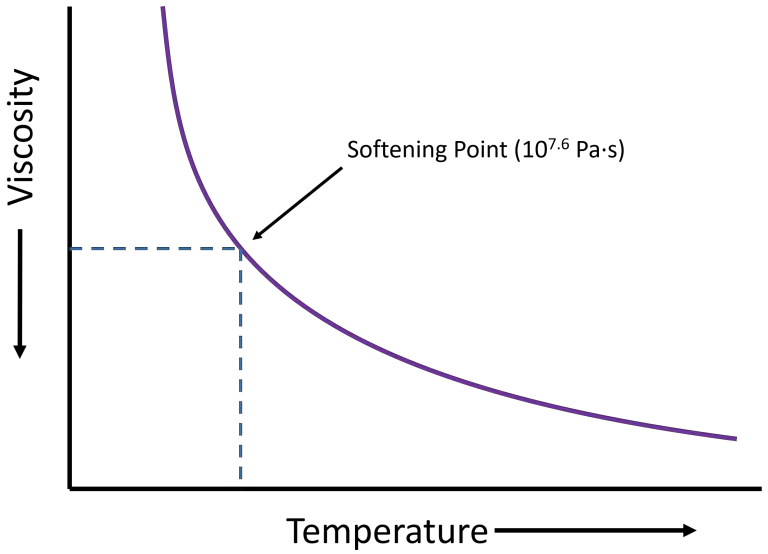

FIGURE 2.8: Generic viscosity vs temperature curve

For fibre drawing, it is important to know the behaviour of the glass viscosity as a function of the temperature, as the glass needs to reach at least the softening point to start softening and then necking, which is the beginning of the fibre drawing process. A way to understand the viscosity behaviours is to perform thermal mechanical analysis (TMA) [78], as shown in Fig. 2.8. It is clearly seen that as the temperature increases the viscosity of the glass decreases, some glasses could have a steep viscosity curve, where the viscosity changes quickly with temperature, making the fibre drawing a complicated process [79]. To obtain a standardized and reliable viscosity curve the ISO 7884-4 norm can be applied to the three-point bending technique commonly used in TMA. The viscosity as a function of temperature and be extracted using equations 2.3 and 2.4 [80].

$$I_c = \frac{h^3 b}{12} \tag{2.3}$$

Equation 2.3 Rectangular cross-section

Where h is the thickness and b is the width of the sample, respectively, in millimetres.

$$\eta = 681\frac{I_s \Delta t m}{I_c \Delta f} \tag{2.4}$$

Equation 2.4 Viscosity according to ISO 7884-4 standard

Where η is the viscosity in $dPa \cdot s$, Δf is the difference in position during the measuring time Δt in seconds, I_c is the cross-sectional moment of inertia in millimetres to the fourth power, m is the mass of the load in grams and I_s is the span in millimetres. In this work the viscosity measured using the ISO 7887-4 norm corresponds to the span from 10^{12} $Pa \cdot s$ to 10^{6} $Pa \cdot s$, for the rest of the plot the data was extrapolated as explained in chapter 5.

2.6 Optical properties of bulk chalcogenide glass

As seen earlier in this chapter chalcogenide glasses have a covalent bonding [48], which promotes glass formation by associating a giant network modifier with a dominant glass forming atom [81]. The electronegativity between cations and anions predicts the type of bonding within the glass' atoms, if this difference is greater than 1.7 the type of bond is ionic, if lower than this value it is defined as a covalent bond [82, 83]. Chalcogenide glasses transmit much longer wavelengths than other glasses (e.g. oxide glasses). This is a key feature and from great importance for applications such as fibre sensors operating for example in the fingerprint region (2-20μm) of the IR spectrum and for laser power delivery for laser operating at wavelengths longer than 2μm, where silica glasses become opaque. The higher the mass of the elements, the broader the transmission window for chalcogenide glasses, as the vibrational energies of the bonds constituting the molecules are lower while increasing the mass [3, 46, 84, 85] as seen in equation 2.5.

$$\upsilon = (1/2\pi c)\sqrt{\kappa\mu} \tag{2.5}$$

Equation 2.5 Frequency of vibrational modes [86]

Where υ is the vibrational wavenumber in cm^{-1}, κ is the stiffness of the bond, and μ is de reduced mass. As seen in Fig. 2.9 the heavier the chalcogen element the wider the transmission window, here it can be seen that Te which has an atomic weight of 127.60 can form a glass with transmission up to 20 μm compared to silica that contains oxygen which has an atomic weight of 15.999 [87].

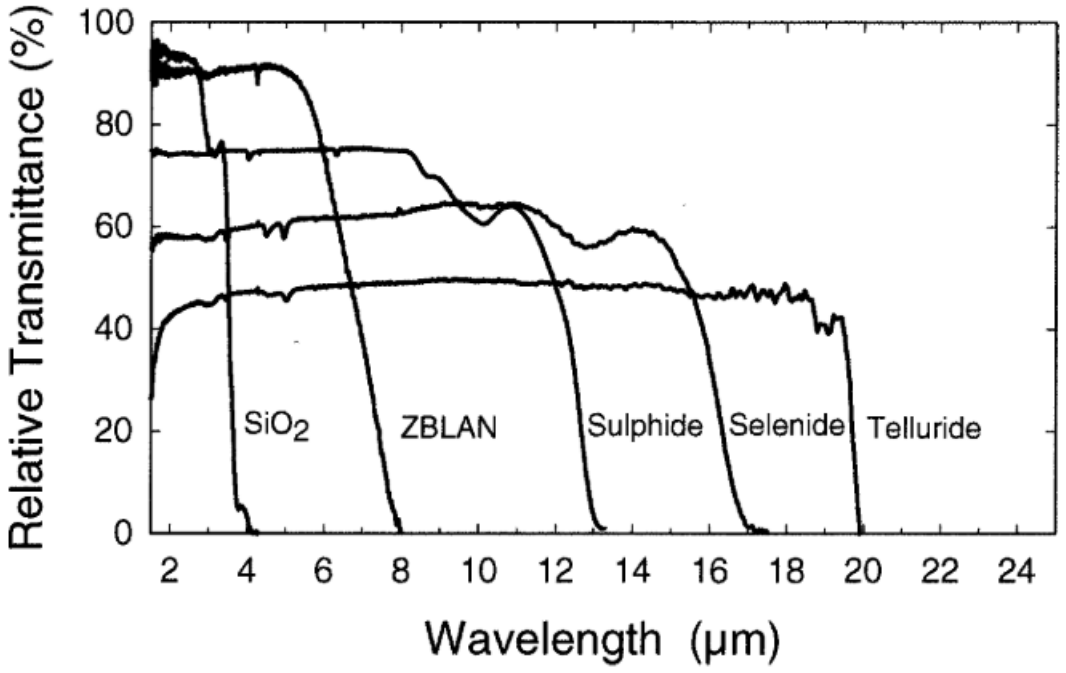

FIGURE 2.9: Comparison of the IR transmission for different glasses, the heavier the anion the further in the IR the transmission window widens [2]

2.7 Intrinsic and Extrinsic Losses

For most glasses, intrinsic losses comprise three mechanisms: Urbach tail, Rayleigh scattering and multiphonon absorption, each one a different loss mechanism and with its own wavelength dependance, as seen in Fig. 2.10. The heavier the atomic mass of the composition the less absorbance in the LWIR. In the region above 8 μm, as shown in Fig. 2.11 there are several absorption bands due to different multiphonon processes, meaning that the multiphonon edge in chalcogenide glasses is a superimposed absorption structure on this edge. This observed multiphonon structure is the result of a combination of different fundamental phonon modes. For the longest wavelengths two, three LO and/or TO phonons combine in an nth order process consequently obtaining the total intrinsic absorption. As said before

chalcogenide glasses are strongly covalently bonded, which would lead to a less overlap within phonon bands, thus giving a defined multiphonon structure [3].

Chalcogenide glasses apart from the Urbach tail at short wavelengths, Rayleigh scattering, for mid wavelengths, and multiphonon, for the long wavelengths, losses it also presents an additional absorption due to the weak absorption tail (WAT), being this the dominating absorption process in short wavelengths, as result from electronic transitions to lower lying bandgap states, Fig. 2.10. These bandgap states are due to impurities or defects in the glass structure such as dangling bonds [3].

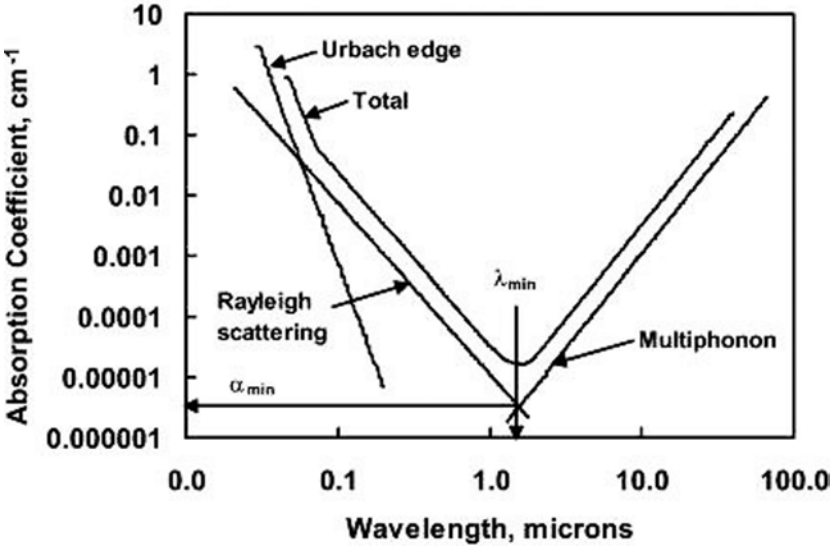

FIGURE 2.10: Intrinsic loss processes in optic materials [3]

Extrinsic losses in bulk glasses are mainly caused by impurities and scattering centres, with additional losses sometimes induced by the fibre drawing process and fibre geometry. It is important to notice that during the manufacturing of chalcogenide glasses and in particular during the quenching process, if the steps have been not fully optimized, there could be nanocrystal formation that could act as scattering centres [81]. Impurities related to hydrogen can also bond with the glass formers and result in specific extrinsic absorption bands, S-H fundamental stretching absorption occurs at 4.0 μm, and Se-H absorption is around 4.6 μm. In all glasses, a common contaminant is OH, which has an absorption near 2.9 μm [3].

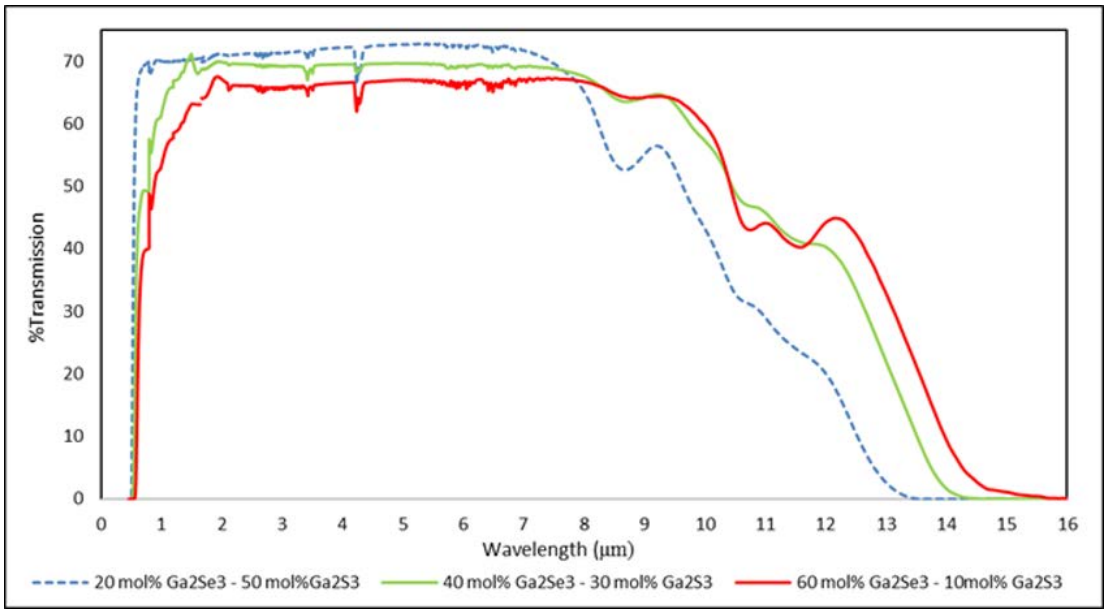

FIGURE 2.11: GLS-Se glass transmission window with different compositions produced by Dr Andrea Ravagli at the Optoelectronics Research Centre [4], thickness of the measured samples 1mm. The absorption peak at 8.6 μm corresponds to S-O vibration, and the peaks at 10.8 and 11.6 μm are due to the presence of Se-O bonds in the glass [54]

2.8 Refractive Index

In chalcogenide glasses, the elements that constitute the glass are more polarizable than fluoride or oxide glasses, this added to the fact that glass densities are also high leads to higher refractive indices n∼2-3 [3, 46, 52]. The refractive index for chalcogenide glasses can be measured with a Woollam®M-200 ellipsometer over a range of wavelengths between 0.370 and 1 μm. Ellipsometry is a technique based on the measurement of the change in polarization of a beam of light reflected from a glass surface. This technique has been used to measure the refractive indices for GLS-Se glasses and then fitted to the Sellmeier equation 2.6 for longer wavelengths than 1 μm [88].

$$n(\lambda)^2 = \frac{A\lambda^2}{\lambda^2 - A_1} + \frac{B\lambda^2}{\lambda^2 - B_1} + \frac{C\lambda^2}{\lambda^2 - C_1} \tag{2.6}$$

Equation 2.6 Sellmeier equation [88]

Where $n(\lambda)$ is the wavelength dependent refractive index and A, A_1, B, B_1, C and C_1 are fitting parameters. Equation 2.6 allow us to predict the behavior of the refractive index at longer wavelengths.

To confirm the difference in refractive index of different compositions and to be able to produce a suitable optical fibre preform, as shown in the following chapters, a Metricon 2010/M prism coupler at 1550 nm measurement, was used. This measurement needs a polished face of the glass sample to be measured, which will be in contact with the prism surface. A laser at 1550 nm is directed to the prism, with an incident angle, passing through the prism, reaching the sample and where it is then reflected to the opposite side of the prism that then is directed to the detector. Then both the sample and the prism are rotated changing the value of the incident angle until the critical angle is found θ_c. When the critical angle is reached the detected signal will start to drop form which the software yields the value of the refractive index [89] by using equation 2.7 where n_p is the known refractive index of the prism, n_g is the refractive index of the glass sample calculated with the critical angle θ_c [90].

$$n_g = n_p \sin \theta_c \tag{2.7}$$

Equation 2.7 Critical angle of refraction

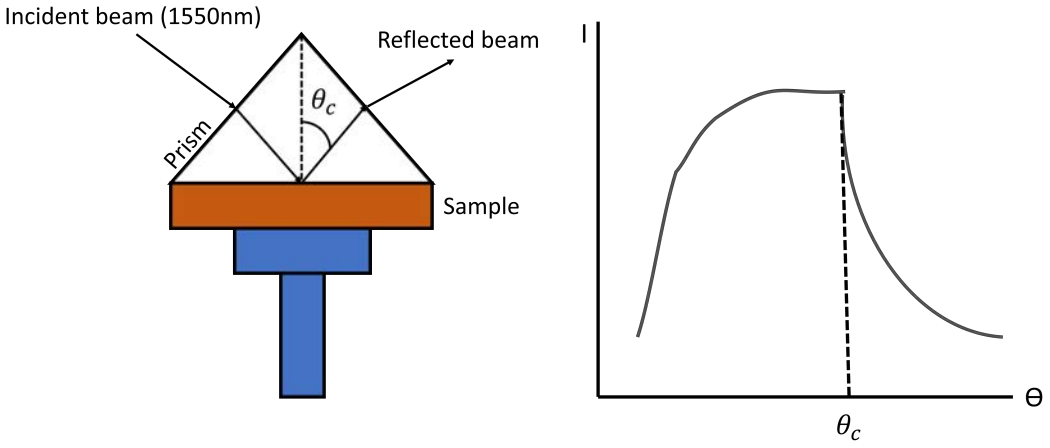

FIGURE 2.12: Metricon®measurement to obtain the critical angle for total reflection from which the refractive index at 1550 nm is determined

2.9 Conclusion

In summary, chalcogenide glasses have been produced, tested, and improved, in the Novel Glass Group, with modifications allowing the glass to be transparent with a

wide transmission spectrum, which goes from the visible up to the LWIR. Efforts have been made to produce a reliable glass in the GLS family, and most recently have obtained enhanced optical characteristics of IR glasses by producing a new family of chalcogenide glasses by doping with selenium. These modified glasses can now be fabricated with a reliable manufacturing process, with thermal stability, longer wavelength transparency and characteristics suitable for the production of optical fibres. The challenges in further processing these glasses, for example by extrusion remain to be addressed. The challenge remaining is maintaining the characteristics of the bulk glasses while the material undergoes a change of geometry that is required for the fibre drawing process.

Chapter 3

Extrusion

3.1 Introduction

Extrusion is a well-known process for metal and plastic manufacturing where rods, tubes or complex structures have been produced [91]. Since 1970, E. Roeder has studied extrusion in the glass field [92]. Before E. Roeder, the lack of use of extrusion for glass materials was due to the fact that most of the shaping glass methods were based on casting, blowing or rolling [93]. Nevertheless, the need for new kinds of glasses with special compositions is becoming crucial [94] and with that comes the need for new glass processing methods. These novel glasses, as a consequence of their compositions, can make their shaping by traditional methods a complicated task. In this regard, extrusion is particularly suitable for glasses with a strong tendency to crystallization [95].

As the optical fibre technology advanced, the need for different type of fibres with complicated geometries [32] and/or novel optical materials [96] started to rise, there was a commitment to overcome this newly created demand by producing different shapes of preforms with compositions that exclude silica. One method explored was capillary stacking [97], which consumed a lot of human effort, time and there is no flexible range for mistakes. Continuing with this need in mind and applying the efforts of E. Roeder, the extrusion process with emerging materials for novel applications started to be explored and the outcomes began to show that it was a reliable method of fabrication [98], moreover the obtained application results started to be trusted [99].

Glass extrusion described in this work is limited to the family of chalcogenide GLS-Se based glasses, and compositions for which extrusion trials have ever been attempted. In the past, different types of chalcogenide glasses have been tested and used to produce optical preforms by extrusion [100] with good results. The aim of this current work is to prove that this method is reliable and does not compromise the quality of the samples based on the new GLS-Se composition. While in the past this method has been used for GLSO glass samples [101] where the oxygen content has helped as a thermal stabilizer [102], the challenge addressed is to obtain a structured preform but with an oxygen-free chalcogenide glass.

Summarizing, to understand how to manufacture glass rods, or structured preforms, from any glass composition by using the flexibility of the extrusion process and the possible implications of it, there is a need to understand two main factors: a) the type of glass that is going to be used and its thermal characteristics (as described in chapter 2), and b) the extrusion process itself. Considering both factors, there should be a middle ground where the thermal and mechanical properties of the glass are exploited without compromising the already studied and proved characteristics of the bulk glass samples. Following this, we can effectively use extrusion apparatus to produce adequate and reliable glass rods for further processing and drawing into optical fibre.

3.2 Extrusion Fundamentals

Extrusion is a process where a material undergoes a permanent alteration of its dimensions by exploiting its plastic deformation ability, or plasticity, in response to an external applied pressure towards an opening of different dimensions [103]. In simple words it is to transform a defined block of material (billet) with certain dimensions into a new geometry by pushing it against a die opening of a smaller and/or different cross-sectional area under high pressure [104].

On the whole, there are two methods of extrusion: direct and indirect [92], for simplicity and due to the facilities at the Optoelectronics Research Centre this work is conducted only towards the use of the direct method.

To give a schematic and description of the direct extrusion method, it can be established at least four main parts to be considered: a) container, b) piston, c) die and d) billet, as seen in Fig. 3.1, where the billet is placed in the container,

ideally with no air gaps between billet and container. The piston applies pressure to the billets to produce a flow of material towards the die. The die aperture shapes the materials into a defined geometry and the billet is a block of material that is to be extruded.

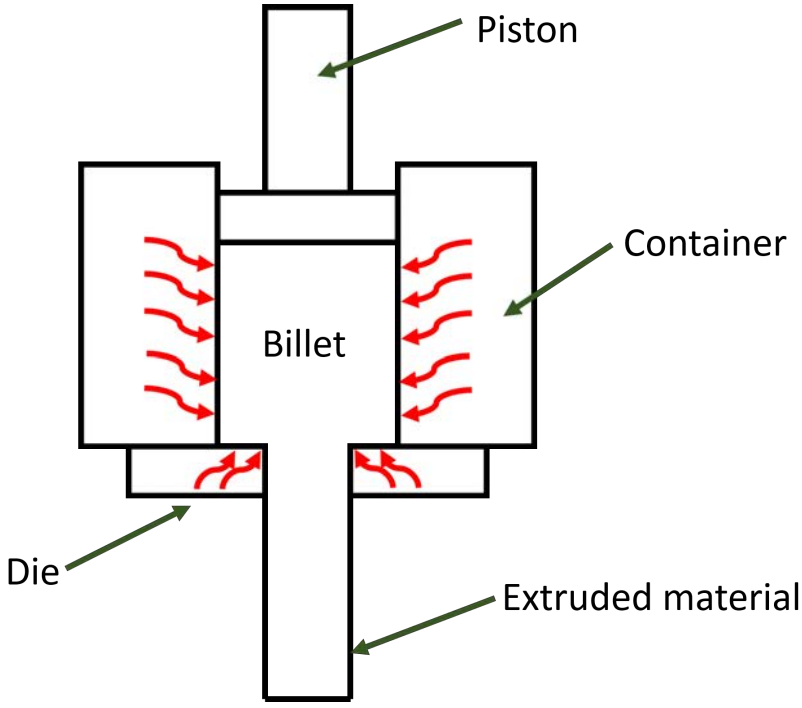

FIGURE 3.1: Schematic of a cross-sectional area view of a direct extrusion method

For metal alloys or polymers the way to obtain a well-defined extruded material exploiting the material plasticity is by carefully designing a die that allows the material to easily flow by solely applying pressure [105].

In this work, we show that as the material to be extruded is glass an important aspect to consider is the viscosity of it. As seen in Fig. 3.1, heat needs to be supplied to the billet to be able to perform the process [106], the reason behind this crucial point resides in the fact that glass would remain in a super cooled state (as seen in chapter 2) unless temperature is increased [107]. Even though heating is required, the extrusion process can be performed at a temperature below the softening point (7.6 dP·s), which is a characteristic of all glasses [108], by using lower temperatures and higher viscosities [109].

E. Roeder suggests that while heating up the glass to a temperature suitable for extrusion, it is not necessary to reach the temperatures that promote nucleation

and crystallization [92, 95], but as reviewed in chapter 6 a temperature above the Tg is needed for GLS-Se glass compositions, therefore some nucleation could take place. As previously observed by E. Roeder, provided extrusion takes place below the onset of crystallization and the cooling of the glass after exiting the die is greater than the critical cooling rate, crystallization is avoided [92].

3.3 Remarks about Direct Extrusion

The characteristic feature of direct extrusion process is that the material flow is in the same direction as the applied pressure [110]. As the billet is surrounded by the container walls with ideally no air gaps between them, and due to the expansive nature of materials in function of the temperature [111] this combination will provoke an increase of the initial load on the billet as a result of frictional forces [112], as seen in Fig. 3.2. The curve shows a rapid increase of the load up to a peak value before the actual extrusion begins, then it decreases during the steady state of the extrusion, and finally it sharply rises when it is close to the end of the billet [113]. In this work, the increased load and frictional force are a result of the coefficient of thermal expansion (CTE) of the GLS-Se based glasses [5].

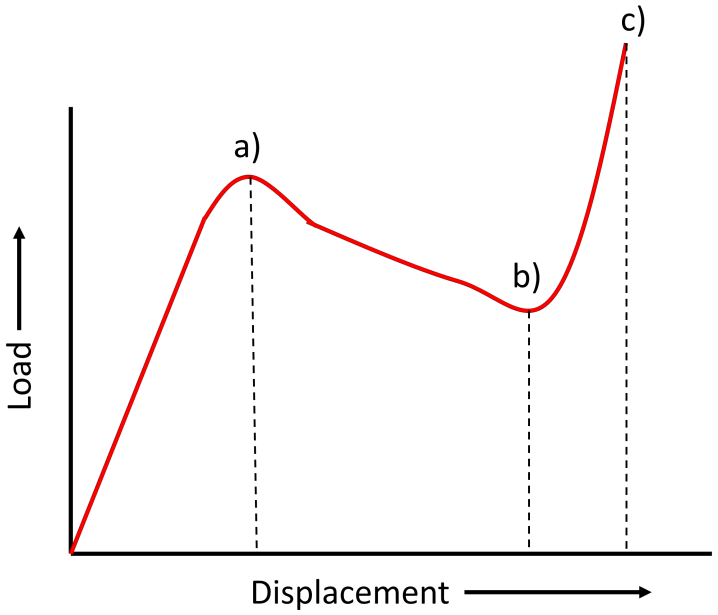

FIGURE 3.2: Load curve versus the displacement of the piston where a) shows a rapid increase in the load before the extrusion begins and the steady flow starts, b) is the end of steady flow and c) displays a rapid increase of load before the end of the extrusion. *Note: temperature is constant*

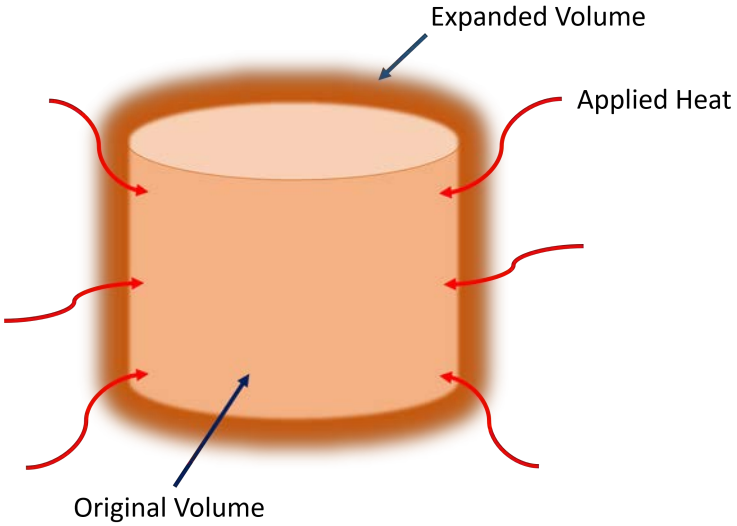

FIGURE 3.3: Schematic of the billet's expansion. Note: expansion not to scale, CTE depends on composition [5]

To relate Fig. 3.2 with the internal behaviour on the billet due to the load, an image of the cross-sectional area is shown in Fig. 3.4, this further explains that at the beginning of the direct extrusion process a breakthrough load is rapidly reached before the extrusion begins. Just as extrusion starts to take place, that is, when the material starts to go through the die, the load decreases as the length of the extruded material increases until a minimum load is reached. As the billet thins up to a critical point the load sharply increases again to continue producing a material flow radially towards the die opening [114].

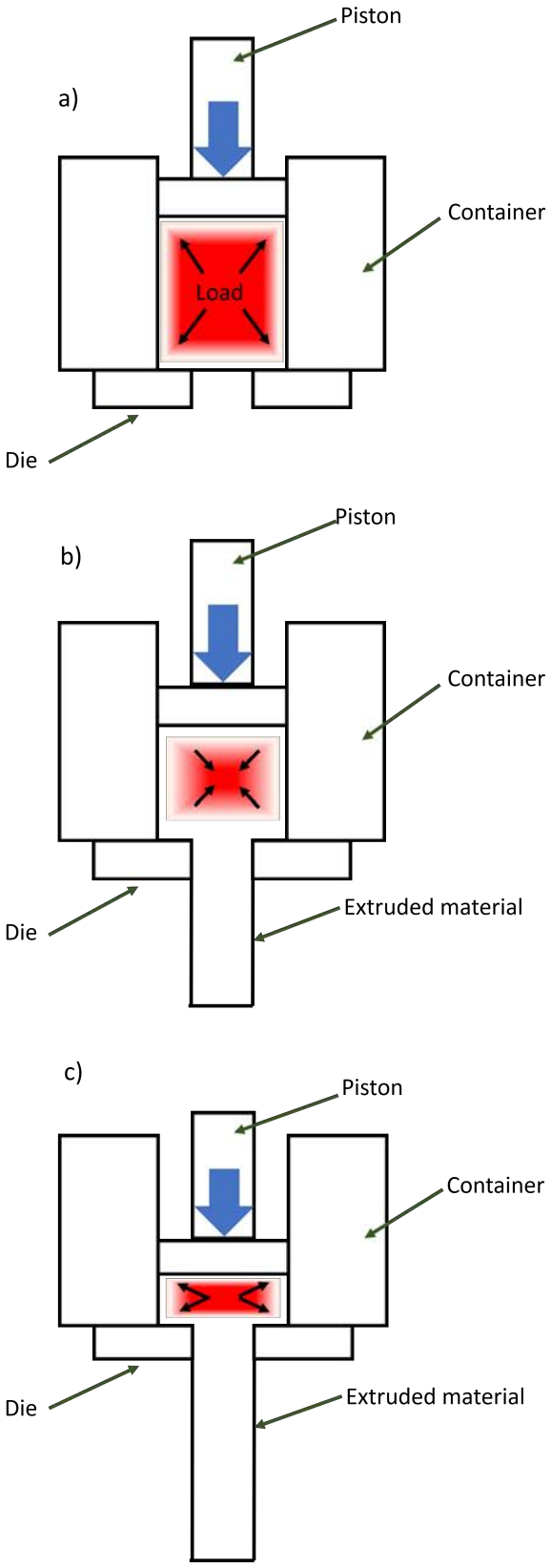

FIGURE 3.4: Material behaviour inside the container throughout the extrusion, as described in figure 3.2

3.4 Description of the extrusion apparatus at the Optelectronics Research Centre (ORC)

At the ORC the extrusion apparatus consists of the following elements, as shown in Fig. 3.5:

1. Piston: to produce a direct extrusion and the load needed.
2. Ceramic shield: to maintain the heat of the entire apparatus.
3. Two heating elements: where one supplies heat to the main body of the billet container of the apparatus and the other supplies heat to the die, this latter resistor is placed just below the die, it helps maintain the temperature of the outcoming extruded material.
4. Two thermocouples: connected directly to a thermal controller and the power resistors, which will maintain the set temperature.
5. A carbon body: that is heated up by the power resistors and that holds the container with the billet.
6. Billet container: divided in three parts: a) sleeve, b) lid, and c) the die itself.

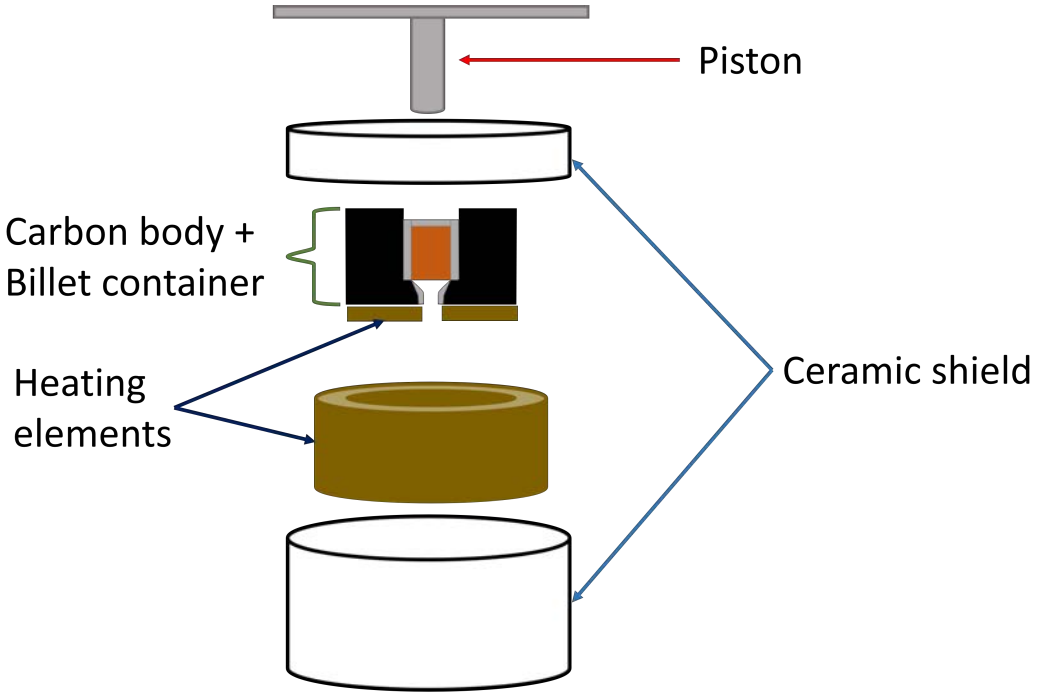

FIGURE 3.5: Schematic of the extrusion apparatus assembly at the ORC

It must be noted that for feasibility and convenience, the sleeve, lid and die are produced in the mechanical workshop with 303 grade stainless steel [115]. The detailed steps of how to prepare the samples and the assembly is further explained in chapter 6. The sleeve has an inner diameter of 29-30 mm and a height of 35 mm, the die has a non-straight gradual slope to an aperture of 10 mm, and the lid has a diameter that fits the sleeve and a thickness of 5 mm. In the cross-sectional area of the assembly of Fig. 3.6 it is shown how the billet temperature profile behaves in respect of its two independent elements (resistors) heating the whole container. The bottom resistor (closer to the die) produces a slight difference (ΔT) in temperature with respect to the main body resistor, this is needed to be sure that the extruded material keeps flowing out of the die by avoiding any possible random cooling that could affect the extrusion at the die aperture.

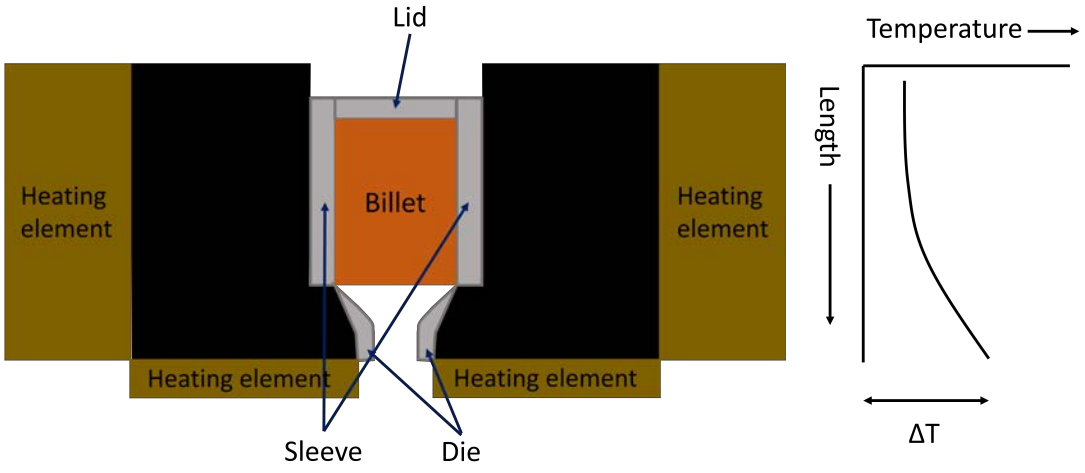

FIGURE 3.6: Cross-section of the billet assembled in the body container (sleeve, lid and die); and temperature profile of the extrusion apparatus

3.5 Glass flow during extrusion

As seen in the previous sections a fundamental element in the extrusion process is the die. It not only defines the geometry of the extruded material but also determines how the glass flows depending on its profile and the coefficient of static and dynamic friction of the material from which it is made. Therefore, the die design is of vital importance as it affects the glass flow during the extrusion process [116]. Thus, one of the characteristics that needs to remain without alteration is the reproducibility of the die manufacture in order to have reliable results and to be confident that the extrusion process can be replicated [117].

The glass flow through a die with a defined circular aperture during the extrusion process presents an isothermal flow through a circular aperture [92], and it is consider to avoid having a slip at the fluid/aperture boundary as stated in Poiseuille's law [118], as the die is made of stainless steel [119].

$$Q = \frac{\pi p r^4}{8\eta l} \tag{3.1}$$

Equation 3.1 Poiseuille's Law for laminar flows [120]

Where Q is the flow rate (m^3/s), p is the pressure gradient between entrance and exit of the die (Pa), r is the radius of the die aperture (m), l is the length of the parallel section of the die with respect to the flow (m) and η is the viscosity of the fluid $(Pa \cdot s)$, as shown in Fig. 3.7. It is to be noted that in this figure P_2 represents a value of 101.325 KPa [121] which corresponds to the ambient pressure. This value is small compared to the extrusion pressure applied by the load, therefore in equation 3.1 the gradient pressure p can be substituted by only the extrusion pressure P_1 [95].

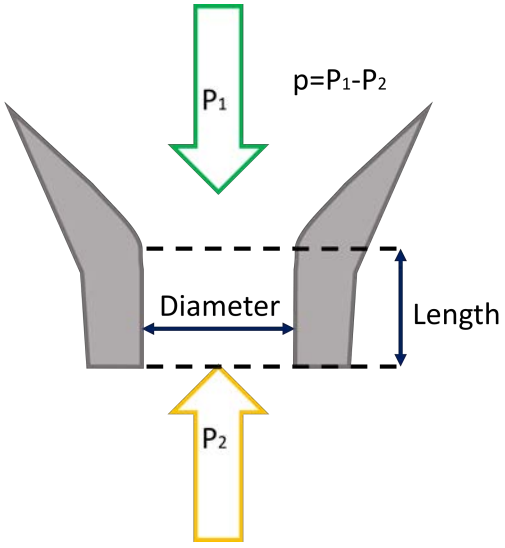

FIGURE 3.7: Diagram representing Poiseuille's law in the die

The extrusion pressure P_1 is given by the applied load F (N) over the die cross-sectional area A_D (m^2) as defined in equation 3.2 [122], the flow rate V (m^3/s) can also be calculated with the extrusion speed v (m/s) times the area A (m^2) of the cross-sectional area of the die aperture, shown in equation 3.3 [123].

$$P_1 = \frac{F}{A_D} \tag{3.2}$$

Equation 3.2 Pressure defined by the applied load over an area

$$Q = Av \tag{3.3}$$

Equation 3.3 Volume flow rate given by the extrusion speed and the cross-sectional area of the die

As during the extrusion process the applied load, diameter of the die aperture and the length of the parallel section of the die are known values, we can use equations 3.2 and 3.3 and substitute them in equation 3.1 [124], so it is rewritten as:

$$P_1 = \frac{128l}{\pi d^4}\eta A_D v \tag{3.4}$$

Equation 3.4 Poiseuille's Law using the extrusion speed, diameter and area of the die

Equation 3.4 shows that a steady flow of extrusion (Fig. 3.2) is clearly dependent on the viscosity of the glass and the volume flow rate [125]. The first part of this equation can be taken as a constant as it only includes the dimensions of the die's geometry and it is not dependent on the extrusion settings. This constant, shown in equation 3.5 [116], describes that the friction increases as the die length increases and when the diameter of the die aperture is decreased.

$$K = \frac{128l}{\pi d^4} \tag{3.5}$$

Equation 3.5 Die constant describing the flow through the die friction

As glass is heated and becomes less viscous it can be treated as an incompressible liquid [126], this means that the volume of glass in the billet that is shaped by the die remains the same after the extrusion [127] with the difference of area and

length in each, as shown in Fig. 3.8. In other words, any portion of glass flowing through the die can modify its geometry, but it must maintain the same volume. It is to be pointed out that the volume flow is the same at any point along the geometry of the billet container [128], but as the area along the extrusion process decreases the speed of the glass needs to increase to maintain the same volume flow [129]. By using equation 3.3 and with help of Fig. 3.8 the volume rate can be written in the form of the continuity equation [130], equation 3.6.

$$A_1 v_1 = A_2 v_2 \tag{3.6}$$

Equation 3.6 Continuity equation

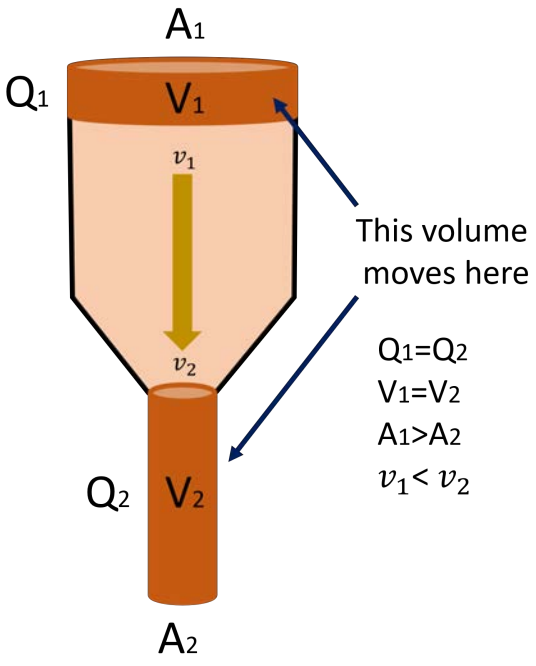

FIGURE 3.8: Schematic of an incompressible material during extrusion, V= volume and A = area

For simplicity in terms of the calculations to obtain the extrusion speed, the die equation 3.6 can be transformed into terms of the diameters of the billet and die, as seen in equation 3.7, where v_1 is the speed of the piston that produces the extrusion, v_2 is the speed of the glass in the die, D_B is the diameter of the billet and D_d is the diameter of the die [131].

$$v_2 = \left(\frac{D_B}{D_d}\right)^2 v_1 \tag{3.7}$$

Equation 3.7 Speed of the glass in the die

After the glass flows out of die, there is a phenomenon that could slightly modify the diameter of the final extruded rod, referred to as die swell [132]. The glass goes through internal expansion through axial pressure towards the walls of the body container (sleeve and die) during extrusion and once the material is out of the die, this expansion and pressure provoke the Barus effect [133] by relaxing its elastic stresses contained in the flowing glass, as seen in Fig. 3.9.

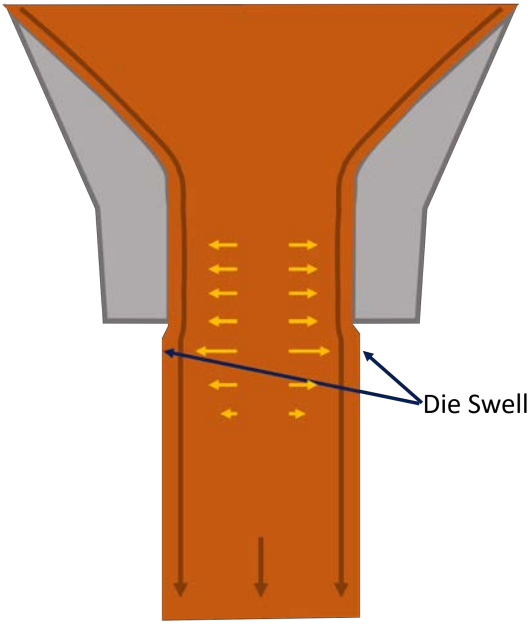

FIGURE 3.9: Die Swell and the Baraus effect schematic, the brown arrows show the flow of the glass, and the yellow arrows portrait how the internal stresses relaxes throughout the flow after the die

The final point to take into account is the maintenance of a uniform shape of the extruded glass rod (or tube) during the extrusion process. If the shear stress between the wall of the die and the glass is high enough to exceed some critical value the shape of the glass would become irregular [122]. At high temperatures the glass behaves as an ideal viscous fluid (Newtonian liquid), where the rate of shear γ is directly proportional to the applied shear stress τ , as seen in equation 3.8, where η is the viscosity.

$$\tau = \eta\gamma \tag{3.8}$$

Equation 3.8 Rheological model for the flow glass behavior [95]

The best and most convenient way to increase the extrusion speed is to increase the temperature by which the viscosity would decrease [134], and by dropping the viscosity we can diminish the shear stress, thus obtaining better control and a more regular extruded shape. However, an increase in temperature to lower the viscosity can promote crystallization [95]. As a result, the optimum extrusion parameters need to be developed for each type of glass.

3.6 Preform fabrication by extrusion

As reviewed on chapter 2, chalcogenide glasses have several optical properties that want to be exploited. To make use of these properties and develop applications or devices, a useful waveguide is desirable, such an optical fibre, therefore one previous step is the production of preform that can be drawn into fibres. A convenient optical configuration to guide light is a core/clad structure [42], as you can control the wavelength to be used, NA, etc. for SMF. Some techniques to produce core/clad preforms include: rod-in-tube technique [135], core-suction technique [136], in situ melt cooling to produce rods and cladding [40], different research groups have explored the viability of producing rod preforms in the past by extrusion process [41] and finally co-extrusion (using two glass compositions and extruded at the same time) [42].

In this work extrusion and co-extrusion are explored, the experiments were carried out in temperature regions where the viscosity is still at a high value ($10^{11} - 10^{9} Pa \cdot s$), where the crystallization rate is kept to a minimum and with this maintain the amorphous structure of the glass [137]. For a single composition glass rod, Fig. 3.6, only one billet is needed however at least two billets with different compositions need to be extruded at the same time (co-extrusion) to produce a structured preform [138], where the composition that acts as a cladding is located in the bottom of the body container and the core on top of it, as seen in Fig. 3.10. To determine which compositions are to be used as a cladding and as a core a study

about its thermal, mechanical and optical properties (i.e. refractive index) [41] are needed to be studied and understood beforehand.

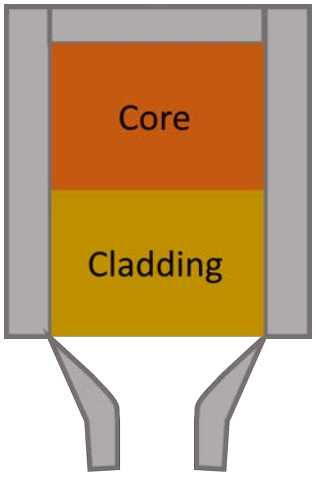

FIGURE 3.10: Co-extrusion using two billets of different compositions, illustrated here for achieving a core/cladding preform

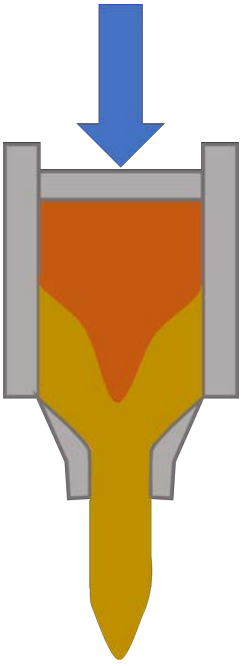

FIGURE 3.11: Initial flow of the co-extrusion process

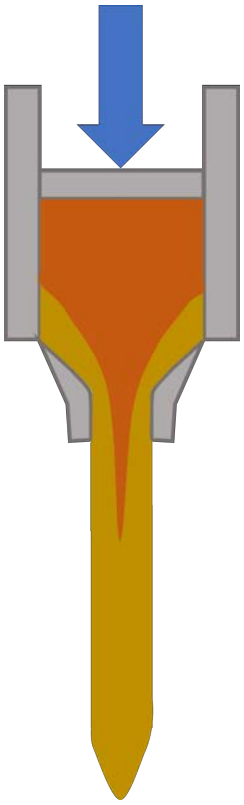

FIGURE 3.12: Structured preform flow as the co-extrusion process continues

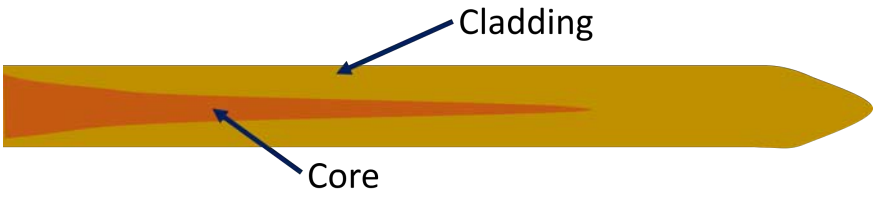

FIGURE 3.13: Final extruded structured preform schematic

One key point for the success of extrusion, and afterwards its drawing into an optical fibre, is to obtain a uniform preform to minimize any fluctuation along its geometry [42]. If the viscosity reaches a low value and the mass of the preform is heavy enough a tapered preform might be obtained. As seen in Fig.3.11 the first composition to be extruded is the cladding, this means the initial portion of the preform is coreless and that the core starts at a minimum value and increases in diameter as the extrusion process keeps going [139], Fig. 3.12.

The core-clad interface, where the evanescent field propagates [140], needs to have no imperfection or impurities as this contributes mainly in the losses along the

preform once it is drawn into a fibre [141]. This requires developing a complete and reliable cleaning and polishing process to prepare the glass billets prior extrusion.

As reviewed in this and the previous chapter chalcogenide glass fabrication methods have been studied for decades, it there exists a trusted method of producing high quality bulk glasses. The key point of any further process (i.e. extrusion) is to not only to maintain these high-quality bulk characteristics, as stated in previous sections, but to develop a reliable process for this purpose. This means that after glass fabrication and prior extrusion there are several steps in between that are also required to produce a successful GLS-Se structured preform as explained in chapter 6.

3.7 Conclusion

Chalcogenide glasses are a reliable material for the IR, but we need an optical fibre geometry so we can extend the number of applications where we can apply them. The first step to produce optical fibres is to obtain a preform with chalcogenide glasses which maintains the optical, chemical and mechanical properties of the bulk glass. There are different methods to obtain rods and tubes from molten glass, but in the current facilities and trying to avoid any possible interaction with the environment, as well as maintaining the quality of the GLS-Se glasses, extrusion is suitable for preform fabrication. As being part of the compound glass family, they need lower temperatures to be moulded, compared to silica based glass, which is an important factor to avoid any possible internal structure modification, such as crystallization. The process that can be easily exploited for structured preforms is co-extrusion, as parameters like temperature, glass volume, speed of extrusion, and quality of the optical surface have been studied and improved to obtain the best possible chalcogenide preforms, after which it might be possible to obtain reliable optical chalcogenide fibres.

Chapter 4

Chalcogenide optical fibres fabrication and applications

4.1 Introduction

Chalcogenide optical fibre fabrication is one of the areas of application of the chalcogenide photonics research [142] aiming to develop novel waveguides or optical fibres to exploit the properties of the chalcogenide glasses, such as non-linearity, transparency in the far infrared, amongst others [32]. Several potential applications include sensing for the civil, medical and military areas, as they these materials offer transmission over much of the molecular fingerprint region (2-25 μm) [46].

A classification of chalcogenide optical fibres according to their composition could be passive [135], when only glass forming elements are used in the manufacturing process, or active [143], when there is an addition of rare earth or transition metal ions into the glass matrix. Passive optical fibres can be used to transport light from one location to another [48], optical signal processing [144], generation of mid-infrared wavelengths [145], supercontinuum generation [146], high efficiency self-modulation and wave mixing [147] or to produce non-linear effects [148], just to name a few examples. Active optical fibres exploitation include mid-infrared lasers [149] and optical fibre amplifiers [150].

As reviewed in the introductory section of chapter 3, there have been different approaches to produce optical preforms from chalcogenide glasses from which optical

fibres can be drawn. However, losses continue to be a problem for chalcogenide fibres and their usage is limited to short fibre lengths [151]. Despite the fact that low losses have been predicted [43] and that one of the lowest values obtained in chalcogenide fibres is 23 dB km^{-1} at 2.3 μm [152] has been achieved, the chalcogenide fibre process requires meticulous attention at each step of the process. From the glass melting process and the carefully production of optical preforms, it is the last step that can decide the success or failure of an optical fibre, that is the fibre drawing process itself. For example, drawing of the fibre requires careful control of temperature to ensure the fibre drawing temperature is sufficiently far from the onset of crystallization while in structured optical fibres the high losses arise due to the core-cladding scattering [153], caused by structural imperfections or trapped particles within the interface of both compositions that can get enhanced in the fibre drawing process [154].

The aim of this work is in part to produce a practical fibre drawing process for GLS-Se based glasses. The aim of this chapter is to detail the equipment required for the drawing of GLS-Se glasses. In the past, several chalcogenide compositions [155], with numerous different results, have undergone fibre drawing trials with the premise that each composition needs a fibre drawing process to be developed. The challenge in GLS-Se glasses is that the drawing temperature is close to its crystallization temperature, a characteristic of chalcogenide glasses [156]. Therefore, the aim is to study how a GLS-Se based preform behaves under the fibre drawing process and optimize every step for a reliable process to be repeatable to further improve the production of GLS-Se glass based optical fibres.

4.2 Fibre fabrication

Chalcogenide fibre drawing is not a straight forward process as is the case for silica optical preforms [3] since crystallization is a major effect in most non-silicate glasses compositions [157] specific temperatures need to be applied in the process. As shown in Fig. 4.1 in this process a fibre drawing tower is required. It consists of a mechanism of preform feeding, a heat source to soften the glass (furnace), diameter gauge to measure the fibre diameter, a coating mechanism that applies a polymer to protect the fibres, a UV lamp that cures the applied polymer and a drum to collect the fibre [17]. The principle behind the fibre drawing process is the conservation of mass law [158], which describes that the total mass of preform draw

per unit time equals the total mass of fibre produced, therefore the parameters ruling the final fibre diameter are the feeding preform and fibre drawing speeds, as seen in equation 4.1 [159].

A suitable heating temperature, above T_g, and heating steps are essential to achieve an optical fibre of good quality [160]. The preform is slowly and continuously fed into the susceptor region of the furnace to soften the glass preform [161]. After the glass viscosity is reduced sufficiently it can be pulled down by applying an appropriate level of tension [162], which in most cases is the weight of the glass itself when the softening point is reached [163]. During the fibre drawing process the geometry of the preform experiences a profile reduction from a specific diameter (i.e. 10 mm) to a fibre diameter (i.e. 125 μm), this is known as a neck-down profile [164]. The neck-down profile occurs due to a viscosity change in the preform as a consequence of the radiative heating from the susceptor towards the glass (Fig. 4.2) [165], the glass flow in the neck-down profile is steady, incompressible and laminar [166]. Initially the temperature on the surface preform is higher than in the centre [167], as the heat continues to radiate towards the preform the centre temperature begins to rise and the glass stretches downwards until the preform temperature is high enough and evenly distributed for the fibre drawing process (Fig. 4.3).

During the fibre drawing process, chalcogenide optical preforms can suffer from crystallization [168], as seen in chapter 6, this drawback effect has some possible causes: contamination within the glass [169], excess temperature [170], time consumed in the process (dwell time in furnace) [171], preform surface quality [172] or residual oxygen and moisture surrounding the glass [37].

$$D^2V = d^2v \tag{4.1}$$

Equation 4.1 Calculation of the drawing speed

Where D is the preform diameter, V is the preform feed speed, d is the fibre diameter and v is the drum rotating speed (Fig. 4.1). In the past GLSO based optical fibres have been produced [53] by increasing the temperature to achieve a known low viscosity at which the preform necks to form a thin fibre that it is attached to the drum, the preform feed is activated and then the temperature is modified accordingly to allow stable fibre drawing. In chapter 7, the steps needed

to develop a successful GLS-Se optical fibre for the first time and all the trials and modifications are explained in detail.

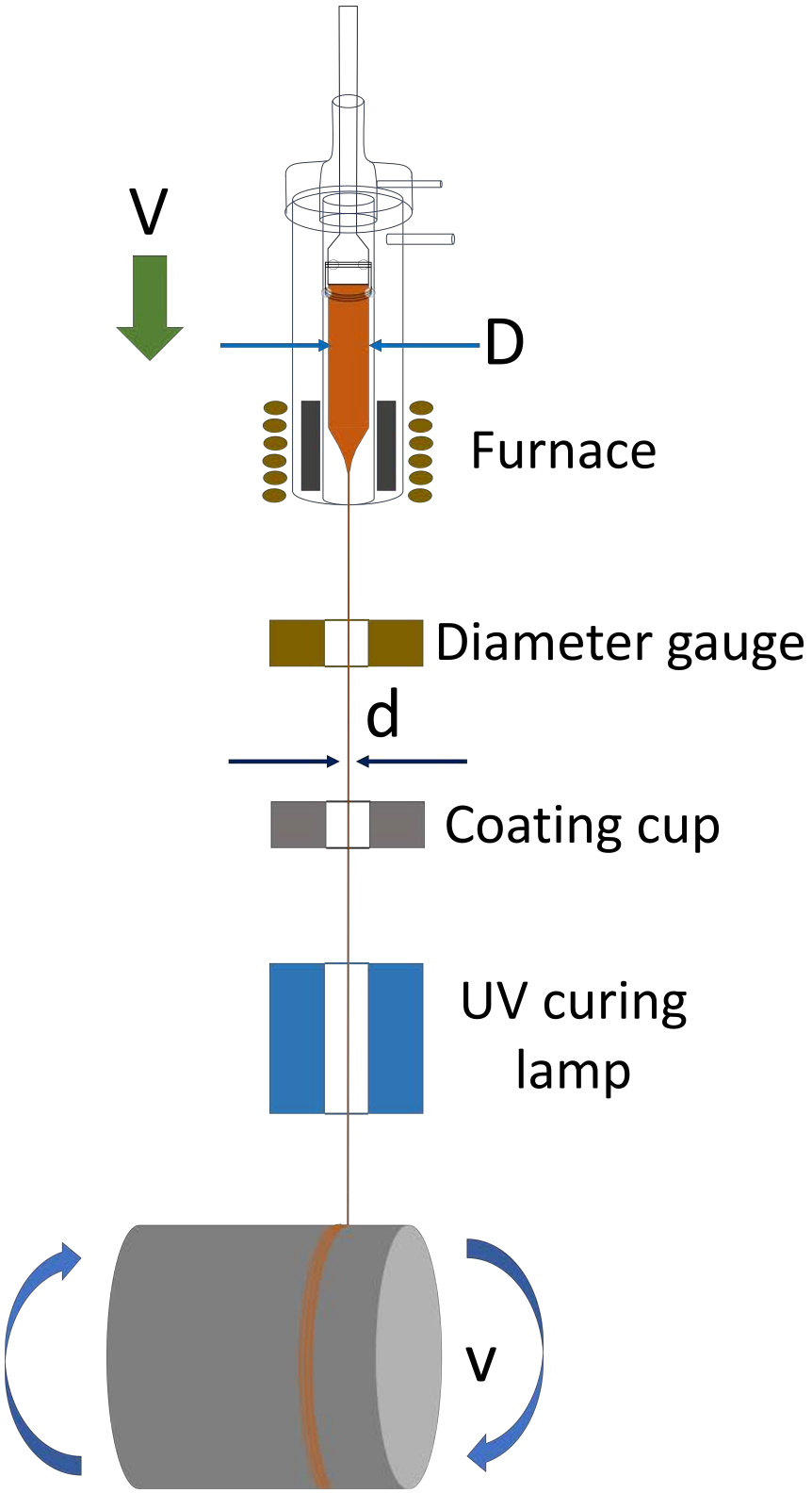

FIGURE 4.1: Novel Glass Group's fibre drawing tower schematic

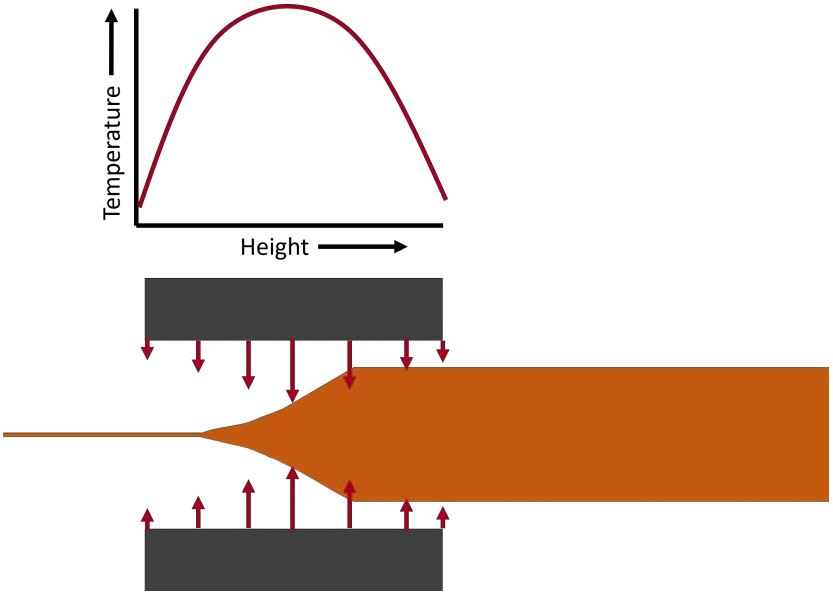

FIGURE 4.2: Thermal radiation towards the preform neck-down for fibre drawing

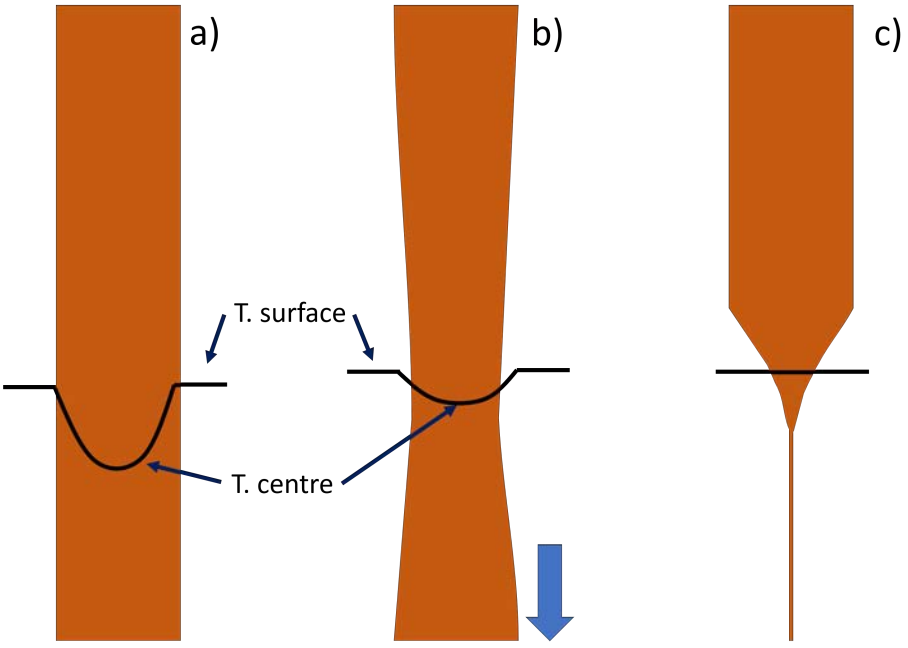

FIGURE 4.3: Temperature behavior between the surface and the centre temperatures of the preform where a) T. surface > T. centre, b) ΔT starts decreasing and preform starts to stretch downwards and c) ΔT $\sim$0 °C, complete neck-down profile

4.3 Novel Glass Group fibre drawing tower furnace for rod drawing

Compared to silica fibre fabrication that uses temperatures above 2000 °C to produce optical fibres [36], GLS-Se glasses need temperatures below 800 °C [5] to be soft enough to start the fibre drawing process. Therefore, in the Novel Glass Group a furnace was designed to be flexible enough to be modified depending on the preform composition and geometry [173], as seen in Fig. 4.4. It is composed of the following components:

1. Two vessels of glassware: made of silica, as it is resistant to the temperatures used for chalcogenide glass preforms, one part acts as a susceptor container and as separation between the preform and the susceptor, and the second part acts as a cap to seal and complete the glassware.
2. Carbon susceptor and RF coil:preform heat supplier, the RF frequencies interact with the carbon susceptor to heat it up, depending on the selected temperature is the power the RF coil supplies.
3. Thermocouple: monitors the temperature of the susceptor and controls the RF power.

Also, each part of glassware has an inlet for an argon flow to preserve the susceptor [174] and to produce a purged environment to prevent the reaction of the glass with the oxygen in the cleanroom [175].

The temperature profile of the susceptor (Fig. 4.5) defines the position where the preform needs to be set to develop an ideal neck-down profile [176]. For GLS-Se glass preforms, this temperature profile must be controllable and reliable as it is needed to heat up a short volume of glass, to avoid promoting crystallization in the nearby material, at a temperature high enough to soften the glass enabling it to be drawn into a fibre. Thus, an optimal GLS-Se optical fibre drawing process needs to take into account every single parameter such as temperature applied, susceptor temperature profile, time, volume of the glass, composition related viscosity, preform feed and drum speeds.

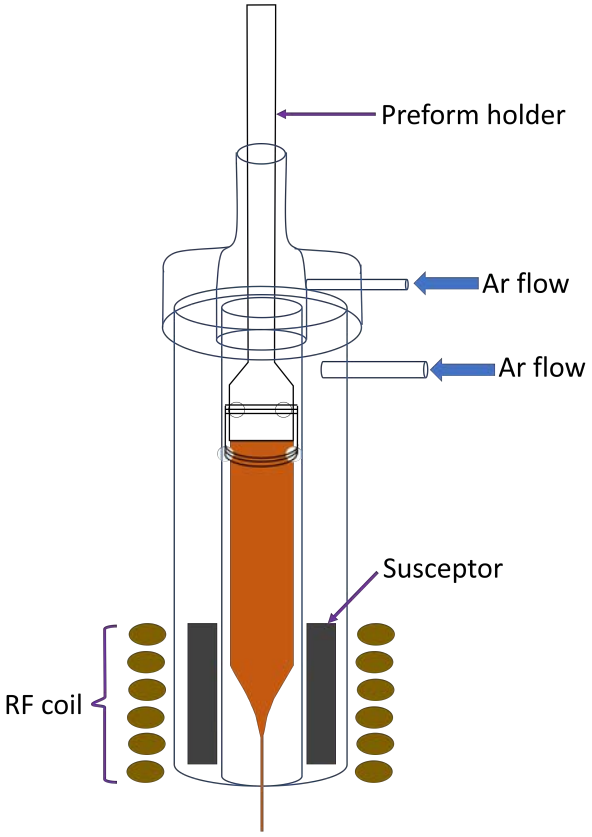

FIGURE 4.4: Diagram of the furnace used for rod drawing

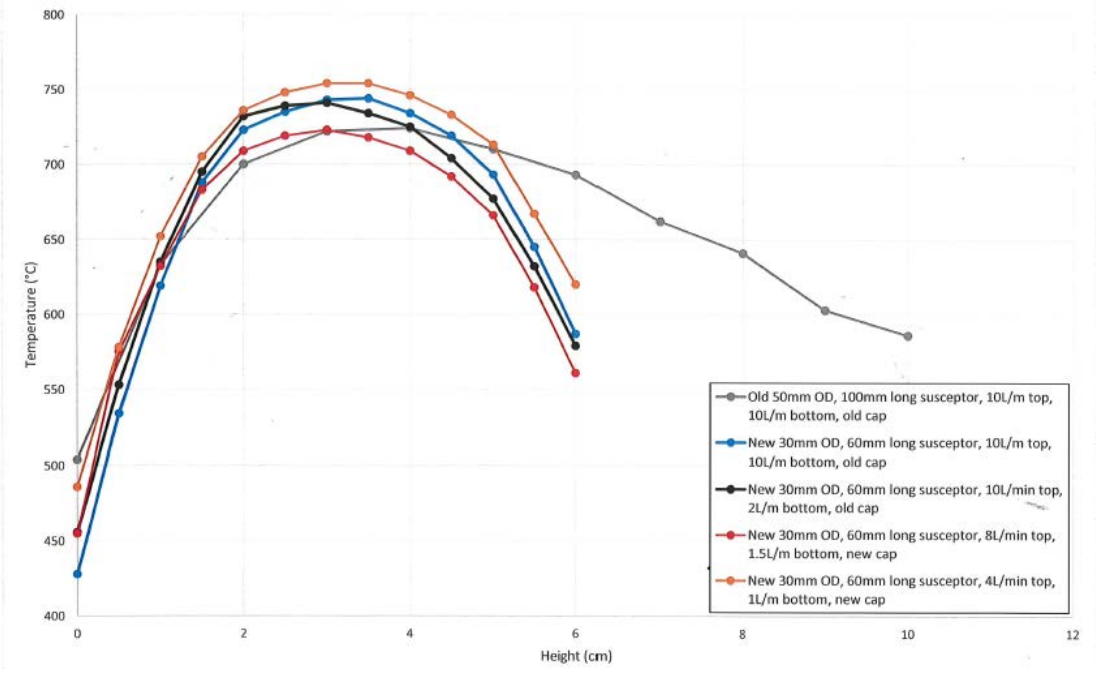

FIGURE 4.5: Temperature profile of the susceptor along its length, where the origin represents the bottom part closer to the furnace exit (profile registered by Bruno Moog at a set temperature of 800 °C)

4.4 GLS-Se optical fibre principles

The propagation of light through a waveguide is enabled by the reflection of light at the boundary between dielectric materials [177]. In a core-clad optical fibre these materials are defined by two glasses with different compositions and therefore different refractive indices (n), where the core presents a higher refractive index than the cladding surrounding it [36]. The basic principle of the guiding mechanism in an optical fibre is the total internal reflection (TIR), meaning that all incident light at the interface of the two materials is reflected back to the core with the same angle of incidence [178] as long as the angle of the incident light is bigger than the critical angle. If the incident light has an angle smaller than the critical angle, part of the light is refracted towards the cladding and represents a loss in the transmitted light in the core [179].

$$\theta_c = sin^{-1}\left(\frac{n_1}{n_2}\right); n_2 > n_1 \tag{4.2}$$

Equation 4.2 Critical angle of incidence for total internal reflection

Where θ_c is the critical angle of incidence, and n_2 and n_1 are the refractive indices of the core cladding respectively. The refractive indices also define the maximum angle of acceptance [180] of incoming light at the input of an optical fibre by means of the numerical aperture (NA) [181], as seen in Fig. 4.6.

$$\theta_a = sin^{-1}NA \tag{4.3}$$

Equation 4.3 Acceptance angle for an optical fibre

Where the numerical aperture is defined as:

$$NA = \sqrt{{n_2}^2 - {n_1}^2} \tag{4.4}$$

Equation 4.4 Numerical aperture for a structured optical fibre

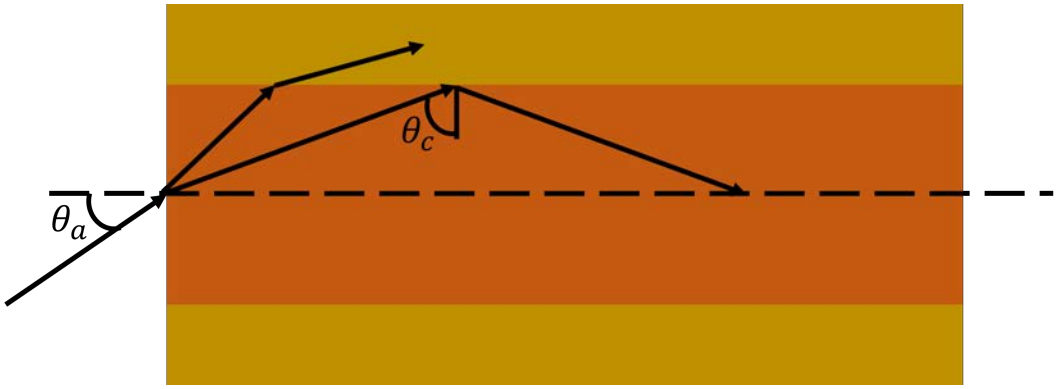

FIGURE 4.6: Angle of acceptance and critical angle for total internal reflection

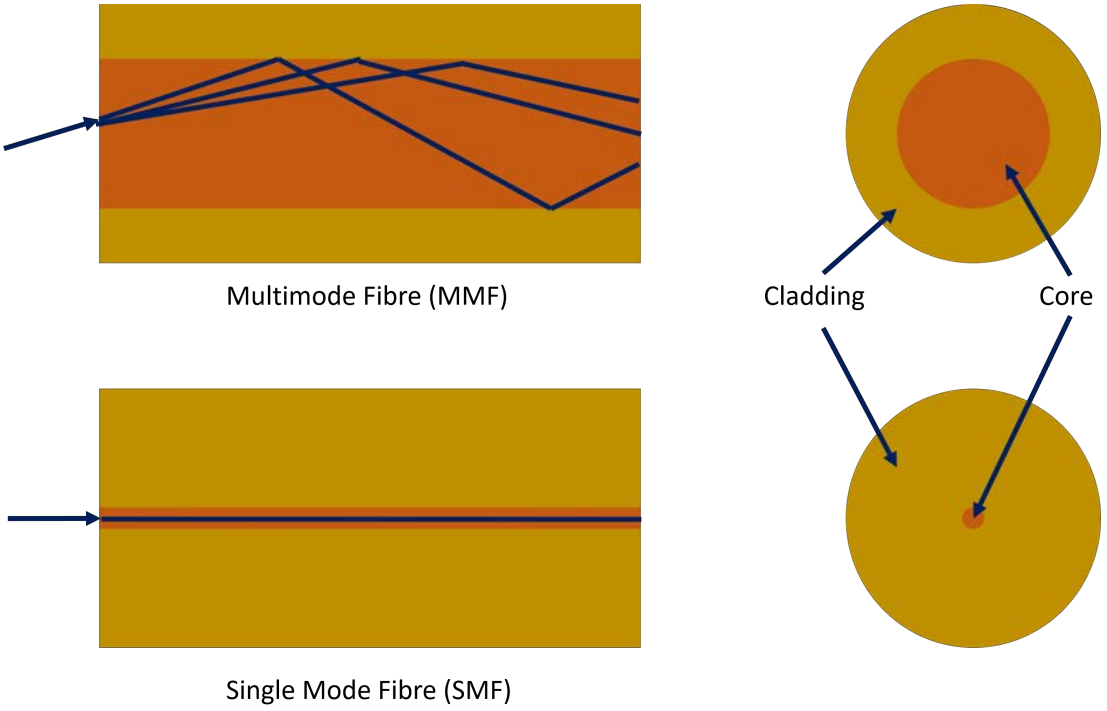

FIGURE 4.7: MMF presents a bigger core diameter compared to a SMF

In an optical fibre the core size is an essential criterion that aids defining the guided modes supported by the structured waveguide, varying between multimode or single mode [182], as seen in Fig. 4.7, and defined by means of the V number parameter [3].

$$V = \frac{2\pi a}{\lambda} NA \tag{4.5}$$

Equation 4.5 V number parameter to determine the mode operation

Where a is the radius of the core and λ is the propagating wavelength. By varying the refractive index, the diameter of the core and the operation wavelength, the modal behavior can be determined. The initial considerations to decide the compositions ultimately used for manufacturing of a structured preform and optical fibre were defined by the previous studies of GLS-Se compositions [54] where the compositions correspond to a GLS-Se glasses with a 35 and 30 mol%, for the core and the cladding respectively (Fig. 4.8), of Ga_2Se_3. In Fig. 4.8 it can be seen that the signal intensity increases until it produces a knee, when the signal drops down, at this point is where the critical angle is obtained and then the refractive index is extracted, as described in chapter 2. As the closer the value of refractive indices the lower the value of NA and therefore a V number value closer to a single mode operation ($V \leq 2.405$) [183]. Preparation of the samples for the extraction of refractive index measurements is discussed in chapter 5.

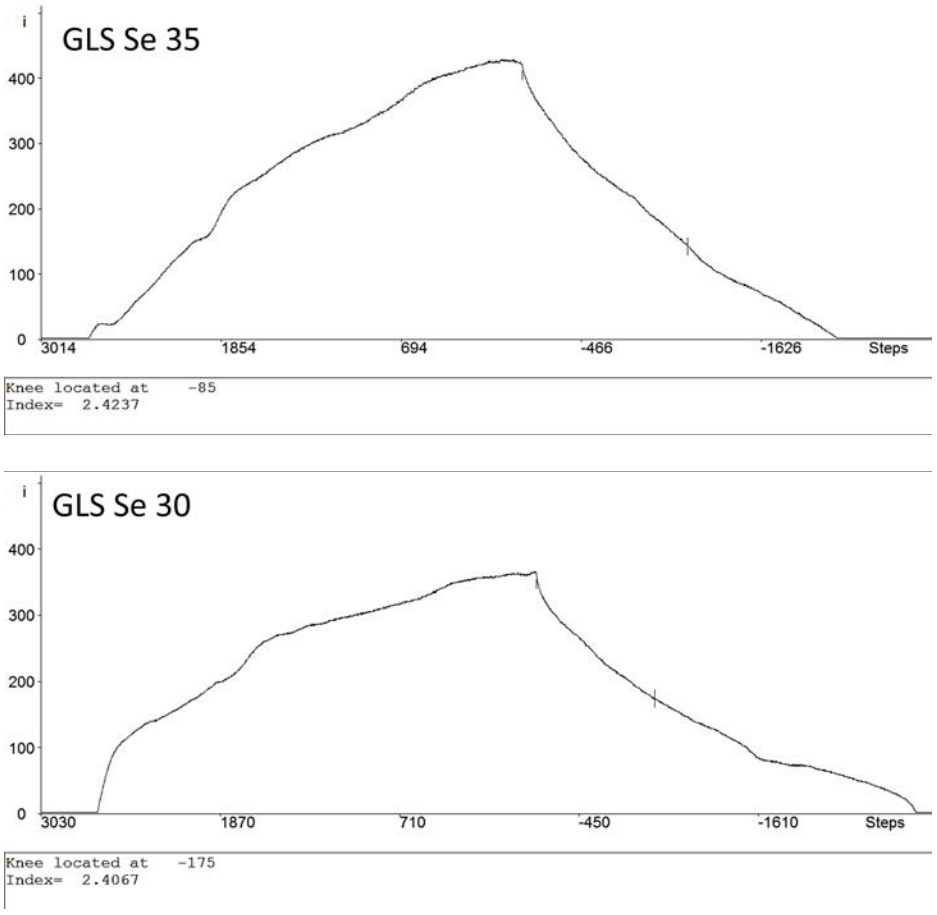

FIGURE 4.8: Examples of refractive index measurements with the Metricon®at 1550 nm for compositions with a difference of 5 mol% in Ga_2Se_3 content between samples for a structured preform fabrication

TABLE 4.1: Refractive index difference and fibre parameters at 1550 nm for GLS-Se compositions

Composition	Refractive index (n)	±	Samples measured	NA	$\theta_c(°)$	$\theta_a(°)$
GLS-Se 35	2.42	0.01	LD1929, LD1960, LD1961	0.31 ± 0.1	82.62 ± 2	18.08 ± 6
GLS-Se 30	2.40		LD1934, LD1962, LD1964			

The refractive indices values in the measurements are consistent between samples of the same composition (Table 4.1), demonstrating the repeatability of the established melt-quenching process, as described in chapter 2, for manufacturing GLS-Se glasses for multiple purposes. Therefore, this validates the reproducibility of production of bulk samples for the fabrication of preforms, eliminating with this any doubt that could have arisen about any possible mismatch between batches of each new glass manufactured.

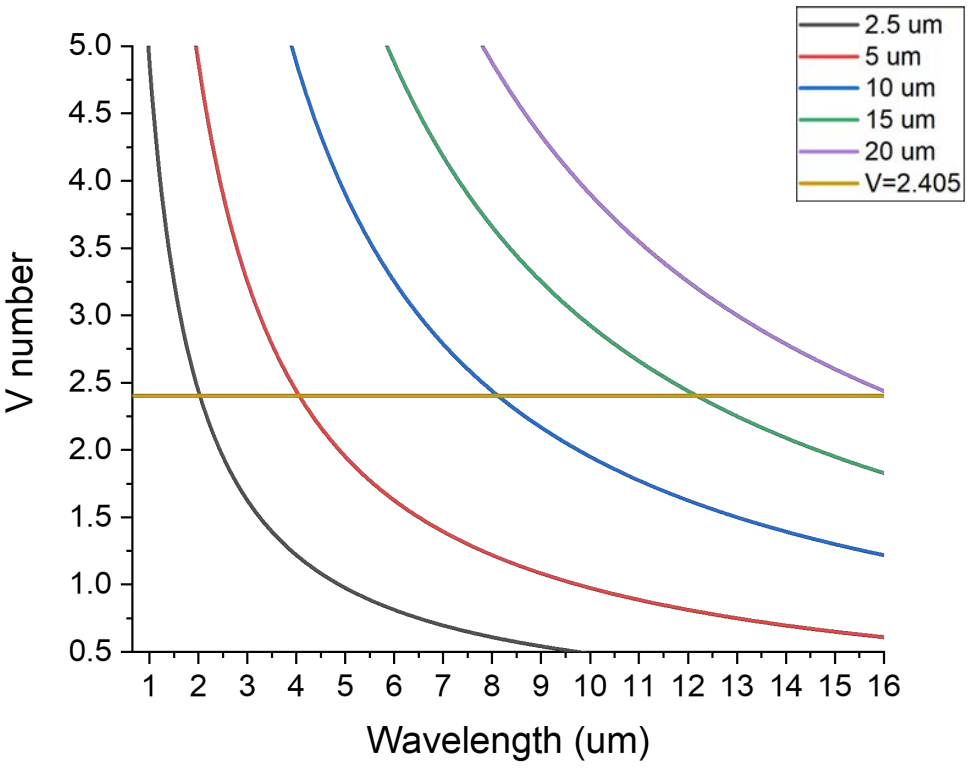

FIGURE 4.9: V number with a NA=0.31 for a structured fibre of GLS-Se glass compositions with 35 mol% and 30 mol% of Ga_2Se_3, for the core and cladding respectively, the different line colours represent different sizes of core radius, where V=2.405 is the cut off for single mode operation

As seen in Fig. 4.9 and Table 4.2 GLS-Se glasses have a clear advantage for single mode operation for mid and far IR wavelengths by virtue of their wide transmission

window [34]. The challenge resides in adequately exploiting their refractive indices and controlling the diameter during the preform fabrication.

TABLE 4.2: Cut off wavelength for a single mode operation dependent on the core radius

Core radius (μm)	λ cut-off (μm)
2.5	2.03
5	4.06
10	8.11
15	12.17
20	16.22

4.5 Mode propagation in a structured GLS-Se optical fibre

Optical fibres, as seen in the previous section, can support one or more modes of propagation depending on their intrinsic characteristics (i.e. refractive index, core diameter, etc.). The fibre geometry controls the set of electric field distributions of light that can propagate in the optical fibre [3]. In other words, the fibre constitution and optical characteristics establish the modes of propagation allowed in it. After calculating the V number parameter to define the operation of the optical fibre, as multimode or single mode, the number of modes M that can propagate in a multimode fibre can be defined as:

$$M = \frac{V^2}{2} \tag{4.6}$$

Equation 4.6 Number of modes of propagation [184]

As seen in Figs. 4.10 and 4.11, with the help of COMSOL®, the characteristics of GLS-Se glasses (Table 4.1) influence the multimode operation. These figures demonstrate that the core radius is a crucial parameter in the number of modes that are allowed to propagate through the core. These figures illustrate the challenge, which is obtaining a small core, that needs to be overcome in order to achieve single mode fibre fabrication, as this work is only focused on the feasibility of structured fibre fabrication.

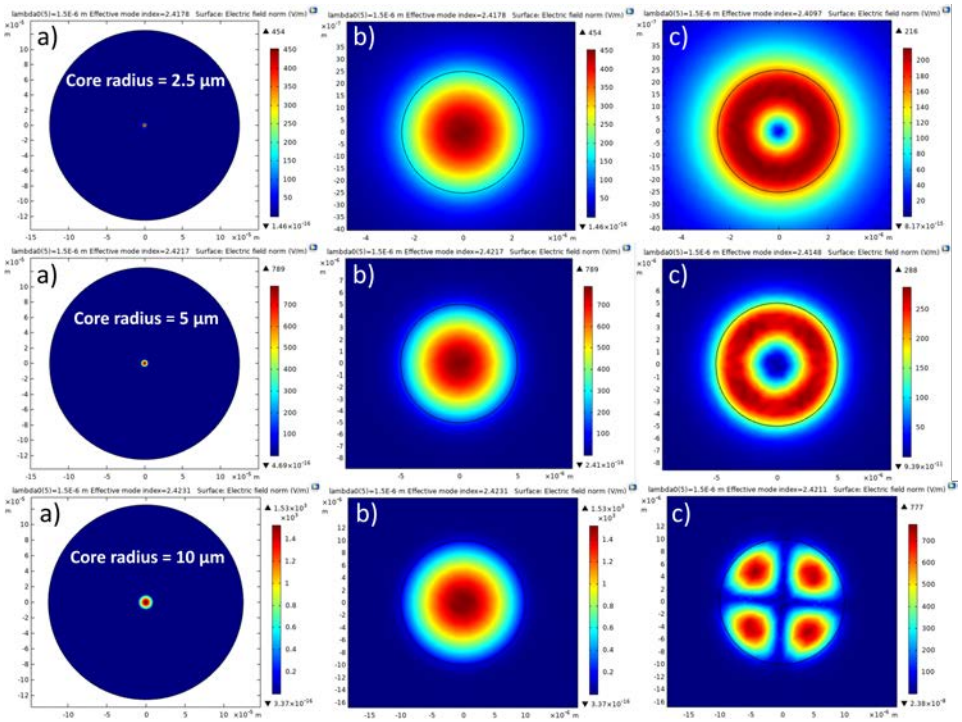

FIGURE 4.10: Mode behavior for different core radius at 1550 nm, where a) is the cross-sectional area of the fibre, b) is the fundamental mode and c) a higher order mode for GLS-Se optical fibres

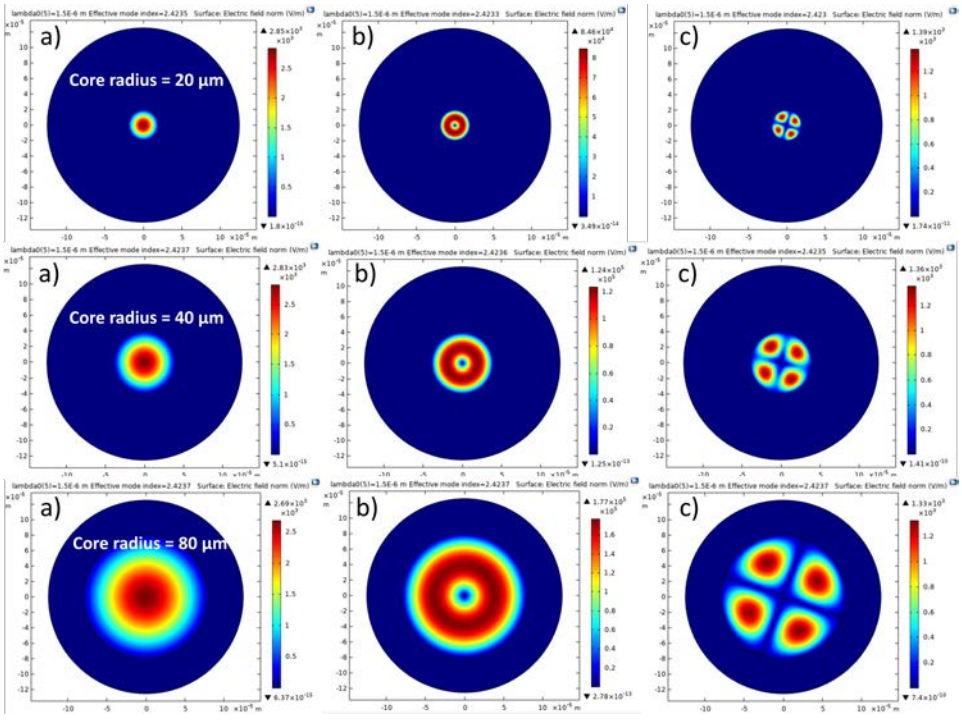

FIGURE 4.11: Mode behavior for different big core radius at 1550nm, where a) is the cross-sectional area of the fibre with the fundamental mode, b) and c) are higher order modes for GLS-Se optical fibres

4.6 RE doped GLS-Se glasses suitable for possible optical fibre fabrication

Research has established that SiO_2 is not an ideal host for RE ions as they tend to form clusters in the silica network [173]. On the other hand, a limited set of the chalcogenide glasses can dissolve sufficient amounts of RE ions making them suitable for optical amplifier and laser applications [185–187]. Some interesting RE transitions are those of Pr^{3+}, Dy^{3+} and Tb^{3+}, as these RE ions possess transitions in the span of 3-12 μm [33] and they can also be potentially used as amplifiers at 1.3 μm [151]. Despite the fact that some chalcogenide glasses are suitable for RE hosting, surpassing a critical concentration can lead to quenching [188]. One explored RE ion in GLS-Se glasses has been Nd^{3+}, where concentrations up to 5 mol% of Nd_2S_3 have been achieved (Fig. 4.12) while maintaining the thermal properties of the GLS-Se glass network [6], as Ga is a strong acceptor of RE ions [189]. This previous study opens the door for future possible structured doped core preforms fabrication, based on GLS-Se glasses as a proper host exploiting its low phonon energy and its high solubility to further study far IR wavelength absorptions and emissions.

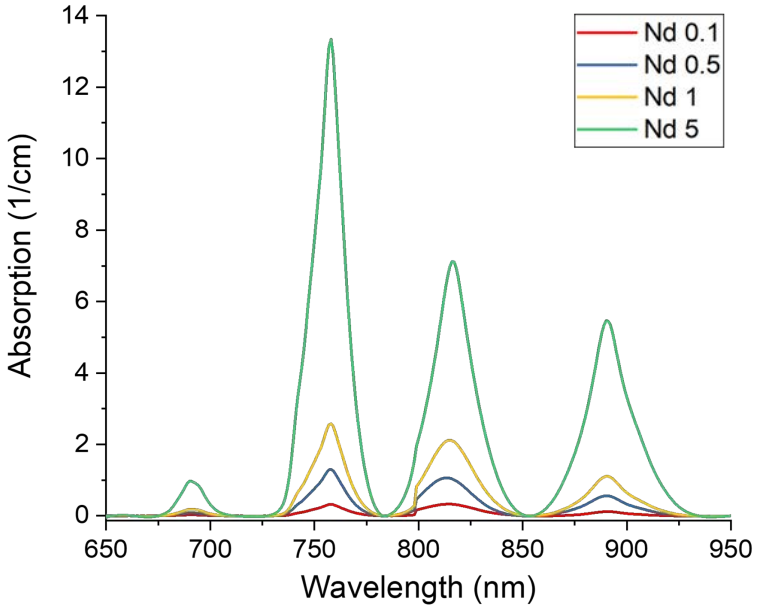

FIGURE 4.12: Spectral characterization of GLS-Se glass doped with different concentrations of Nd_2S_3 [6] (study led by Dr Andrea Ravagli, reproduced with permission as co-author)

4.7 Examples of possible applications for a structured GLS-Se optical fibre

In the past, promising results for GLS optical fibres have been obtained at power handling levels up to 5W at 1064 nm into a 150 μm fibre core, with no decrease in transmission. In addition, due to their high transition temperature they are suitable for high power lasers [135, 190]. Optical sensing is one of the most common uses for chalcogenide optical fibres, based on systems that generally expose the core of the fibre to an environment to be sensed and monitored by which the transmission is altered after the evanescent wave interacts with the medium. This technique is known as fibre evanescent wave spectroscopy [191], helpful in monitoring chemical species [192]. More applications include supercontinuum generation, which has also been exhibited between the span 2-13 μm in small core $AsSe$ fibres [193], laser performance with a low threshold operation and a decent slope efficiency of 17% [194], more has to be achieved since the first demonstration of GLS glass laser operation [150].

4.8 Conclusion

GLS-Se glasses are suitable for optical fibre production, if they maintain their optical properties. Passive applications could be suitable as a waveguide to transmit light, as the relatively high refractive index of chalcogenide glasses inhibits a proper guidance through the glass of the optical fibre. For active applications, RE doped GLS-Se glasses have been produced and tested with promising results, capable of demonstrating emissions in these chalcogenide glasses. More studies with different compositions, controlled core diameters for MMF or SMF, and different RE ions doping need to be carried out. GLS-Se optical fibres need to be fabricated and characterized in order to determine their viability as waveguides and to improve the process steps accordingly. This work focuses in passive GLS-Se glass compositions, as they have never been fabricated in an optical fibre form before.

Chapter 5

GLS-Se glass billets fabrication and preparation for extrusion

5.1 Introduction

In this work, the first step towards the fabrication of GLS-Se optical fibres is the manufacturing of glass billets to obtain between 20 or 23 cubic centimetres of volume needed for the extrusion apparatus described in chapter 3. These billets need to comply with the optical, thermal, and mechanical characteristics previously demonstrated [5] by the GLS-Se glass family, that is, there should be no change in the glass properties during the extrusion process. The importance behind this first step resides in ensuring the repeatability in production according to cleanroom capabilities while only adapting the geometry and volume of each of the samples.

It is important to understand that a key point in a reliable process is to trust the previous research. As thousands of hours, equipment and human efforts have been invested in developing a trustworthy GLS-Se glass fabrication process. It is vital to understand every step taken in previous works [1] to have a solid base for further experiments. Thus, in this work no modification has taken place in the melt quenching process throughout this research as this has already been well established.

By not modifying the melt quenching process, the research efforts can then be directed towards the GLS-Se optical fibre fabrication (i.e. extrusion or fibre drawing). In order to be able to produce a successful melt quenching technique for billet fabrication, several hours of training and resources were invested to ensure that we can obtain amorphous transparent glass samples from every batch of raw materials.

Preliminary results were used to understand the intrinsic characteristics of the glass samples [34] in order to start planning the best possible approach for preform fabrication. These initial results and experiments aimed to explore every possible variable or parameter that needed to be considered and allowed for the modification of the glass samples through the preform and optical fibre fabrication processes, which might affect the already proven intrinsic characteristics of the GLS-Se glass family. Therefore, this chapter underlines the current glass melting capabilities within the Novel Glass Group, and the results that defined the guideline to have a successful melt quenching process by acquiring data to see the possibility of further improvements for preform fabrication, if needed.

5.2 Glass melting

The melt quenching technique is fully described in chapter 2, as reported previously [54]. The first attempts were performed to understand the process and to ensure the repeatability of the glass fabrication. Steps include the raw materials batching (Fig. 5.1), preparing the horizontal furnace, transferring the batch to carbon crucibles (Fig. 5.2) and the melt quenching technique itself for GLS-Se glass production, where the Ar purge flow is applied to eliminate any by-product or volatile impurities from the raw materials [190], (Figs. 5.3 - 5.7). As a new horizontal furnace was installed and the availability to melt glass needed to be proven, all these steps were performed and recorded in said furnace. Previous studies [195] describe that the melting temperatures for the materials are as follows: 1090 °C for Ga_2S_3, 1005-1010 °C for Ga_2Se_3 and 2100-2150 °C for La_2S_3. The melt quenching technique is carried out at 1150 °C where this temperature is enough to melt two of the raw materials, and once melted they act as a solvent for La_2S_3 [196] mixing it by effect of the convection currents naturally occurring in the crucibles during the process [197].

FIGURE 5.1: Example of raw materials batching for GLS-Se compositions

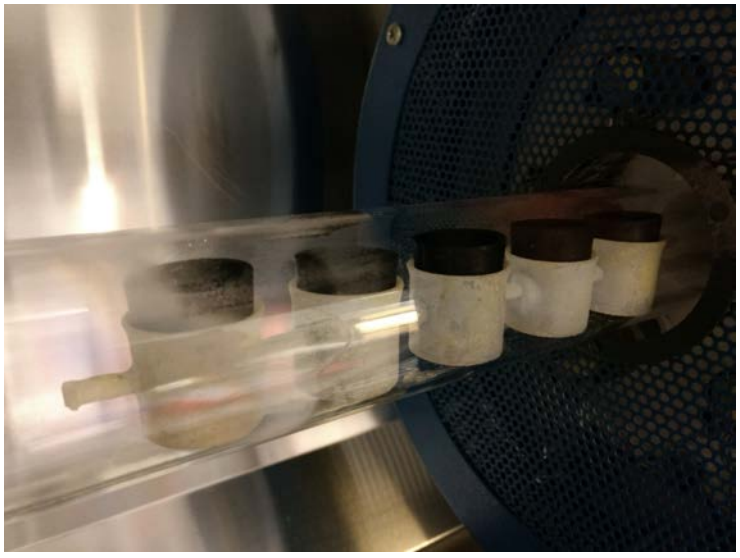

FIGURE 5.2: Raw materials in carbon crucibles positioned in the horizontal furnace before the melting

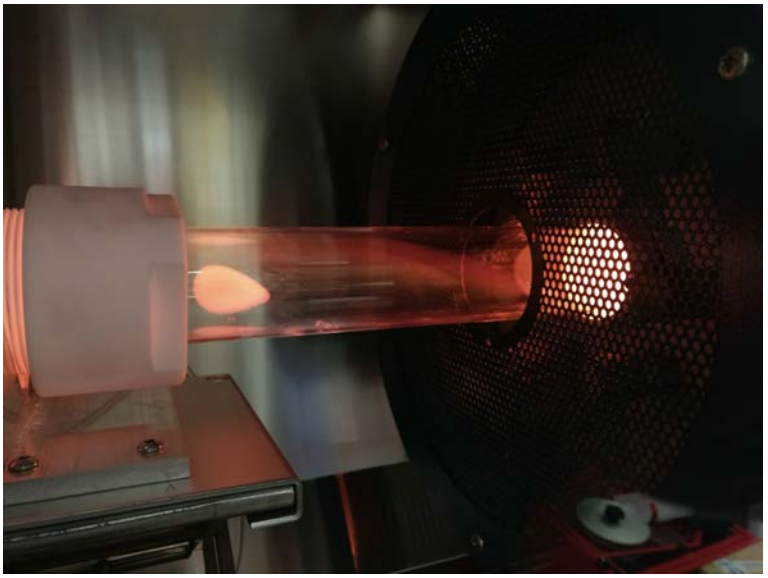

FIGURE 5.3: Left side of the furnace where the Ar purge flow starts to be applied

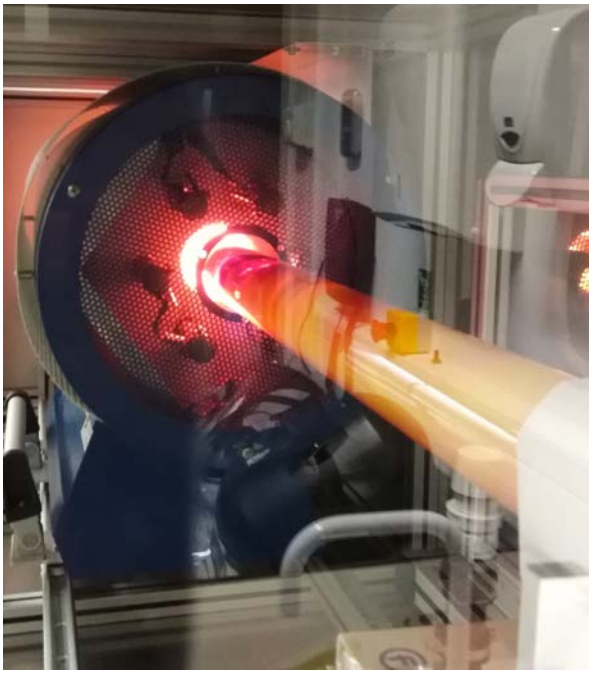

FIGURE 5.4: Right side of the furnace where the volatile impurities are carried by the purge towards the extraction

FIGURE 5.5: Glass vessels to filter any volatile particle from the melt before the extraction

FIGURE 5.6: Crucibles after the furnace was removed to begin the quenching step

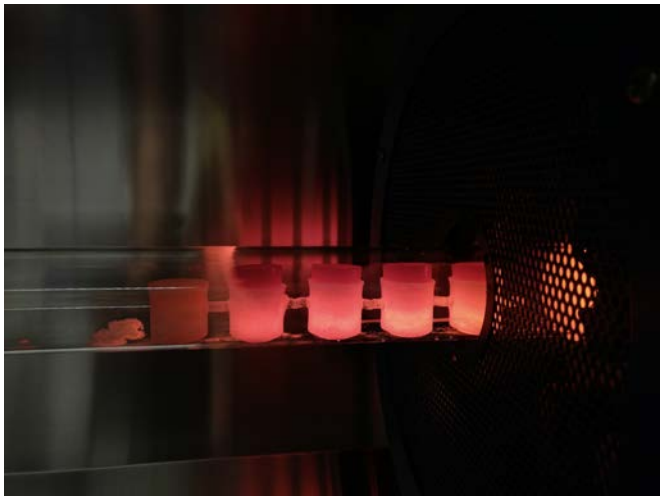

FIGURE 5.7: Crucibles cooling down, brightness fades away as the temperature goes down

Figs. 5.8 and 5.9 highlight the importance of placing the crucibles in the correct hot zone of the furnace. The wrong positioning of the crucibles does not allow the correct melting of the raw materials as the temperature needed is never reached, plus the quenching rate is slower. Therefore, one common problem in the inability to produce glass samples is not having a temperature profile of the furnace in use, fortunately this can be easily overcome as seen in Fig. 5.10.

FIGURE 5.8: Fully crystallized sample

FIGURE 5.9: Crystallized samples, not usable for further processes

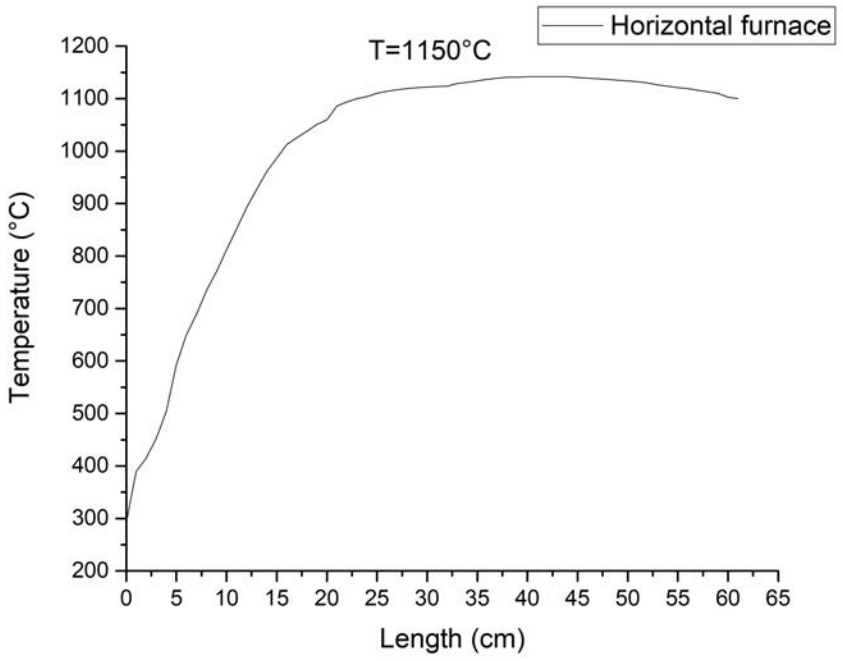

FIGURE 5.10: Horizontal furnace temperature profile with a uniform hot zone of 45cm

After obtaining the temperature profile, the next batching (20 g of raw materials per crucible) was placed in the hottest zone of the furnace. This action as well as increasing the Ar flow from 300 cc to 500 cc after the furnace was removed favoured the quenching rate, and as a result amorphous glass samples were produced as seen in Figs. 5.11 and 5.12. These samples were used for initial thermal analysis and refractive index measurements (as seen in chapter 4) to corroborate that the steps were correctly followed by showing results in accordance with previous studies, including the ∼2% of mass loss during the melting [54].

FIGURE 5.11: GLS-Se glass samples, after a successful melt quenching

FIGURE 5.12: Transparent GLS-Se sample of 20 g

5.3 Glass billets production for extrusion

As seen in chapter 3 the current capabilities of the Novel Glass Group include an extrusion apparatus comprising a billet container for samples of up to 30 mm in diameter. It is used to fabricate glass billets in accordance with said dimensions, considering also a maximum of 23 cubic centimetres in volume, as seen in previous sections of this chapter. After a meticulous selection, the GAZ 3 cylindrical crucibles model from Sigradur®G was chosen as it complies with the diameter specifications required in a high quality carbon. To fit in the horizontal furnace, each crucible was cut 3 mm from the top and a new silica crucible holder was fabricated to keep each crucible in a vertical position to avoid spills (Fig. 5.13).

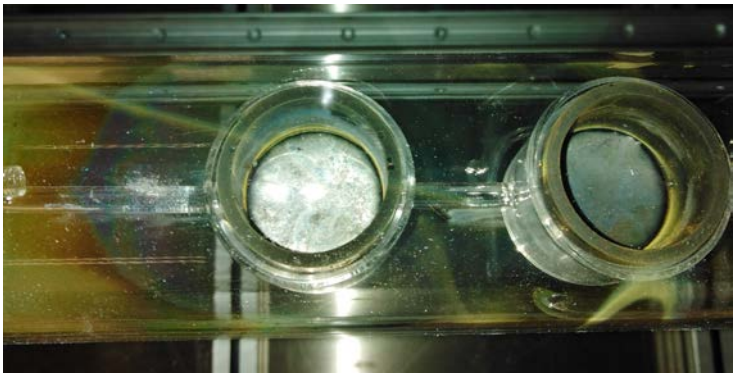

FIGURE 5.13: Glass billet in the crucible of 30 mm in diameter after the quenching was performed

Even though the use of carbon crucibles might infer some possible contamination to the glass samples, chapter 2 and previous studies [54] show that that the spectral region between 4-8 μm does not show the characteristic carbon absorption peaks [65] most likely due to the inertness of the vitrious carbon used for the crucibles. This validates the use of this type of crucibles for the glass melts. These crucibles have a maximum capacity of 30 g of raw materials and glass billets produced with this mass of materials have a thickness of around 8 mm (Fig. 5.14). For a core-clad extruded preform (i.e. using two different glass compositions) thicker billets are needed. Therefore, the best option to obtain bigger billet volumes is a remelt process. This comprises using two, or more, already produced glass billets (Fig. 5.15) and melting them together or producing a glass ingot (>170 g) and using it for the billets (Figs. 5.16). For this latter option the ingot must be cut (Fig. 5.17) and cleaned in an ultrasonic bath (Fig. 5.18) to remove any particle that might have been introduced. During this process isopropanol is used as solvent as it does not react with the glass [198].

FIGURE 5.14: GLS-Se glass billet using the GAZ 3 crucibles and 30 g of raw materials

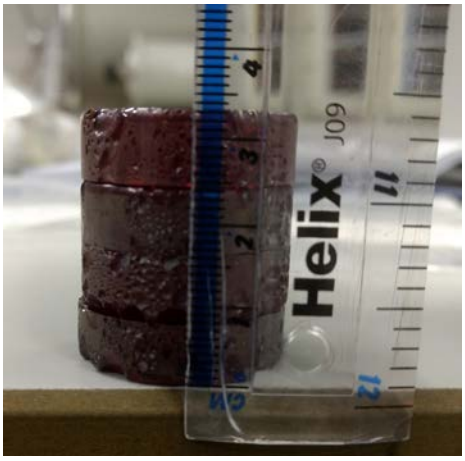

FIGURE 5.15: GLS-Se glass samples stacked, with a thickness around 8 mm each

FIGURE 5.16: GLS-Se glass ingot for billets remelt

FIGURE 5.17: Pieces of cut-glass ingot

FIGURE 5.18: Ingot pieces ready for ultrasonic bath

Each remelt is performed following the same steps as the melt quenching technique described in previous sections, used for the raw materials to ensure that the nature of the glasses and the capabilities of the equipment are maintained. As before, the mass loss is around 1-2% after the remelt is completed. As seen in Fig. 5.19, thicker billets are successfully obtained for extrusion. One throwback of the remelt that needs further investigation is the effect of the loss mass at each remelt, as the glass could be pushed to its glass forming region, and also a different cooling rate might be needed to avoid the crystals promotion.

FIGURE 5.19: Thicker GLS-Se glass billet for co-extrusion

5.4 Billets and samples polishing

After annealing the samples, further steps consist of using the lapping and polishing plates (Fig.5.20) to smooth the end faces for further measurements and to remove any carbon residual. As GLS-Se glasses could react with water, ethanediol is used as a lubricant. Three different sizes of alumina powder are used (9 μm, 1 μm and 0.3 μm) to give the samples an optical finish. The jig must be adapted depending on the size of the glass samples or billets, this adds an extra step during the polishing process and is crucial as any wrong positioning or pressure applied can damaged the sample or even the lapping plate. Before the lapping and polishing steps samples need to be cut to flatten the end faces (Fig. 5.21), as this helps reducing the consumed time and avoids wasting material (i.e. alumina powder).

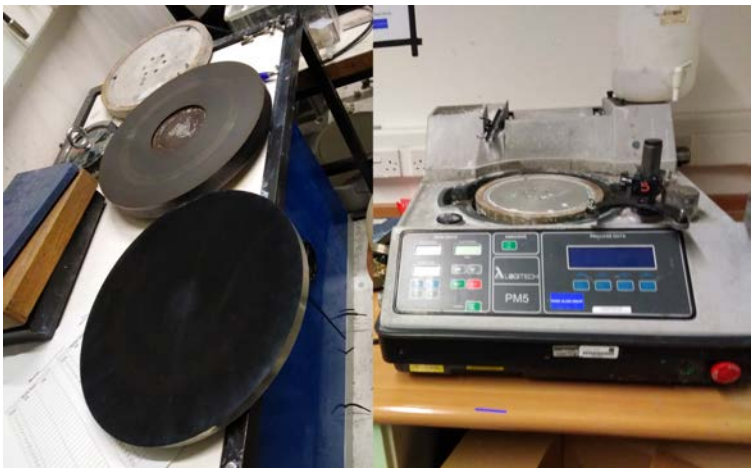

FIGURE 5.20: Lapping and polishing plates for the PM5 system

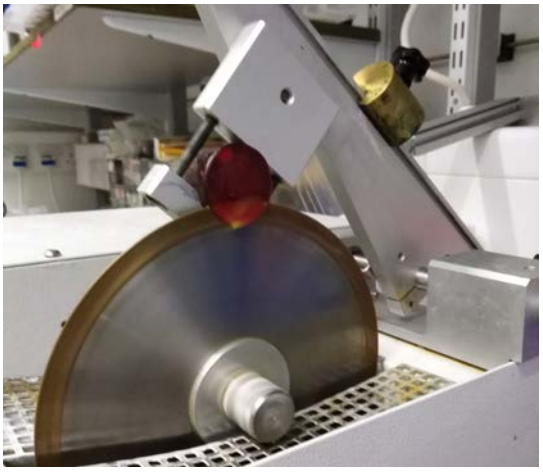

FIGURE 5.21: Billet being cut by a diamond blade

The conditions for lapping and polishing might change depending on the glass compositions; the quality of the final optical finish depends on the optimization of the material removal rate and surface defects can be reduced by controlling the physical actions [199]. As a mechanical process, experience has showed that when the size of the alumina particles is reduced, the applied pressure must be increased. Although there is no way to quantify the pressure in the existing equipment, further studies could be established to develop the best possible parameters for lapping and polishing GLS-Se glass samples to avoid any possible scattering from the surface quality [200]. Current lapping and polishing expertise are enough for the initial measurements and experiments, as possible surface roughness does not affect the glass properties considered in this work [201].

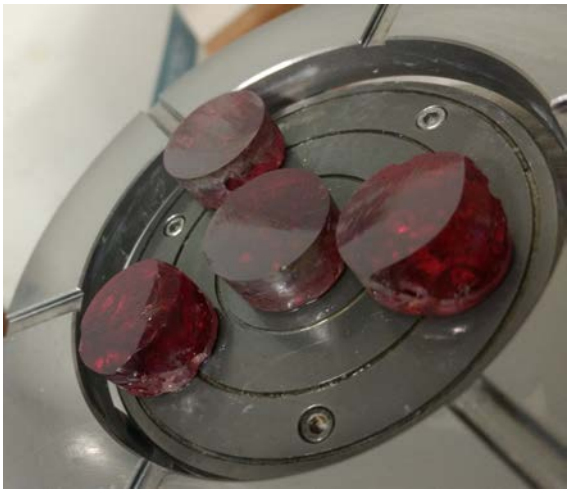

FIGURE 5.22: GLS-Se 20 g samples polished simultaneously to save resources

FIGURE 5.23: GLS-Se sample after optical finish ready for measurements. *Note: the bubbles are only in the bottom part of the billets*

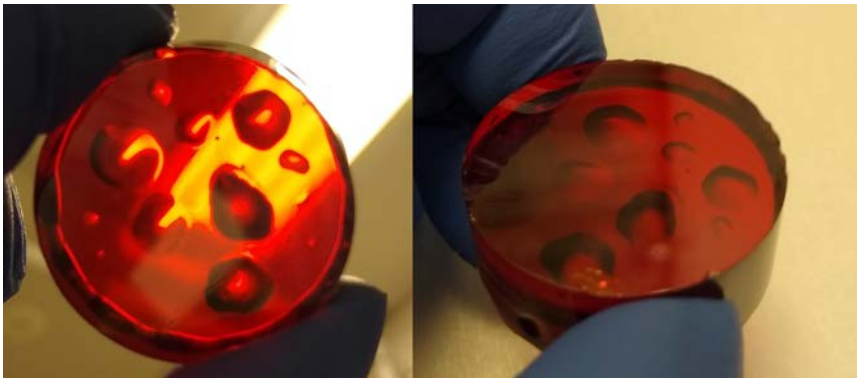

FIGURE 5.24: GLS-Se billets for extrusion after polishing both faces

Initial extrusion experiments in this work did not consider polishing the cylindrical surface of the billets, as it was previously thought that this would not affect the extrusion or fibre drawing processes. As explained in chapters 6 and 7 carbon residuals were contained within the preform core-clad interface after the co-extrusion process, but the effects were only seen after the fibre drawing was performed. Carbon residuals affected the performance of both processes, diminishing with it the quality of the preforms and fibres. This confirmed the need for polishing the cylindrical surface to enhance the glass quality and facilitate the processes. No equipment was in existence to polish the billet cylindrical surface so with the help of the mechanical workshop, a two piece stainless steel billet holder (Fig. 5.25) was produced to use an already available lathe.

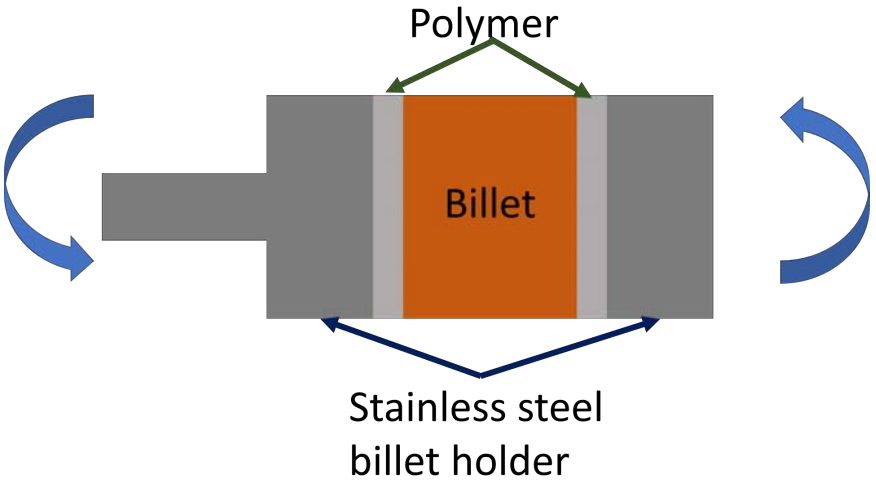

FIGURE 5.25: Billet holder to polish cylindrical surface, the polymer prevents scratching the end faces

Each billet cylindrical surface was polished using diamond films from Thorlabs®up to a 1 μm finish. As this had not been performed before all the cylindrical surface polishing was performed manually, this was problematic for the user as the surface gets hot by friction [202]. Finding a better way to do it or developing the proper equipment for this would require further studies and efforts. Polishing the end faces and cylindrical surface of each billet ensures that any possible carbon deposition from the crucibles is eliminated, which avoids any induced crystallization as a result of deliberately added heterogeneous nuclei [55].

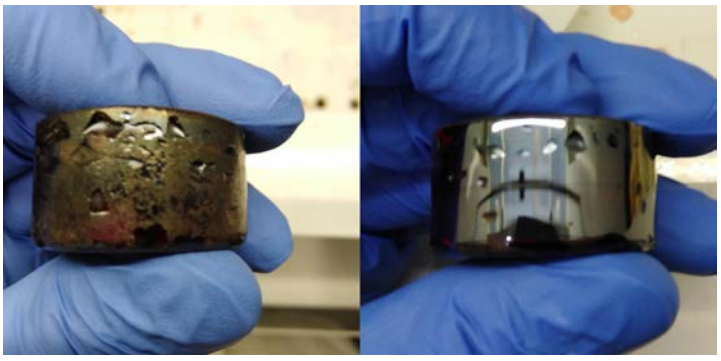

FIGURE 5.26: Polished cylindrical surface of a billet

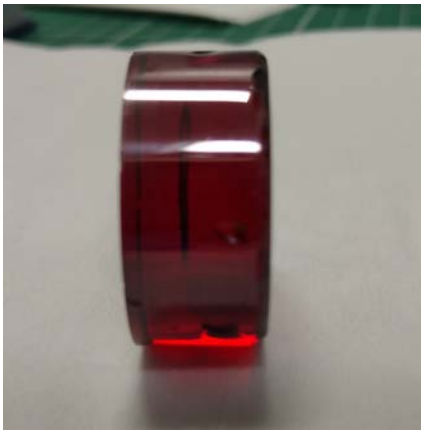

FIGURE 5.27: Billet cylindrical surfaces can be polished for different thicknesses

5.5 Billet initial thermal and mechanical analysis

For initial glass melting trials and measurements (chapter 4) only two compositions were considered: GLS-Se with 30 mol% and 35 mol% of Ga_2Se_3. This

was firstly to ensure that the glass was produced according to specifications and that the characteristics were maintained before further processes. As described in chapter 2, one way to ensure that the glass was produced according to previous studies [5] and that the quality was maintained was for the glass samples to undergo a differential thermal analysis (DTA) and a thermomechanical analysis (TMA). These characteristic temperatures are a good indication of batch to batch uniformity for the glass. Full details about the exact values obtained for the thermal and mechanical analysis are disclosed in chapter 6. For the DTA (Fig. 5.28) samples between 10-20 mg were placed in the Perkin Elmer Diamond TG-DTA after the annealing process. Comparison between previous studies [54] under the same conditions (i.e. raw materials used) show a maximum variation of 1% between reported values and the DTA values showed in this work. This helps to confirm that the glass samples are melted accordingly, and that the thermal characteristics prevail. As the billet production needs a remelt, further studies need to confirm if at a certain amount of remelts (taking into account the time of remelt) the thermal and mechanical characteristics are modified and to quantify them, this to avoid any structural change and to assure that the characteristics of the glasses are maintained at all time.

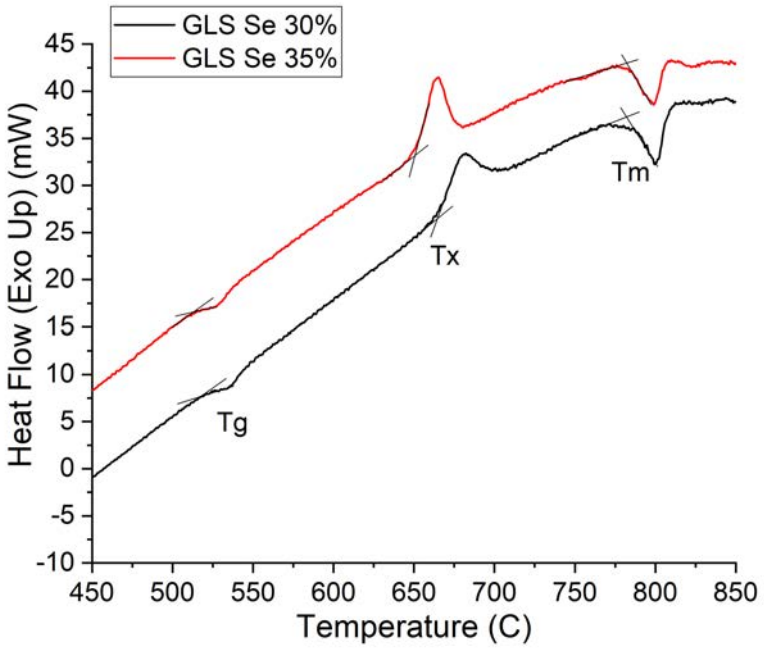

FIGURE 5.28: Example of a DTA performed for two different GLS-Se glass compositions

For the viscosity curves a three-point bending TMA was performed. A Perkin Elmer Diamond TMA was used. Samples were cut with a length of 7 mm, a thickness of 1 mm and 4 mm width. The ISO 7884-4 standard [80] was applied to obtain the viscosity curve of each sample, where a tip of a probe was placed perpendicularly on the surface of the sample at the centre of the longest edge, a load of 100 mN was used to press the sample against the stage, and then the temperature was incremented at a rate of 10 °C/min up to 950 °C (Fig. 5.29). After using the standard ISO 7887-4 the viscosity data was fitted to the Vogel–Fulcher–Tammann equation [203]:

$$log(\eta) = k + \frac{a}{T - b} \tag{5.1}$$

Equation 5.1 VFT equation to fit the viscosity

Where T is the temperature of the sample, k, a and b are fitting parameters. The curves were plotted from the transition temperature according to the DTA to 950 °C (Fig. 30). The softening point range is in accordance with previous studies [5] and demonstrates in Chapter 7 that the fibre drawing temperature might vary according to composition and preform quality.

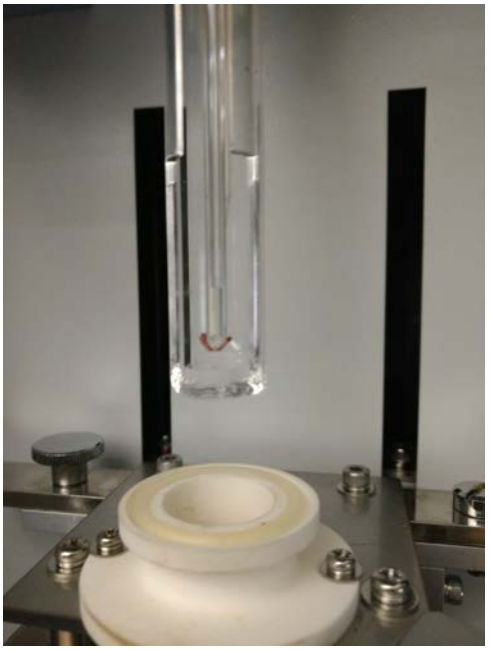

FIGURE 5.29: GLS-Se sample after the TMA

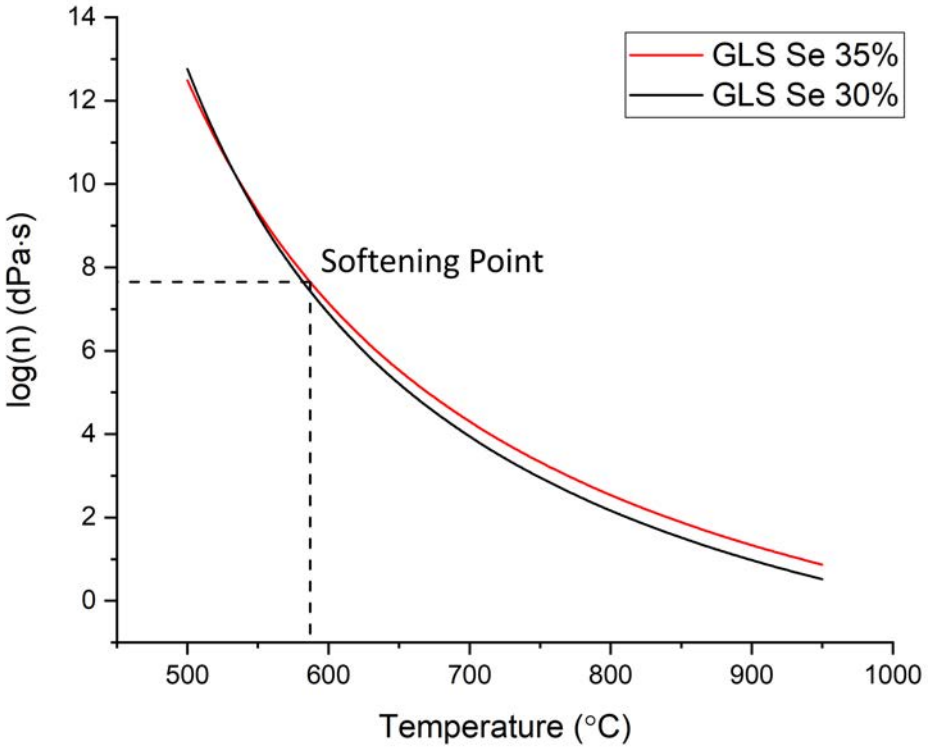

FIGURE 5.30: Initial TMA of GLS-Se glass samples

For fibre drawing and to avoid crystallization, a temperature below the T_x is preferable. However, another variable to take into account in the processing at temperature of GLS-Se glass compositions is time. Time is a crucial factor as a long exposure to a heat source even if is below the T_x can lead the sample to crystallize. In the extrusion and fibre drawing processes high temperatures are preferred to produce a nice glass flow, but even if the glass is thermally stable it can crystallize if a time threshold to temperature is surpassed. A thermal-time study was carried out, setting up a temperature close to T_x (around 650 ∘C) and waiting for one hour to establish the amount of time that the samples take to fully crystallize (Fig. 5.31). The results were consistent with the first thoughts: at a temperature close to T_x it only takes around 20 minutes to fully crystallize. This shows that once the samples are heated up, the extrusion or fibre drawing has to be fast enough to avoid crystallization, and the cooling rate is also a factor that could lead to evade said undesired effects. More studies were carried out to obtain the optimum temperature for extrusion or fibre drawing from GLS-Se preforms and to establish the minimum time to carry out the processes (chapters 6 and 7).

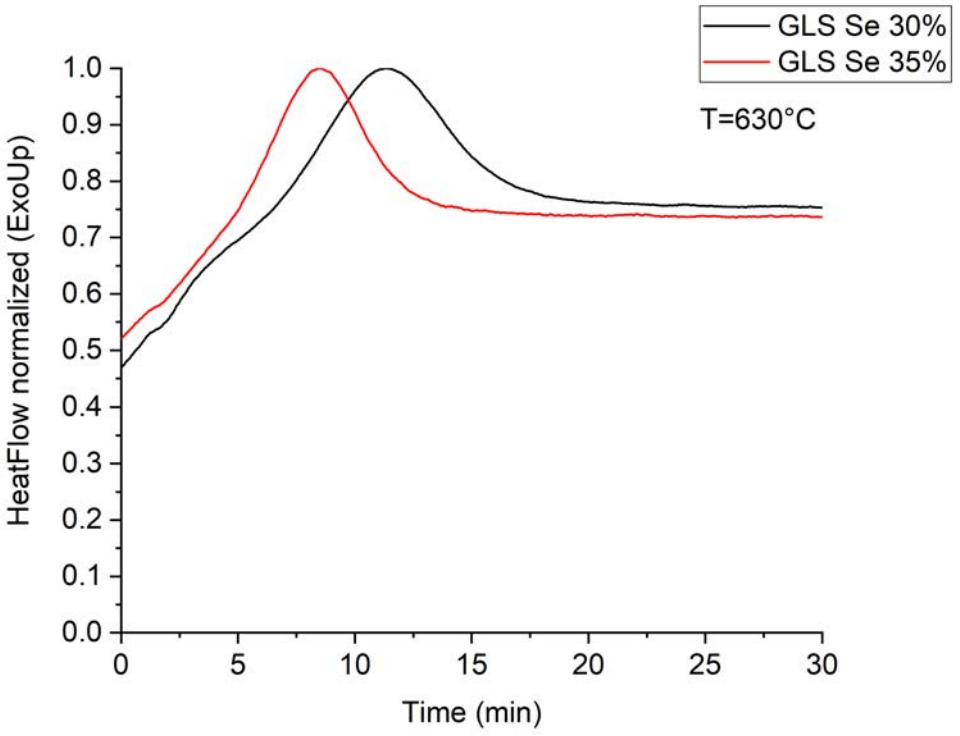

FIGURE 5.31: Heat flow vs time, showing how much time is required to crystalize the samples at a given temperature

5.6 Conclusion

GLS-Se glass samples and billets were fabricated throughout the already well-established melt quenching technique. As long as the temperatures and procedures already established are followed it does not matter in which furnace the materials are melted. Bulk samples have undergone different polishing steps to obtain an optical finish and were optically measured previously (chapter 4), demonstrating the reproducibility of glass manufacture. Moreover, thermal and mechanical studies show that the glass samples are in accordance with the expectations and these initial results are the basis for further experiments and measurements. Once the steps to reproduce the GLS-Se glass family are proved under the current situations and equipment, it can be established that it is reliable to mass produce GLS-Se glasses for any application needed in industry or for further experiments.

Chapter 6

Extruded GLS-Se glasses for fibre drawing preforms

6.1 Introduction

Previously, the promising properties of a new family of bulk glasses based on gallium and lanthanum sulphide (GLS) that have been modified with selenium (GLS-Se) have been demonstrated [4]. Through this substitution of sulphur by selenium, the long wavelength transmission increased from 9 μm for GLS to 15 μm for GLS-Se, whilst maintaining the visible transmission. However, to date, optical fibres based on GLS-Se based glasses have yet to be demonstrated.

Optical fibres are most commonly fabricated by heating and drawing from a preform [204]. For silica fibres, preforms which provide the internal core-clad structure of the resulting fibre are formed by chemical vapour deposition (CVD) [205] which provides a glass that is highly stable and can be heated to its softening temperature without subsequent nucleation or growth of crystals, results in low loss optical fibres [36]. No equivalent CVD process has been developed for preform fabrication from chalcogenide glasses and therefore alternatives for modifying the bulk chalcogenide glass into a preform or directly into fibre form have been explored. These different techniques include: rod-in-tube technique [38], crucible technique [39], in situ melt [40], suction technique [136] and extrusion [41].

Crucible drawing techniques, which draw fibre directly from the molten glass, have been favoured for conventional chalcogenide glasses, which have low melting

temperatures, typically 300 - 500 °C [206]. However, glasses based on gallium and lanthanum-based chalcogenides have much higher characteristic temperatures, with melting temperatures on the order of 1000 °C [195]. As result, crucible drawing is more difficult, not necessarily in achieving the required temperature, but in engineering a fibre drawing tower design which allows the molten glass to cool and solidify before reaching the bottom of the fibre drawing tower, where is it wound and spooled.

To get over these difficulties, chalcogenide preforms are often made through the extrusion process [207]. An important aspect to consider is the viscosity of the glass that is to be extruded, short glasses such as chalcogenides are those that present a steep viscosity temperature curve, which could prevent the material from being extruded appropriately; examples of the difficulty encountered are provided later in this chapter [92, 95]. Extrusion is typically performed in a narrow range of temperatures above the softening point ($10^{7.6}$ Poise) using lower temperatures than conventional oxide-based glasses. [108, 109]. The ideal extrusion temperature may therefore be close to the crystallization temperature of the glass, and as crystals must be avoided in the final fibre form, this could be problematic.

The first part of this chapter shows the initial experiments to confirm extrusion is a compatible process with GLS-Se glasses. Afterwards a full study is undertaken to further prove the suitability of reliable extrusions and extruded glass properties are examined post process. The extrusion of GLS-Se glasses into rods for three single different Ga_2Se_3 concentrations, and structured (core-clad) preforms using the initial results shown in chapters 3 and 5 are described. To characterize the glasses after extrusion some techniques are used such as: Raman spectroscopy, thermal analysis and refractive index measurements to investigate structural changes of the glass, x-ray diffraction (XRD) to look for evidence of crystallization, and optical spectroscopy to verify the absorption or if scattering losses were introduced. With this it is demonstrated that the extrusion process is a viable solution for preform fabrication in these materials, as their desirable characteristics are maintained after the extrusion process, ensuring their properties can be exploited also in optical fibre fabrication form for multiple applications.

6.2 Extrusion apparatus assembly and considerations

The Novel Glass Group extrusion apparatus and all the components comprising it are fully described in chapter 3. For successful extrusions the correct operation increases the chances to successfully obtain fully useful rods and structured (core-clad) preforms. Some considerations need to be taken into account before starting any process. Billets after polishing need to be cleaned by a 1-hour ultrasonic bath to remove any trace of ethanediol after polishing, as seen in chapter 5. The billet container (die, sleeve, lid), is also cleaned in isopropanol to remove any residual grease left by the mechanical workshop, this needs to be done for at least one hour. Dies are polished by a laser machine, but as seen in Fig. 6.1 it is not a completely smooth surface, this will produce some strays into the glass surface (Fig. 6.2) that are detrimental for fibre drawing. These strays are unavoidable, but a complete die cleaning might avoid adding impurities to the glass while being extruded producing with this some crystallization [207] or even surface scratching.

Before starting the assembly of all the parts that comprise the apparatus, it is necessary to check each single element that is going to be used. If no precaution is taken it might lead to an unsuccessful extrusion, damaging of the equipment and even the users can be at risk. In the past, there have been various examples of errors which resulted in breakage of glass samples, thermocouples being burned by the heating elements, or even damaging the piston (Fig. 6.3). Any of these avoidable mistakes, might give a poor extrusion process or could lead to the apparatus being out of use for several weeks until the damage has been fixed.

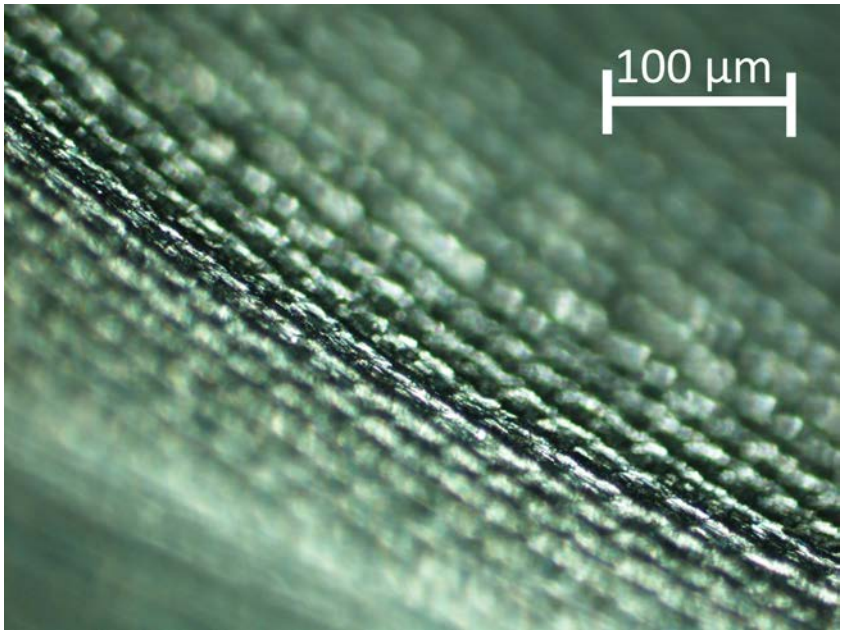

FIGURE 6.1: Microscope image of the die surface used for extrusion

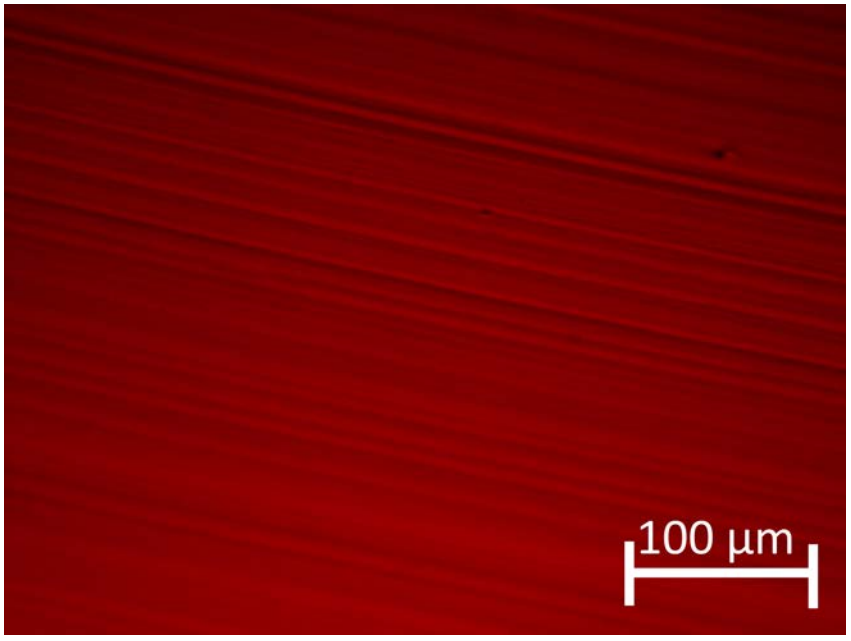

FIGURE 6.2: Strays on the surface of an extruded GLS-Se preform

FIGURE 6.3: Damaged piston after mispositioning it in the extrusion apparatus

The assembly steps for the extrusion apparatus are listed as follows:

- The billet container after being cleaned (Fig. 6.4), is placed in the carbon body and the glass samples are placed accordingly (Fig. 6.5).

FIGURE 6.4: Cleaned billet container (die, sleeve and lid)

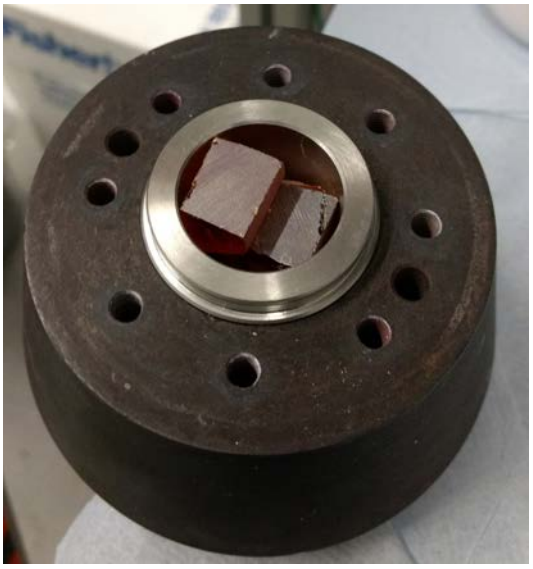

FIGURE 6.5: Glass samples placed in the billet container

- The lid is placed on top of the glass billets (Fig. 6.6). It is best if there is a gap between the lid and the edge of the sleeve, as this helps positioning the piston, and avoids any possible damage during the process. Also, the thermocouples are placed to measure the temperature of the top and bottom part of the carbon body, as described in chapter 3.

FIGURE 6.6: Billet container, showing a gap between the lid and the sleeve favouring the positioning of the piston

- Afterwards the carbon body and the billet container are placed on top of the bottom heating element and the second heating element, for the carbon body, is then allocated (Fig. 6.7).

FIGURE 6.7: Partially assembled extrusion apparatus showing the main heating element before the ceramic shield is placed

- The ceramic shield is then used to cover the rest of elements, as this helps maintaining the heat applied to the billet container [208] and favouring the control in temperature. Then the piston is put in position, and the equipment is ready for the process (Fig. 6.8).

FIGURE 6.8: Completed assembly of the extrusion apparatus and ready to start the process

Although the steps to follow are systematic and repeatable, the user needs to be careful and respect the guidelines of the process. The misunderstanding of any steps might lead to undesirable consequences, for example they might affect the billet container and breaking the glass samples (Fig. 6.9). In this work the extrusion apparatus used a silica tube under the die to facilitate maintaining a straight extruded glass and in case of breakage for user safety.

FIGURE 6.9: Example of crushed glass, as the lid and piston were positioned incorrectly

6.3 Initial extrusion experiments with GLS samples

The Novel Glass Group has previously explored extrusion at a temperature range between 620-640 °C [53] with various results as part of a study of GLS glasses, but not as a main goal. To be able to further develop the family of chalcogenide glasses, the next step is to explore the feasibility of extrusion with GLS-Se glasses. After studying the pros and cons of extrusion, as seen in previous chapters, the first step is to understand the behaviour of chalcogenide glasses during extrusion. Initial tests were carried in already produced GLS glasses, to set the best approach and temperature values for a continuous and complete extruded glass rod. The preparation of the samples was as discussed in chapter 5. The extrusion apparatus has a temperature heating rate around 18 °C/min and a maxim set temperature of 700 °C. It has two independent temperature controllers for each heating element

(Fig. 6.10): one for the carbon body itself (main heater) and one for the die (ring heater). The latter requires a higher temperature as the die needs to maintain the temperature to avoid having glass stuck in the die and promote the glass flow. The GLS glass (65:35) has a transition temperature of 563.8 °C, a crystallization temperature of 679.2 °C [1] and the softening point ($7.6 dPa \cdot s$) is reached around 620 °C [53]. For extrusion to take place, the temperature needs to be set above the transition temperature (T_g) but below the crystallization temperature (T_x), but these are dependent on composition the viscosity chosen might differ.

FIGURE 6.10: Glass extrusion apparatus temperature controllers

Another parameter that can be established in this equipment is the speed of extrusion, that determines the time used for the process to be completed and therefore the thermal history of the glass. Extrusion speed and the viscosity, as a function of the temperature, describe the total load applied by the piston (Fig. 6.11). These two latter parameters define the window of time within the extrusion can be carried out before crystallization begins [209]. The initial thoughts were that getting to the extrusion temperature needed to be done in steps of stabilization, this is choosing the maximum temperature to be used and starting with lower temperature, waiting and then increasing again. This approach, as seen in Fig. 6.12, was proved to be wrong. This figure shows completely ceramized sample, as the chosen temperature was 670 °C for the ring heater and 640 °C for the main heater. It was initially set to a 200 °C temperature, then 400 °C and afterwards 600 °C. Once the ring temperature controllers reached 600 °C the temperature was increased by 10 °C until it reached 670 °C, and the same procedure was used for the main heater to reach 640 °C. The extrusion speed chosen for this trial was 0.1 mm/min, this plus the time required to reach the highest temperature in the controller, lead to an initial trial with up to 6 hours process time.

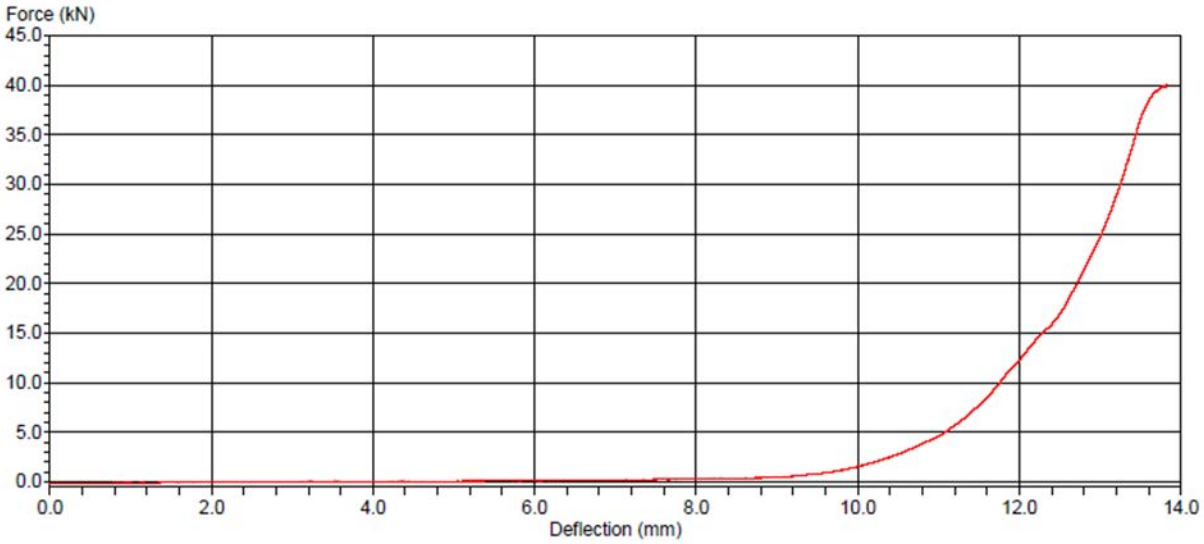

FIGURE 6.11: Extrusion load curve, the horizontal axis shows the distance the piston has travelled inside the billet container, the sharp load rise is due to the ceramized sample

FIGURE 6.12: Ceramized GLS sample after a failed extrusion attempt

After this failed initial attempt the choice was made to try the opposite approach: start at a low temperature of 570 °C for the main heater and 610 °C for the ring heater. Extrusion speed was increased to 0.5 mm/min to reduce the time of the process, and temperature was increased directly to the chosen temperature with no intermediate steps. Once the temperature controllers reached the set values there was a dwell time of 5 minutes before starting the process. As seen in Fig. 6.13, this approach was again proven wrong as the glass sample was not in a temperature high enough to be extruded and on the contrary, the glass was being crushed. The load curve sharply increased, and several cracking was heard. To overcome

this the temperatures were increased progressively every minute until the load dropped. Contrary to the previous attempt the piston went further in the billet container, meaning that extrusion was taking place. Unfortunately, the initial low temperature and glass crushing led to a short crystalized extruded sample (Fig. 6.14) as the glass powder particles could have acted as nuclei, but this partially successful trial led to the confirmation of the possibility to extrude glass if the conditions were improved (i.e. correct temperature) and that extrusion needs to start at a low temperature and increase in small steps until the load curve is steady.

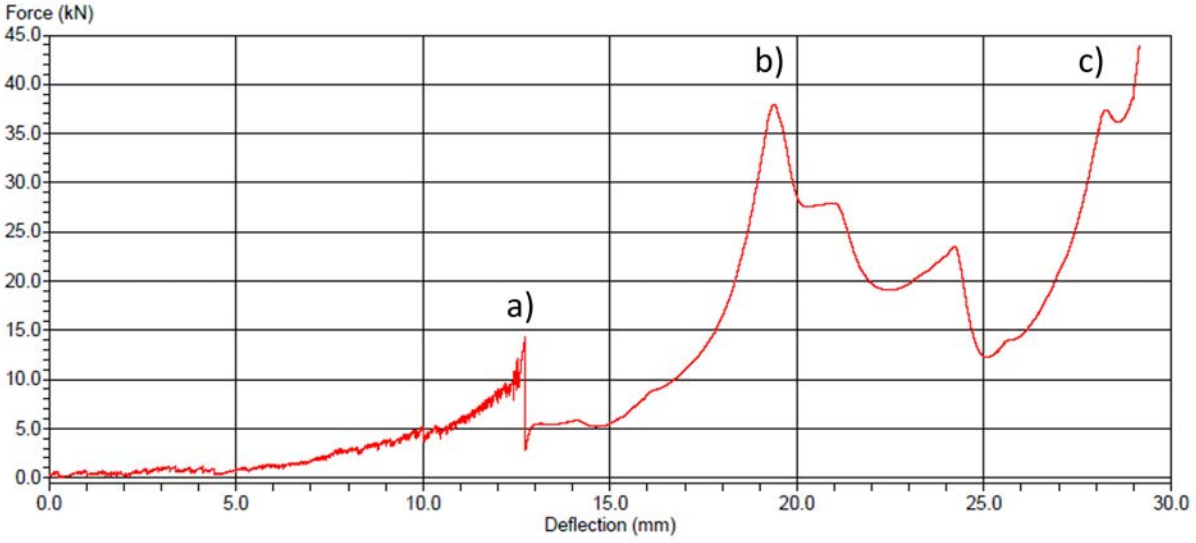

FIGURE 6.13: Extrusion load curve where it can be seen the section a) that belongs to the part with low temperature and therefore crushed class, b) temperature was increased to decrease the glass viscosity and extrusion started to take place until a load peak was reached, temperature was gradually increased and as result load kept decreasing, and c) the end of extrusion

FIGURE 6.14: Extruded GLS sample, heavily crystallized as glass was crushed during extrusion and a wrong temperature was set

6.4 Extruded GLS-Se samples failed attempts

After the GLS extrusion attempts, several improvements were made to determine the steps to be followed for a successful extrusion process with GLS-Se glass billets for rods and structured preforms. This section shows the situations that occurred and parameters that were used leading to unsuccessful extrusions. They are not necessarily in a chronological order as some attempts were performed to further investigate possible situations and parameters that could benefit the process, which in the end did not, and also some were produced by an equipment malfunction. A crucial step described in chapter 5 was the ultrasonic bath after every polishing step, to reduce or eliminate any carbon trace that could affect the extrusion process, a remanent of the polishing process. This realization resulted from the negligence of not cleaning the glass billets and just introducing them into the extrusion apparatus after they were annealed. This resulted in a glass rod with severe crystallization along its length (Fig. 6.15) as the particles on the surfaces promoted nucleation [55].

FIGURE 6.15: Extruded preform partially crystallized as billets were unpolished

To illustrate how crystallized the preform was, a white light source was used to show the scattered light (Fig. 6.16). This proved that a cleaning step (i.e. ultrasonic bath) needed to be introduced to the process to avoid crystallization by particles.

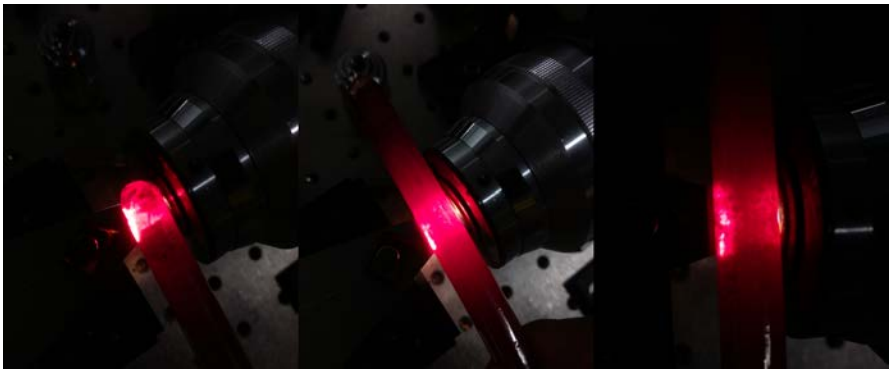

FIGURE 6.16: Crystallized preform under a white light source showing scattering due to the crystals produced in the extrusion process

This failed attempt was done in the pursuit of trying to avoid the polishing and ultrasonic bath steps to save time as preforms can take up to two weeks before being ready to be drawn into fibre. However, in this attempt the temperatures were close to be suitable for a continuous uninterrupted extrusion. Another way to ensure the quality of an extrusion is by maintaining a pre-determined extrusion load curve. It was thought that the higher the temperature, and therefore the lower the viscosity, the more straightforward the extrusion process would be. The latter means that the load curve would be almost linear until the very end of the extrusion (Fig. 6.17).

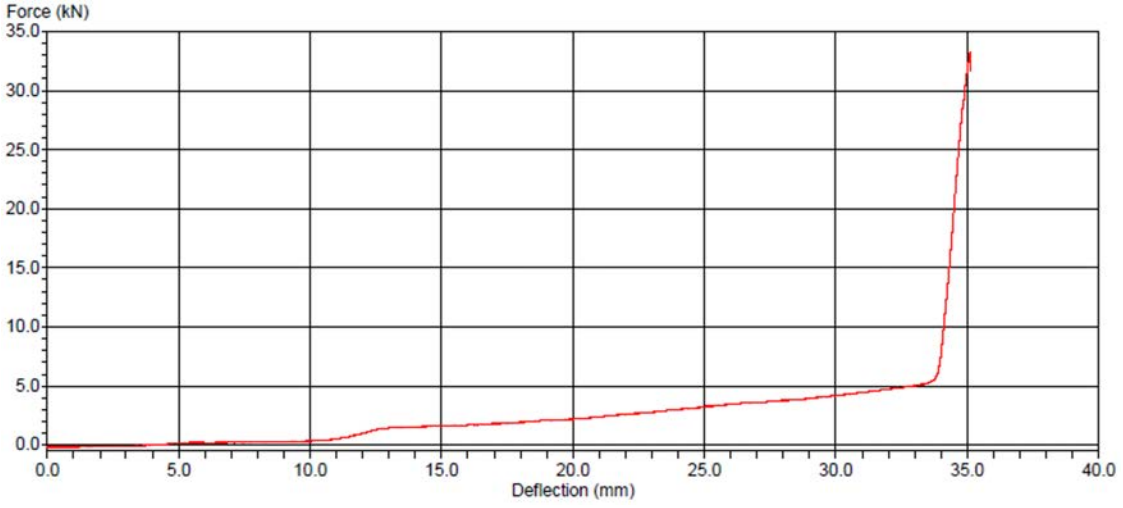

FIGURE 6.17: Almost linear extrusion load curve that produced crystals in the preform as the temperature set was 620 °C

According to the curve, the extrusion seems perfect, but the preforms contained some visible crystals within it. Compared to other successful trials, the difference

in temperature was only 10 °C higher. After multiple extrusions, it was corroborated that once the set temperatures were reached in the controllers, at least 5 minutes are needed to stabilize the temperature in the billet container. If extrusion is started before this waiting time, there is a high probability that the first part of the glass comes out of the die sharply bent provoking an unsuccessful extrusion. This result was due to a high viscosity of the glass and a high load applied by the piston [210], as the internal pressure in the die builds up when the glass comes out of the die the pressure difference provokes an acceleration in the glass flow provoking that the material stops behaving as a laminar flow resulting in a random flow that provokes a sharp bending angle. Although some bending is unavoidable, it must be reduced as much as possible, so that the useful length of the extruded glass is maximized.

The dies produced by the mechanical workshop, as described in chapter 3, have an aperture of 10 mm in diameter. One extrusion trial was to produce canes of 1 mm in diameter directly from the glass billets and for this purpose a new die was designed. The problem that arose from using smaller die apertures was that the inner roughness of the die cannot be controlled properly. Moreover, the smaller the die aperture, the higher the load that needed to be applied [122]. These factors cause different types of imperfections in the surface of the canes (Fig. 6.18). For varying die diameter apertures, further studies need to be carried out, and new parameters need to be stablished.

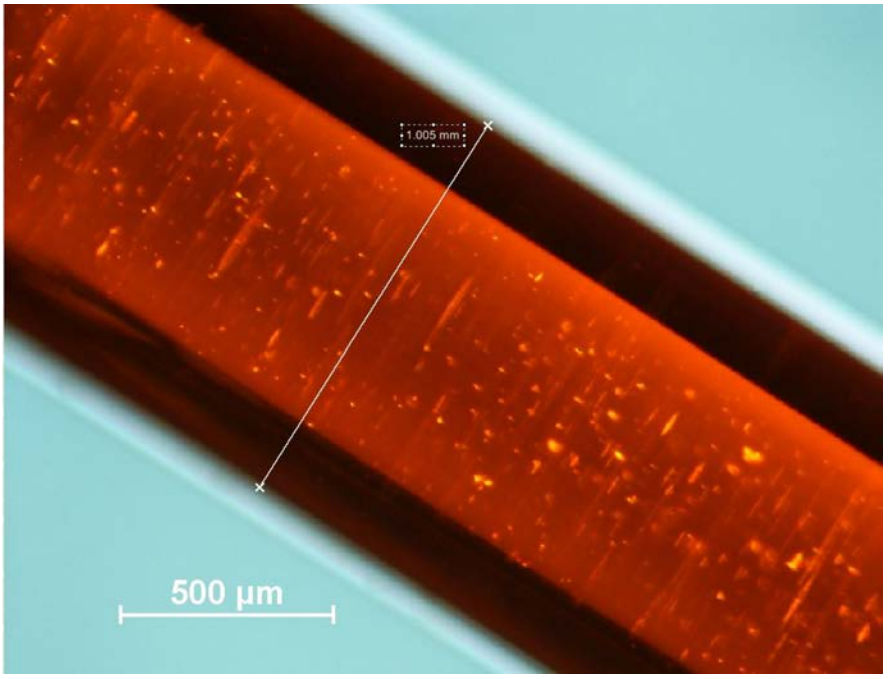

FIGURE 6.18: Extruded cane of 1 mm in diameter showing surface imperfections

In previous studies [98], it has been of interest to exploit the high nonlinearity of the chalcogenide materials for hollow fibres. These types of fibres confine the light in the core very efficiently due to their structure. To facilitate the fabrication of these type of fibres the extrusion process has been applied successfully for GLSO glasses [101]. As background it is shown that GLS based glasses can be used to produce hollow fibres and this example was used as basis to try to replicate the same type of extrusion with GLS-Se glasses. The challenge for extruding GLS-Se glasses in complex dies is that their extrusion viscosity is in the range of $7dPa \cdot s$ which can be though as a high viscosity for the process, and also the die design needs to promote a proper glass flow to cover all the space in it. A note in this work, is to not misunderstand a high viscosity with the Vickers hardness [54] of the glass, as this property is only for solids, but do note that the glass Vickers hardness is higher than that of stainless steel [211]. Viscosity must be low enough to flow through the geometry of the die for a hollow preform. Fig. 6.19 shows that the use of a temperature related to a high viscosity destroys the die structure and does not produce the desire geometry. GLSO glasses as explained in chapter 3, have an advantage that due to their oxygen content, higher temperatures and thus low viscosity can be obtained, therefore improving the extrusion of any intricate die structures. For complex die structures more studies need to be carried, to obtain the best parameters for a successful extrusion.

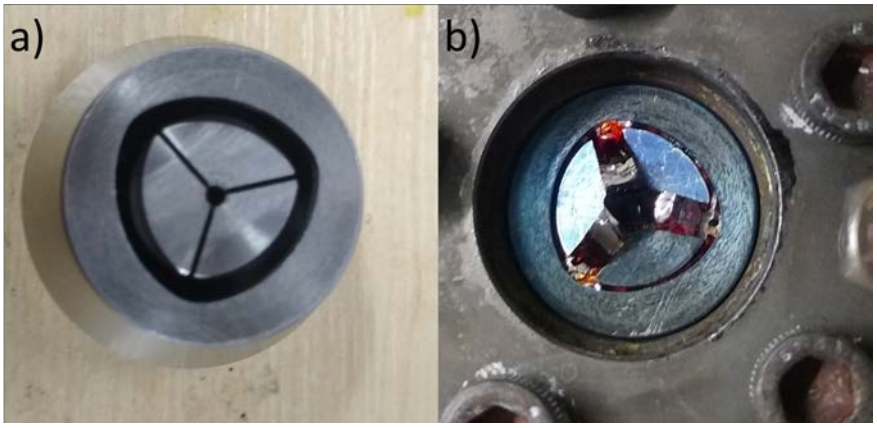

FIGURE 6.19: Failed wheel extrusion attempt, where a) is the original die pre extrusion and b) is the destroyed die by the low viscosity glass

As described in previous sections, one factor that produces unsuccessful extrusions is equipment failure. The most common is that the temperature controller thermocouples have wrong temperature readings as they are damaged. One effect that this might produce is that the die is heated unevenly and that temperature gradient [212] produces a twisted glass preform (Fig. 6.20), as the temperature gradient in the die produces a convection flow in the unevenly heated glass. No further experiments were done with this extruded glasses, but it is probable that the fibre drawing of these could be useful for spun fibre applications [213]. If this type of extrusions have an application, further research needs to be be carried to understand how to replicate them.

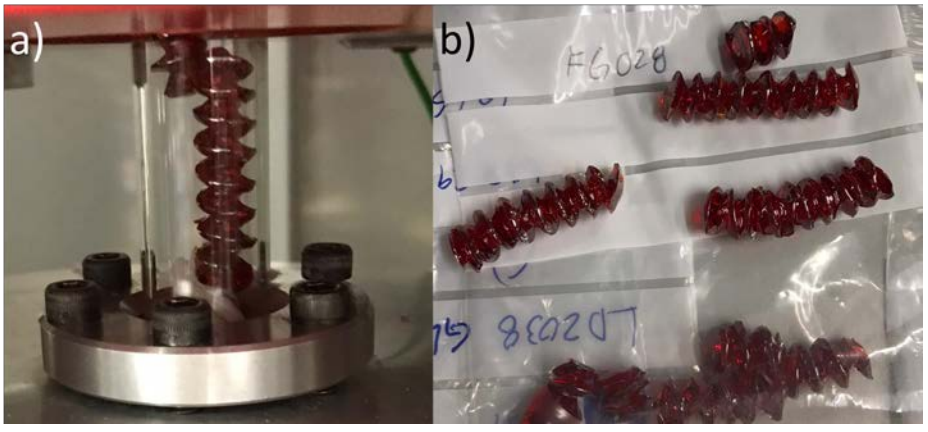

FIGURE 6.20: Twisted extrusion due to a misfunctioning in the heating elements, where a) is the extruded glass inside the protection tube and b) samples of the failed extrusion

As described before, a glass sample, if melt-quenched correctly, always shows its intrinsic characteristics and every part of it is transparent. However, there are some failures in the equipment and this leads to the production glass billets that are not completely glassy (Fig. 6.21), as they were not correctly placed in the furnace affecting with this the whole process. In an attempt to understand how detrimental this effect would be in an extrusion these type of billets were used to obtain an extruded rod. The billets went through the same steps that were already established to prepare and clean the samples before extrusion (i.e. polishing, ultra sonic bath).

FIGURE 6.21: Billets for extrusion not completely transparent, just the bottom part of them presented this anomaly

The extrusion of the billets was thought to have a different load curve and that the not completely glassy sections would be extruded first and pushed out of the billet container, so that the rest of it is useful and completely transparent. None of these ideas occurred, as the temperature used produced the same load curve as other successful extrusions, but what resulted was an extruded rod with the outer surface heavily scratched and with ceramics (Fig. 6.22). Chapter 7 shows that those surface imperfections can be overcome by rod polishing. This confirms that from the raw materials mix until the extrusion process, every step must be respected and replicated to the highest standards established and that before carrying any job the equipment needs to be checked to ensure that no failure affects the glass samples and extrusion process.

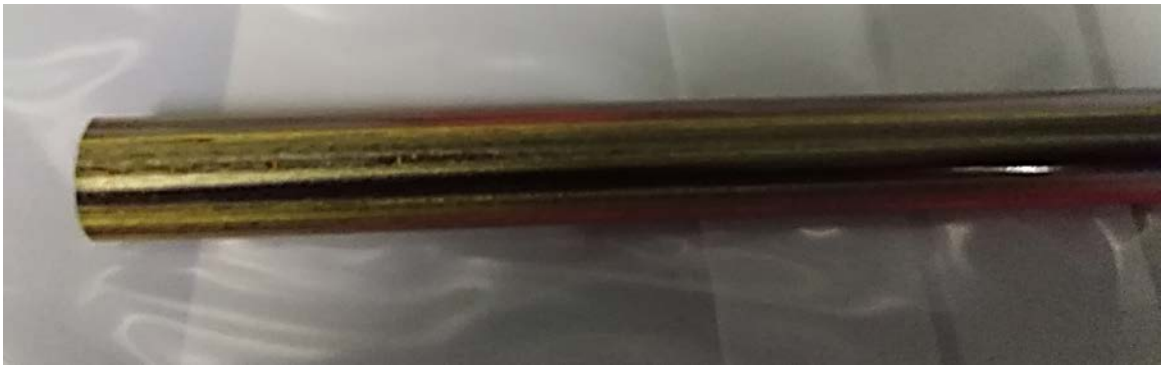

FIGURE 6.22: Extruded rod with surface defects caused by partially crystallized billets

6.5 GLS-Se successful extrusion for rods with single compositions and structured preforms

Following the cleaning and polishing steps, the avoidance of high temperature established the path to follow to obtain the correct temperature for completely transparent and crystals-free preforms. As stated in the previous section, the first approach that started giving positive results was to choose a temperature low enough to avoid crystallization but enough to decrease the viscosity of the glass, even at the expense of the load curve. The first successful trials included a progressive increase in temperature in amount of 5 °C, when the load started to raise and until the load descended to a stable value that could keep the extrusion process going (Fig. 6.23).

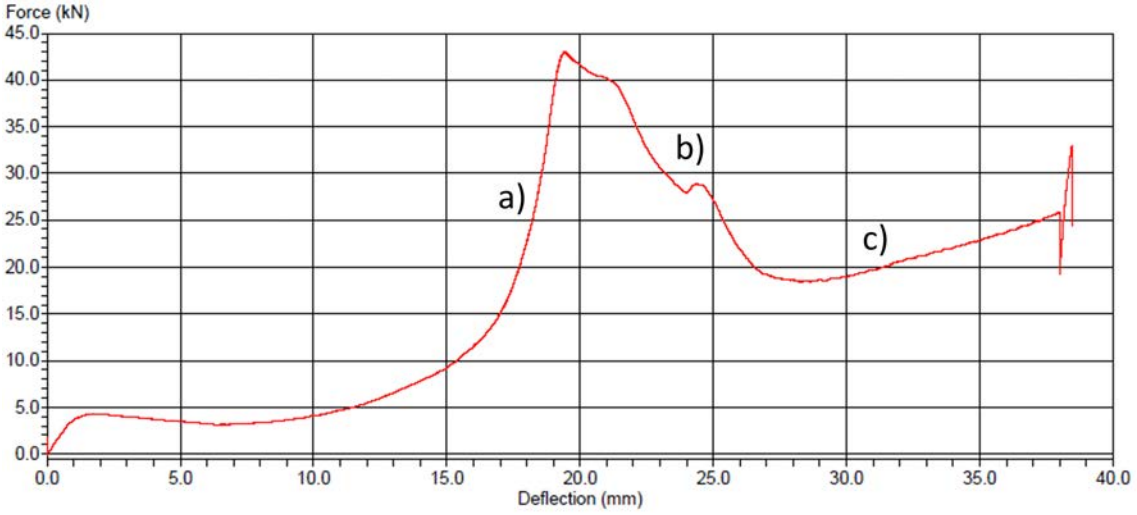

FIGURE 6.23: Successful extrusion with temperature increasing steps, where a) load sharply rises (T=575 °C), b) load decreased as temperature increases by 5 °C per min, and c) constant and stable load (T=610 °C)

From these extrusions with temperature increasing in small steps, the maximum temperature that was useful for a continuous extrusion and to produce glass rods without crystals was obtained. The maximum temperatures selected in the temperature controller were 610 °C for the ring heater and 600 °C for the main heater. The produced load curve is steady and with an increasing load as the piston displaces in the billet container (Fig. 6.24). Depending on the billet's thickness is the maximum length of the extruded rod (Fig. 6.25). Every successful extruded rod has a diameter of 10 mm ± 0.02, which confirms the stability of the extrusion process and the reliability of the fabrication itself.

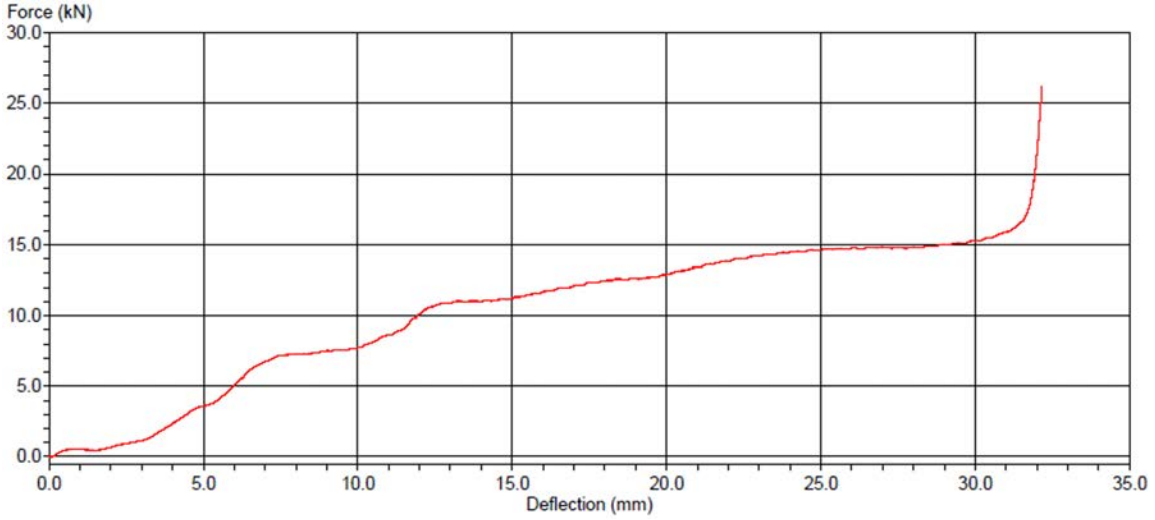

FIGURE 6.24: Example of a load curve for an extruded rod without crystals and with the correct temperature

FIGURE 6.25: GLS-Se extruded rod without crystals and with a maximum length of 26 cm

As described in chapter 4, for structured preforms (core-clad) compositions with Ga_2Se_3 30 mol% and 35 mol% were chosen, as they present comparable refractive indices and Weinberg parameters [5]. This means that thermally they behave similarly making co-extrusion a viable process. Billets were prepared with the same steps that proved being essential for a successful extrusion. Afterwards they were placed in the billet container (Fig. 6.26) and every step was reproduced in the same way for every extrusion. The load curve did not present a big difference compared to single composition extrusions. What needed to be proven was that the co-extrusion process behaves similarly to a single composition extrusion glass flow, to produce a core-clad interface. As seen in Fig. 6.27, successful structured preforms were obtained where the new challenge was to obtain a smooth interface between both compositions, to prevent any scattering from introduced impurities during the process (Fig. 6.28). All efforts have been put to obtain completely transparent preforms with no crystal formation and with the least impurities introduced by the process itself. Further studies need to be carried for different compositions for rod and structured glass preforms.

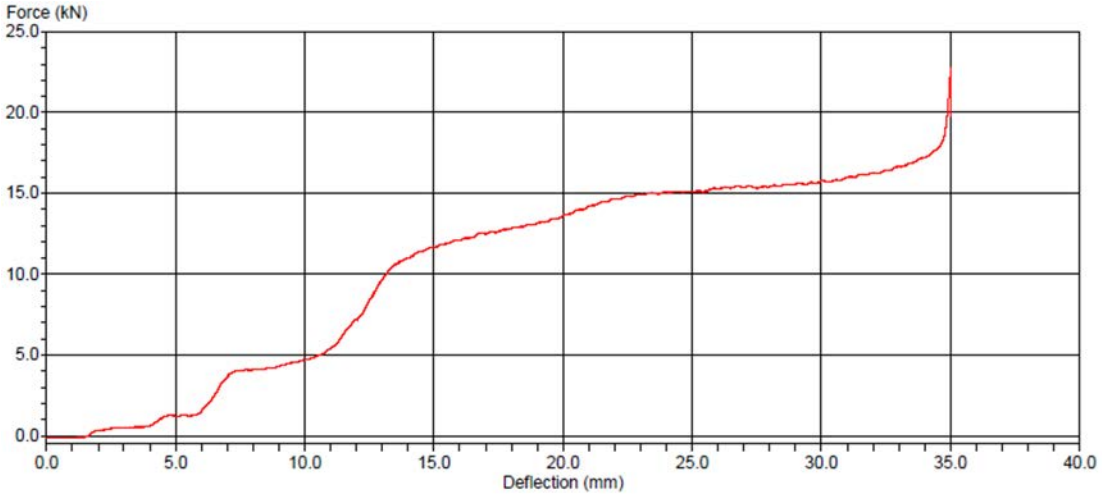

FIGURE 6.26: Load curve for a co-extrusion to produce structured preforms

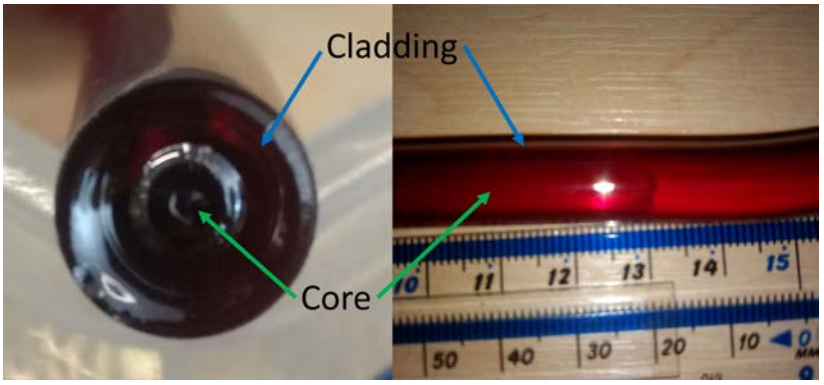

FIGURE 6.27: Successful structured preform after co-extrusion

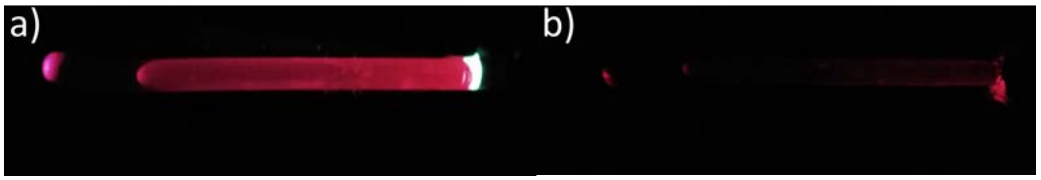

FIGURE 6.28: Structured preforms under a while light source showing the scattering in the core-clad interface, where a) shows a heavily scattering preform and b) scattering was suppressed

6.6 Improvements during the development of successful GLS-Se extruded rods and preforms

Every extrusion attempt provided feedback about the quality of the process, the samples used, and the post extrusion results. After every trial, new considerations towards the correct steps to follow during the process were developed. Each extrusion attempt represented an opportunity to improve the quality of the samples and the parameters involved (i.e. extrusion temperature), to include new steps (i.e. polishing), etc. Figs. 6.29, 6.30 and 6.31 clearly show the difference in quality between extruded samples using 630 °C (high temperature, viscosity $6dPa \cdot s$) and 610 °C (low temperature, viscosity $6.5dPa \cdot s$). The effects of using the wrong temperatures and not including cleaning steps promote poor quality extrusions and high contamination due to impurities and crystallization.

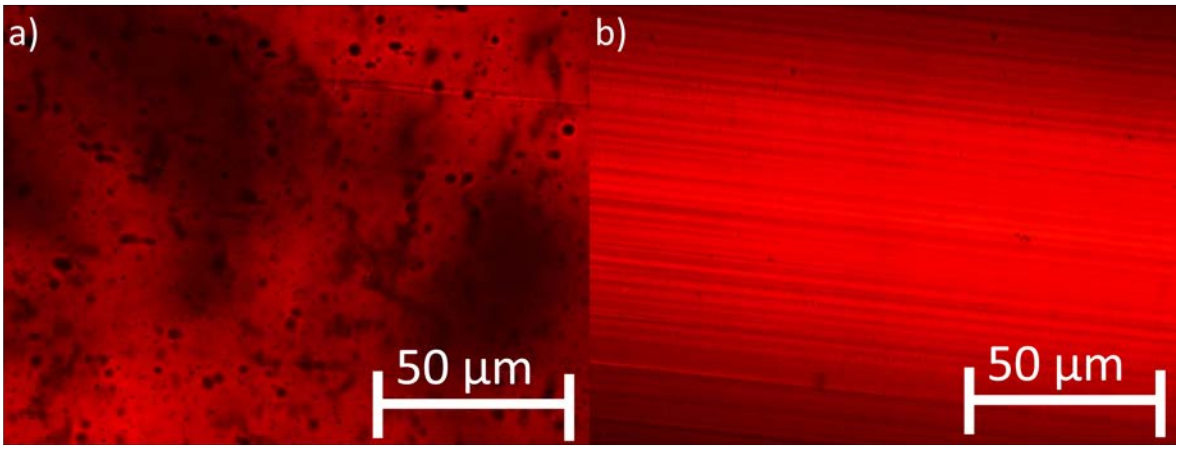

FIGURE 6.29: Surface extruded quality, showing the effects of using a) 630 °C and b) 610 °C

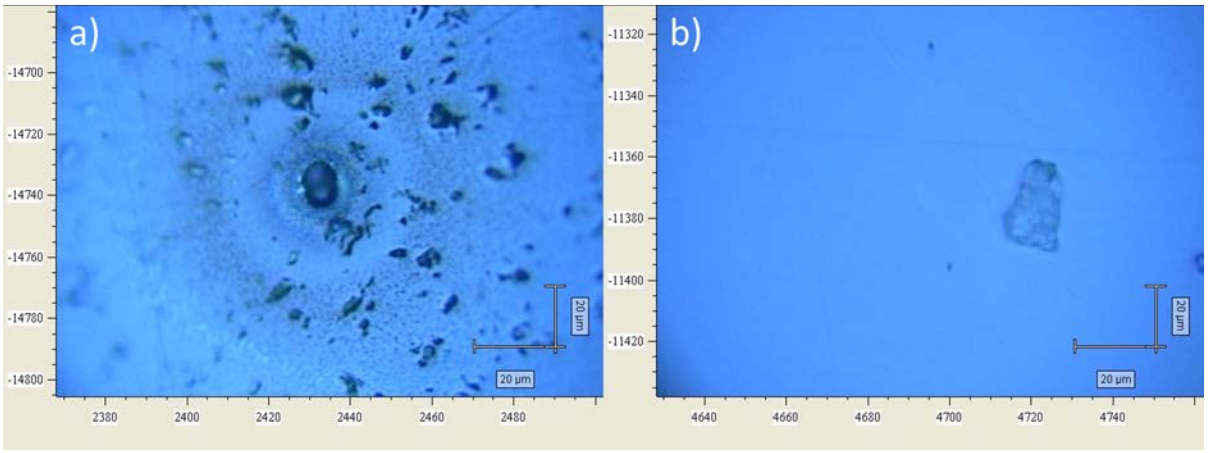

FIGURE 6.30: Difference in the glass quality, due to the effects of using a) 630 °C and b) 610 °C

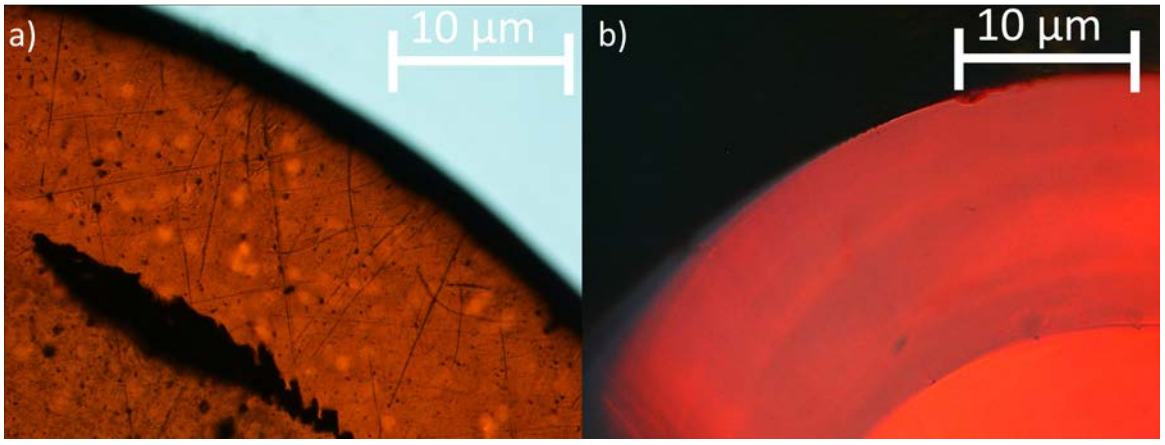

FIGURE 6.31: Structured preform interface differences between extruded samples, showing the importance of the cleaning steps, where a) shows impurities and b) is cleaner

6.7 Thermal characterization of GLS-Se successful extruded rods with single compositions

The failed attempts to produce GLS-Se extruded rods led to an initial understanding that the time and temperature were incorrect. To decrease the time of the process, the extrusion speed was increased to 0.5 mm/min, which helped to reduce the exposure of the glass to heat from 6 hours to approximately 1 hour. The importance of this resides in the fact that the initial extrusions affected the thermal behaviour of the glass (Figs. 6.32 and 6.33). In these pictures we show the exothermic crystallization peak has a higher amplitude and its broadening, or shortening, has a variation between 3-27% compared to the bulk samples before the extrusion process. These variations in the heat flow analysis, specifically in the crystallization peak, are described by the equation [214]:

$$\phi = m \cdot c_p \cdot \beta + \phi_l \tag{6.1}$$

Equation 6.1 Heat flow signal analysis

Where m is the mass of the sample (kg), c_p is the specific heat capacity ($J/K \cdot kg$), β is the heating rate (K/s) and ϕ_l is the heat loss function (mW). This equation shows that the behaviour of the heat flow is related to the specific heat capacity. This latter is likely to differ between the bulk and the extruded samples of the same glass, as extrusion could promote crystallization if the parameters used (i.e. temperature) are not suitable for the process. Further studies need to be carried to define the heat capacity of GLS-Se glass bulk and extruded samples, to fully understand the behaviour of this family of glasses under the influence of applied heat.

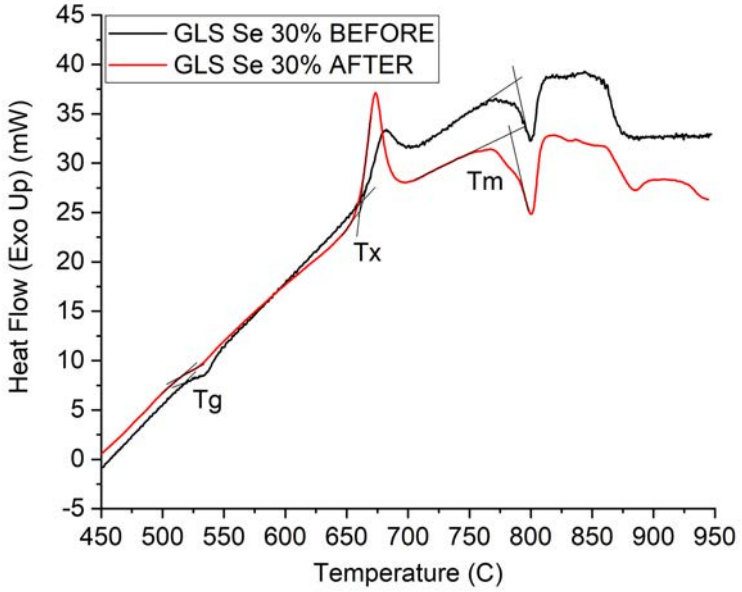

FIGURE 6.32: DTA curve for GLS-Se glass samples with Ga_2Se_3 30 mol% before and after extrusion

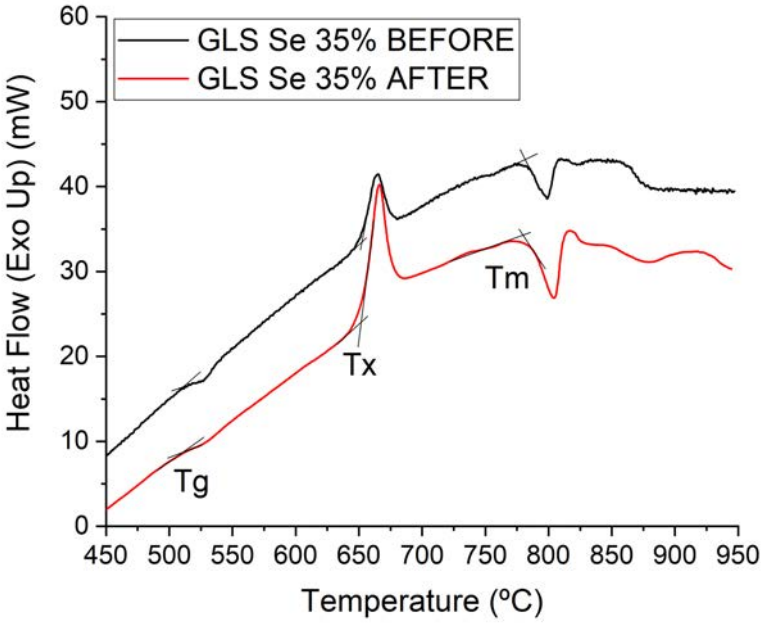

FIGURE 6.33: DTA curve for GLS-Se glass samples with Ga_2Se_3 35 mol% before and after extrusion

Therefore, extruded glasses presented almost the same characteristic temperatures as bulk glass samples. However, changes in the structure of these curves, for example the stronger crystallization peak, suggest that some material changes (i.e. nucleation) are occurring which could affect other bulk properties such as heat capacity. For the most part during extrusion the characteristic thermal properties for different contents of Se are maintained [215], as shown in Table 6.1. As described in chapter 5, the difference between the bulk samples produced in this work and previous studies [54] is of maximum 1%, each temperature in this work presents a ±2 °C approximation within temperatures of the same composition.

TABLE 6.1: Thermal characterization for GLS-Se glass samples before and after extrusion

	Bulk			Extruded		
Composition	T_g (°C)	T_x (°C)	T_c (°C)	T_g (°C)	T_x (°C)	T_c (°C)
GLS-Se 20%	519	678	802	512	679	805
GLS-Se 30%	517	663	786	515	661	783
GLS-Se 35%	511	652	782	510	651	780

Thermomechanical analysis (TMA) showed that the characteristic viscosity of GLS-Se extruded glass was maintained, and the softening point corresponded to previous studies [5] with a maximum difference of 1% between values of the same composition, as seen in Table 6.2. The increasing of Ga_2Se_3 content, in the first instance, decreases the softening point (as its melting point is lower than the melting point of the Ga_2S_3) but as the concentration increases it starts increasing again, as it tends to a maximum in the phases of Ga_2Se_3 [216], as shown in Fig. 6.34. These viscosity curves, in addition of the differential thermal analysis (DTA), are the basis for establishing the parameters for fibre drawing of the extruded GLS-Se glass-based rods and structured preforms.

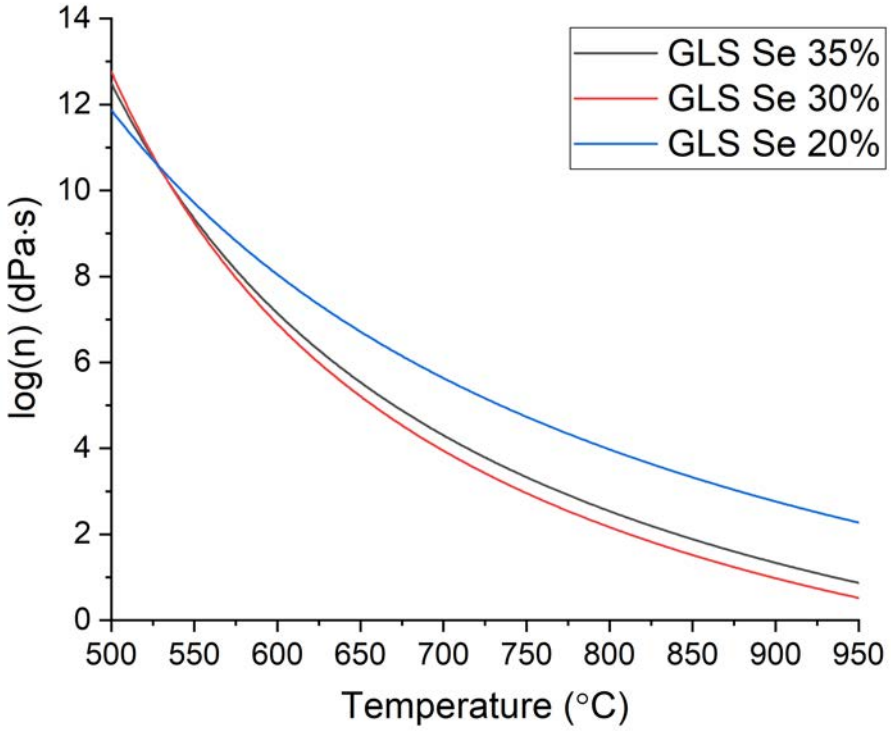

FIGURE 6.34: Viscosity curves for different GLS-Se extruded glasses

TABLE 6.2: Temperature at the softening point GLS-Se glass samples before and after extrusion

	Bulk [34]	Extruded
Composition	Softening point (°C)	Softening point (°C)
GLS-Se 20%	623	616
GLS-Se 30%	581	583
GLS-Se 35%	—	588

6.8 Optical and material characterization for extruded glass

Optical characterization is the next step for the extruded glass to ensure that the extrusion process has not modified the properties compared to the bulk glass prior to extrusion. The results presented in this section are for single extruded compositions, but the same analysis was carried out for the structured extruded preforms (i.e. FTIR spectroscopy). Results obtained are in accordance with the graphs and

tables shown in this section however for clarity structured preforms graphs were omitted. A disc of 1 mm thickness was cut from each extruded rod, and polished using the same process for the billets. Optical transmission was measured using a UV-VIS-NIR (Cary-500) and a FTIR (Cary-670) spectrometers in a range of 500 nm to 15 μm. The optical transmission for the samples corresponds to what is expected from the bulk samples [54], with a maximum difference of 5% for the sample with Ga_2Se_3 35 mol%, considering that some transmission loss due to reflection and scattering produced by imperfections in the polishing might occur. As the concentration of mol% of Ga_2Se_3 increases, the refractive index increases too (Fig. 6.36), this favours the Fresnel reflections during the optical characterization, and results in a lower transmission spectrum as the concentration of Ga_2Se_3 is increased. Also, there is a loss from 10 μm to 12 μm which corresponds to an absorption due to oxide impurities [217], that could have been produced as the extrusion is not in a purged environment and above T_g the glass can react with oxygen [175] (Fig. 6.35. Although no impurities or change in transmission up to 9 μm was seen. Even though the energy-dispersive X-ray (EDX) showed a maximum of 200 ppm of nickel (Ni) in one of the extruded samples, there is no considerate loss at its absorption wavelengths [218].

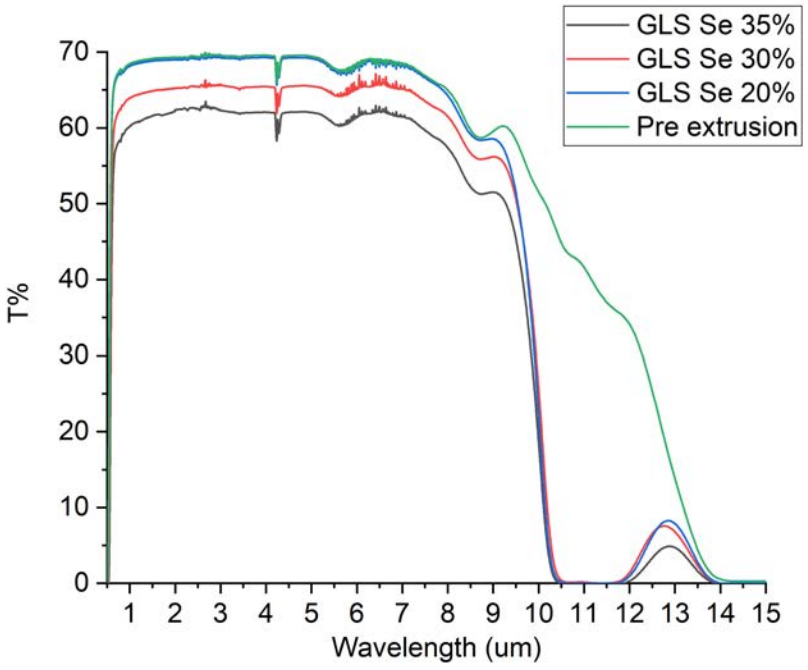

FIGURE 6.35: Transmission spectra of the extruded glasses. *Note: spectra not corrected for Fresnel reflections, the pre extrusion spectrum corresponds to a Ga_2Se_3 20 mol% sample*

The transmission can be affected by a possible phase change from the Ga_2Se_3 during the extrusion, as the greater content of this component, the more the transmission decreases compared to bulk samples. Further studies can consider the purity of the raw materials related to their effects in the transmission of extruded samples.

The refractive index was measured using an ellipsometer (Woollam®M-2000) from 370 nm to 1 μm, the Sellmeier equation was used to fit the obtained values [88], where $n(\lambda)$ is the wavelength dependant refractive index, λ is the wavelength and A, A_1, B, B_1, C and C_1 are fitting parameters. Refractive index shows a change as the amount of Ga_2Se_3 is increased, which corresponds to the previously studied bulk samples [34], as the polarizability of the glass is modified by modifying the composition [219] (Fig. 6.36). Error bars were calculated using Origin®through the standard deviation, and have a maximum error of 0.2%.

$$n(\lambda)^2 = \frac{A\lambda^2}{\lambda^2 - A_1} + \frac{B\lambda^2}{\lambda^2 - B_1} + \frac{C\lambda^2}{\lambda^2 - C_1} + 1 \tag{6.2}$$

Equation 6.2 Sellmeier equation

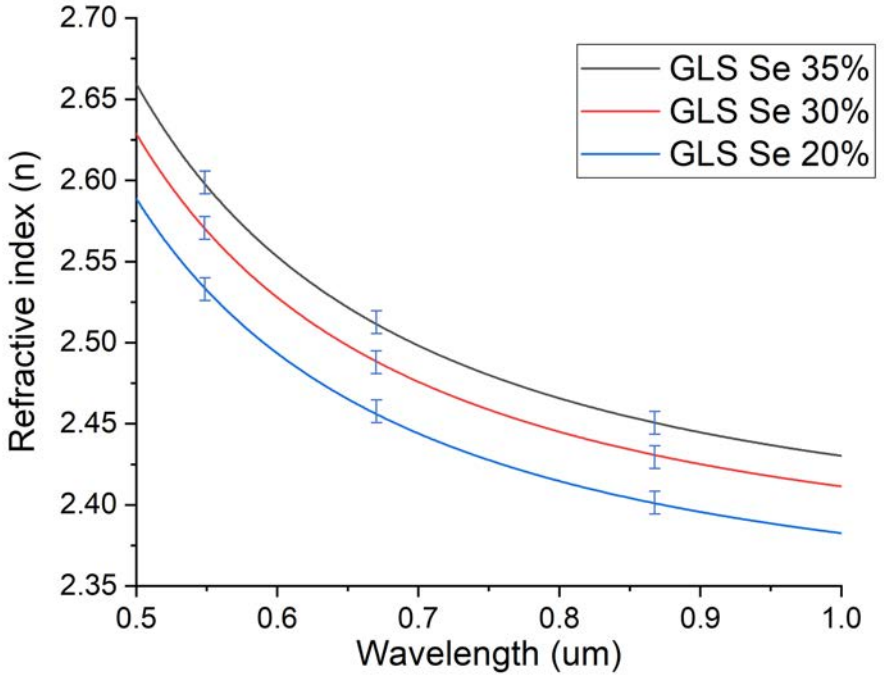

FIGURE 6.36: Refractive index of the extruded glasses

To verify that the transmission obtained was from a glassy amorphous phase in each sample, X-ray diffraction (XRD) and Raman spectroscopy were performed. Raman spectroscopy provides evidence of a glassy amorphous phase in the samples after extrusion as no sharp peaks were found. The peak at 325 cm^{-1} of Ga_2S_3 decreases as expected when the amount of Ga_2Se_3 increases, the peak at 225 cm^{-1} increases and shifts to the left with a higher amount of Ga_2Se_3 in the composition. The last peak at 150 cm^{-1} corresponds to La_2S_3 as is the only compound amount to remain constant through all three samples [5, 220, 221] (Fig. 6.37). The XRD measurements confirm an amorphous phase while Raman spectroscopy showed broadening of the spectra. Adding this to the absence of high intensity peaks in the spectra, at 2θ=25° a slight decrease in intensity was seen as the amount of Ga_2S_3 was substituted by Ga_2Se_3, which also corresponds to an increase of the intensity at 2θ=30°, a crystalline phase should show a sharp peak and intensity on the range of thousands and a width of few degrees [222] (Fig. 6.38). This analysis confirmed the amorphous nature of the extruded samples, and further studies might be carried to quantify the change in the peaks shown.

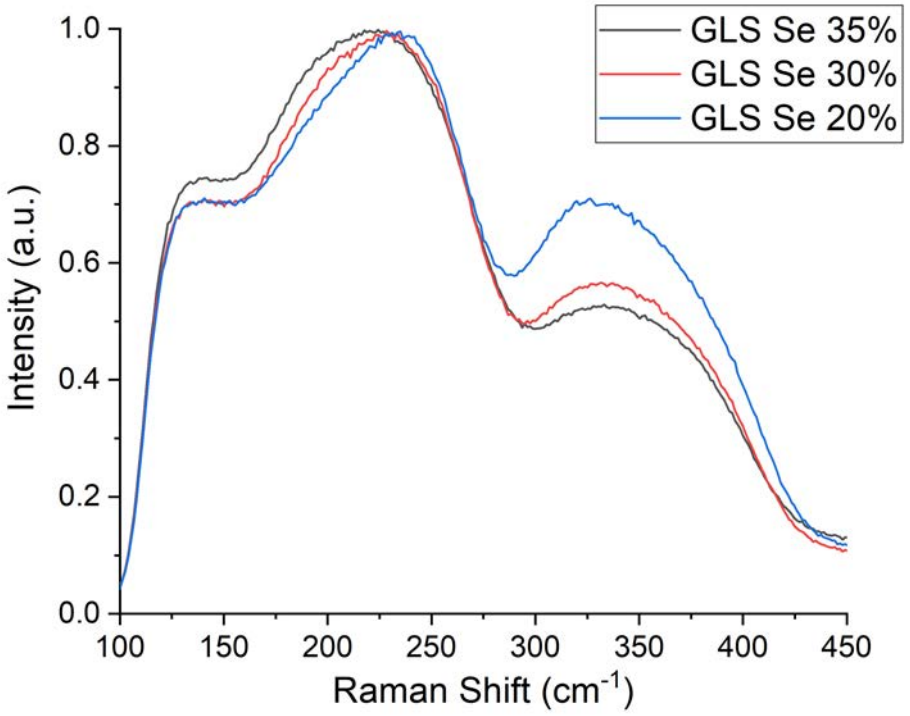

FIGURE 6.37: Normalized Raman spectra of the extruded glasses

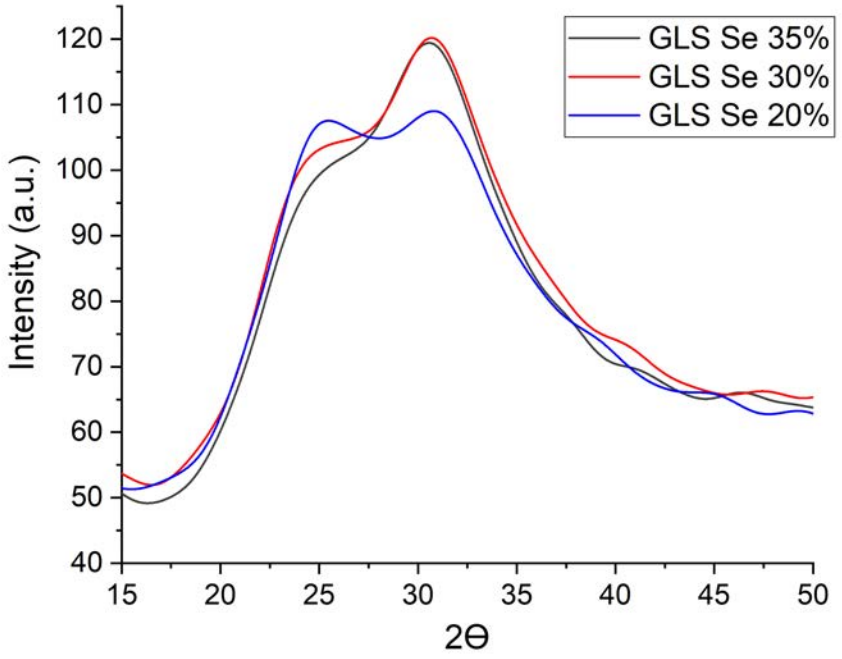

FIGURE 6.38: XRD spectra of the extruded glasses

6.9 Conclusions

The thermal properties of the family of GLS-Se glasses can be exploited as predicted in previous studies, and this opens up the possibility of producing glass rods and structured preforms for fibre drawing. This helps us to get closer to achieving the desired goal of obtaining an optical fibre from these chalcogenide glasses and to further exploit their properties. This study shows that moulding a glass, in this case extruding, is not a simple straightforward process. The intrinsic characteristics of the glasses indicate the parameters that might be useful for the process (i.e. softening point) but deny the possibility of predicting the behaviour of the glass through every step taken. A complete methodology had to be developed to be able to extrude GLS-Se glass rods and preforms, throughout a combination of a literature review and an experimental approach. This study also shows that the optical, thermal and mechanical properties of the extruded glasses correspond to the ones already demonstrated in their bulk form. Optically there was an effect of having less transmission (up to 5%) and a loss between 10 to 12 μm, which could mean that during extrusion there might be some mass loss resulting in a

reduction in Se content due to the unpurged extrusion apparatus. Future work might include isolating or modifying the extrusion apparatus to further improve the quality of the extruded glass, using a different type of material for the billet container and adding steps during the process to keep impurities to a minimum level.

Chapter 7

GLS-Se fibre drawing from extruded rods and preforms

7.1 Introduction

The fibre drawing process for chalcogenide glasses is performed using previously produced glass and rods and structured preforms, produced by extrusion. The principle behind drawing this family glasses into an optical fibre, as seen in chapter 4, follows the same technique as any other known glass [159, 223]. A glass rod is set into a furnace, temperature is raised above the softening point and then the glass is drawn into a suitable optical fibre diameter [224] depending on the application, the geometry and dimensions might vary. Initial thoughts indicated that this process was straightforward as the thermal properties of GLS-Se based glasses have been studied previously [54], and theoretical results have been pictured, making this family of glasses suitable for fibre drawing.

In the past other chalcogenide glasses have been drawn into optical fibres, with different results [225]. An advantage of this type of glasses over silica based glasses, is their feasibility to be drawn into fibres at relatively low temperatures [226], making the process itself simpler and more flexible. The main challenges for chalcogenide glass preforms are the tendency to crystallization [227], as its softening point is close to the crystallization temperature, necessitating the need to reduce the time consumed in the process to avoid promoting nucleation [228] while the glass rod is being heated. Also, the viscosity curve is steep [229], so variations in temperature need to be avoided to have a successful process outcome.

Some theoretical and practical results of previous thoughts and experiments [230] have considered chalcogenide glasses with some oxygen content [231], rods and preforms directly produced from bulk samples [232] and with no imperfections within the glasses. These aspects have helped in the obtaining reliable GLS based optical fibres [135]. As seen in the previous chapters of this work, GLS-Se glasses have been produced and tested before [5] but this was the first time that it is was shown that this family of glasses can be exploited into rod and preform production and subsequently drawn into fibre.

In this chapter we verify that the quality of the glass rod, or structured preform, is a key feature to exploit the fibre drawing process. Chapter 6 shows the difference between preforms of good and poor quality, both were drawn into optical fibres and as expected poor quality preforms showed a high tendency of crystallization or were even unable to produce a continuous fibre drawing process. This chapter explains the steps that were taken to produce an efficient process, from being unable to produce fibre to being capable of producing optical fibre in a non-stop process from the very beginning to the end of each preform. Proving this, that GLS-Se glasses can be exploited in an optical fibre form, sets the beginning of the exploration in this chalcogenide glass family in further applications.

7.2 Rod and structured preforms preparation for fibre drawing

As seen in chapters 5 and 6, each glass sample must undergo some preparation steps before they are suitable for further processing. This same occurs to both the extruded rods and structured preforms. Each extrusion delivers between 15 to 26 cm of extruded glass depending on the volume of the glass billet. The fibre drawing tower furnace configurations has been optimized to accept rods around 10 cm in length which is optimum to be able to maintain control over the samples. This means that each glass rod to be drawn needs to be cut to a suitable length (Fig. 7.1), and notches are produced in both ends to be able to hold the extruded rod inside the furnace and to add the extra weight to promote the necking of the rod to start the fibre drawing process.

FIGURE 7.1: Extruded glass rod of 10cm after being cut to fit the drawing furnace

The first fibre drawing attempts did not consider the surface quality of the extruded rods and structured preforms. Initial experiments only considered the post-extrusion crystallization on the surface to be detrimental for further processing, extrusion attempts showed a variety of results depending on the quality of the glass billets. As explained in chapter 6, apart from using the correct temperature, the quality of the billets affected the quality of the extruded rods. Some of them came out of the die scratched or contaminated, which led to further thoughts about how to overcome the surface imperfections. First thoughts were to repeat the experiments and not use said extruded rods, as some higher quality, extruded rods were obtained (Fig. 7.1) with no apparent surface imperfections and just the strays produced by the friction between the die and the glass flowing outwards. Some of these transparent rods with no surface crystal could not be drawn, as they showed heavy crystallization and weak fibre after drawing. These unexplainable results demonstrated that apart from the use of the correct temperature, the surface quality of the extrusion had some influence. In addition to GLS-Se extruded rods fibre drawing attempts some, GLS (65:35) polished professionally by Crystan®were drawn, with various results, but there was no breakage when the necking started, and crystallization was only seen due to excessive temperature. It is important to note that these trials were done to obtain the skills for fibre drawing, and such attempts are not considered part of the outcome of this work as it is well known that poor surface quality promotes crystallization, the microscopical strays can act as the volume needed to act as a nucleus [233]. Further studies, in how to determine the critical size of particles and nuclei for crystallization to be heavily promoted in GLS-Se glasses needs to be carried out. To overcome any imperfection and produce a smooth surface to assist fibre drawing, each extruded rod was polished down to 1 μm of grit size. For this, a small in-house constructed lathe (Fig. 7.2 and 7.3) and Thorlabs®diamond films were used. This added step

modified completely the surface (Figs. 7.4 and 7.5) up and enhanced the outcome of fibre drawing. One disadvantage though, is that this step was not automated [234] and was done entirely by hand, so a lot of expertise needs to be obtained by practice before being able to produce reliable rod polishing for fibre drawing (Fig. 7.6).

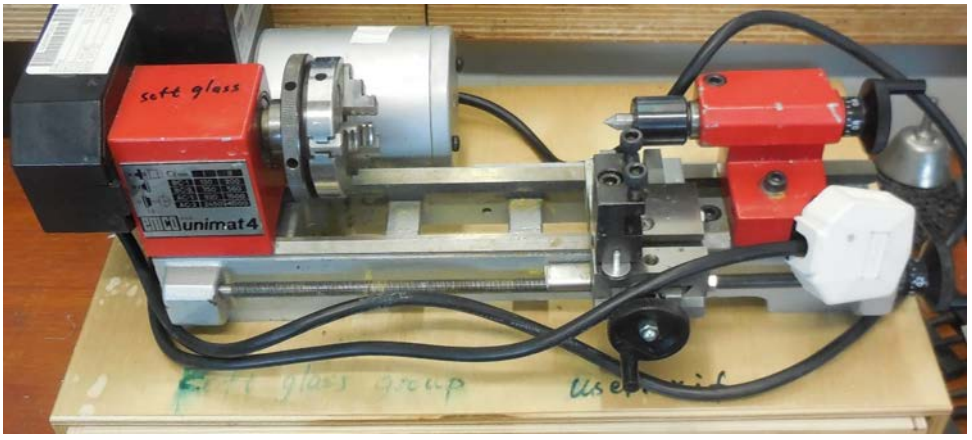

FIGURE 7.2: Lathe for rod polishing

FIGURE 7.3: Extruded rod during the rod surface polishing step

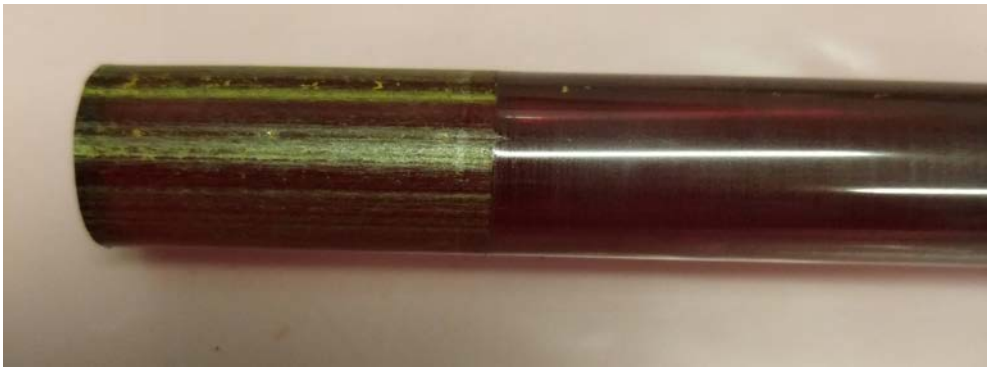

FIGURE 7.4: Surface scratched rod showing the benefits of rod polishing

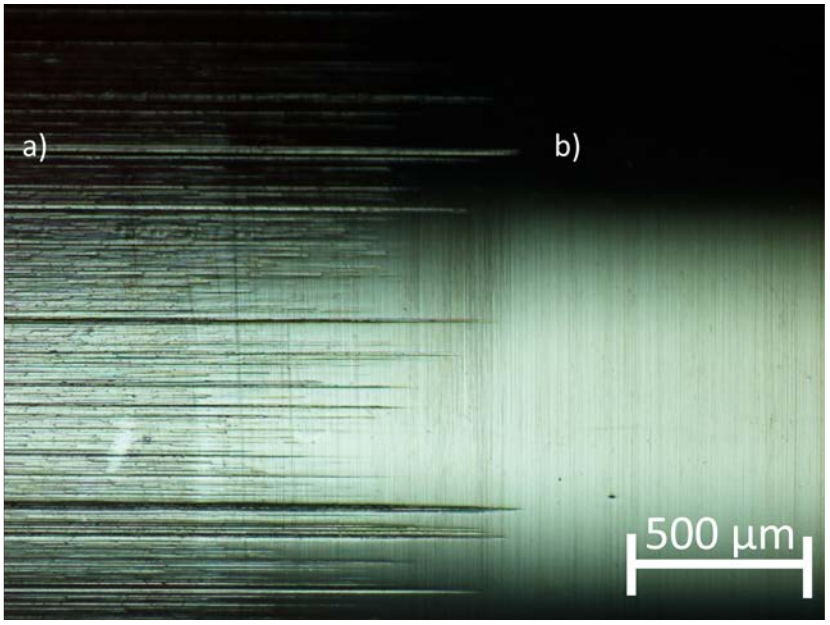

FIGURE 7.5: Extruded rod showing a) unpolished and b) polished surfaces down to 1μm of grit size

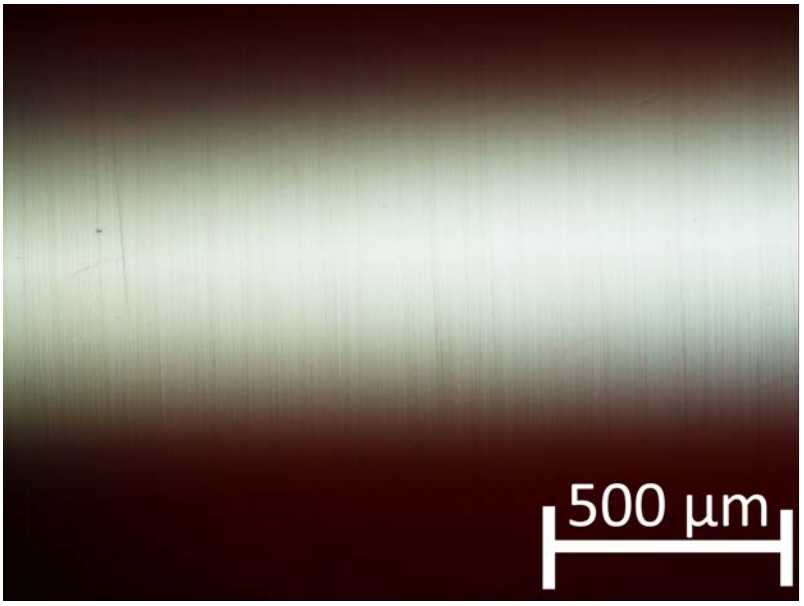

FIGURE 7.6: Completely polished extruded rod surface

After the polishing is finished, another cleaning step is performed, with the ultrasonic bath and isopropanol to remove any residual ethanediol left on the surface. The cleaned rod, or structured preform, is attached to the silica holder and a weight of 80 g is place in the other end, helping to maintain the rod in a straight position and to aim the necking in the fibre drawing process (Figs. 7.7 and 7.8).

FIGURE 7.7: Extruded and polished rod attached to the silica holder and the 80 g weight

FIGURE 7.8: Extruded and polished rod of 11 cm ready to be set on the furnace, surface quality is clearly seen

The next step is to place the preform holder, extruded polished rod (or structured preform) and weight vertically in the fibre drawing tower furnace (Fig. 7.9). This step is crucial as it must be positioned without touching any element of the furnace, as they can be misplaced, affecting with this the process. The rod needs to be positioned exactly in the middle of the furnace, were the centre of the rod is concentric to the centre of the furnace, as this assures an even surface and volume heating of the rod [235]. Any misplacement means that part of the rod gets hotter and this produces a viscosity mismatch; this surface thermal difference is also translated as a need to supply more heat to soften the less hot glass region, incrementing the chance of crystallization.

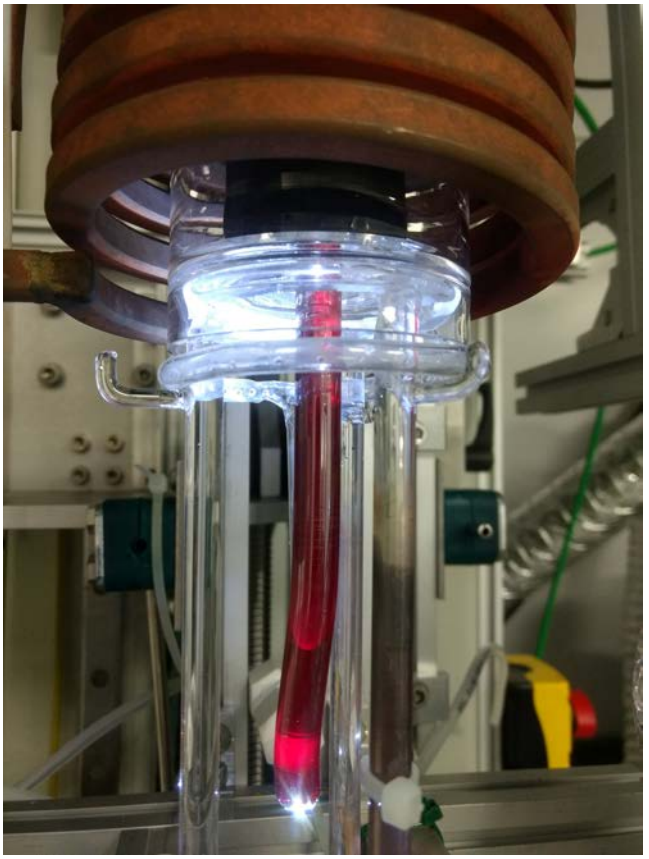

FIGURE 7.9: Structured extruded and polished preform, set in the middle of the furnace before fibre drawing

7.3 Fibre drawing tower and GLS-Se glass rods considerations

Previous studies [236] have proposed that for chalcogenide glasses the best approach to have a successful fibre drawing process is to increase the temperature beyond the softening point and once it is necking decrease the temperature to increase the viscosity and have a steady and stable process. However, this process is problematic for GLS-Se based glasses as their tendency to crystallize is high and fibre drawing has never been tried before, thus affecting the whole process. During the whole experiment it was shown that the best approach to obtain the correct temperature, depending on composition, is to start at a low temperature and gradually increase it until the glass is soft enough to start the process. The first time this approach takes place, it must be noticed that the time required is considerable and this might produce some crystals, but after the ideal temperature

is obtained, this temperature needs to be set as the initial temperature and the time used in the whole process is reduced, as seen in chapter 6 with the extrusion process.

Steps for a successful fibre drawing depends on the composition and type of glass. For GLS-Se extruded rods of 10 mm in diameter there are some helpful guidelines that can help exploit the current equipment capabilities (i.e. fibre drawing furnace and tower, Fig. 7.10):

- Obtain the T_g by DTA of the glass to be drawn.
- Set the temperature in the drawing tower software around the T_g.
- The ramping heat rate of the furnace is: 100 °C/min.
- Once the desired temperature is reached wait until the neck is formed.
- For very first trial of a new composition, increase the temperature maximum 10 °C and wait 2 minutes.
- Keep increasing by the same rate until that the preform starts necking in a slow but constant motion, a neck should be clearly seen
- Stop the temperature increase when a steady slow motion is seen.
- Start the feed rate at 0.5 mm/min.
- Necking should be clearly seen and continuously progressing.
- The decrease in rod/preform diameter should be clearly seen.
- Remove the weight and pull by hand to reach the drum.
- If fibre needs to be coated, wait until the diameter is small enough to go through the coating cup die.
- Check with the microscope that the fibre is aligned in the centre of the die to avoid clusters of coating.
- Set the UV lamp power accordingly, but not above 50% of its power.
- Whether it is coated or not, wait until the tip of the drawn glass reaches the drum.

- Start the drum at 1 m/min.
- Attach the fibre to the drum with sticky tape.
- Check the tension of the fibre and adjust with the temperature and drum speed.
- Check with the diameter monitor the diameter of the fibre.
- Adjust feed and drum speeds accordingly.
- Once the diameter starts decreasing in a fast rate or is below 100 μm without moving any parameter, preform is close to finish.

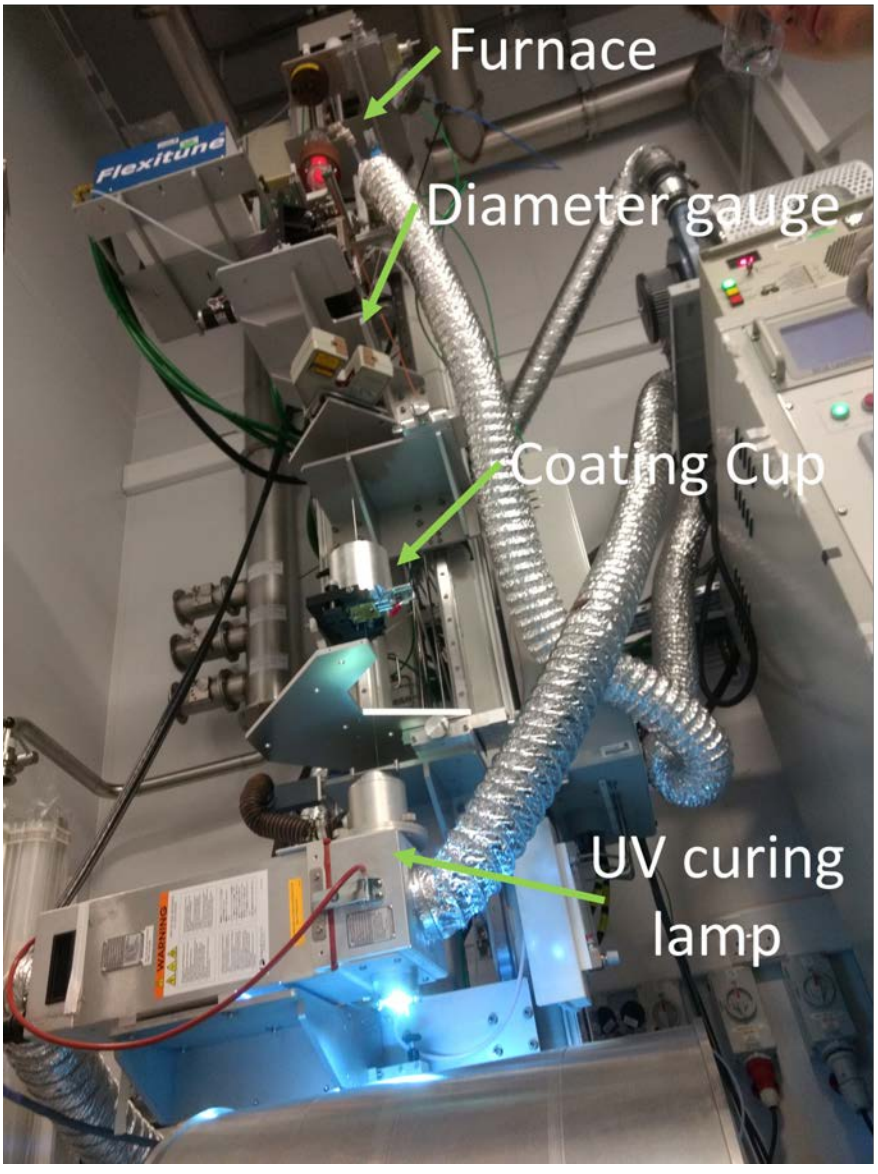

FIGURE 7.10: Novel Glass Group fibre drawing tower at the Optoelectronics Research Centre

7.4 Initial fibre drawing experiments with GLS samples

In order to obtain the expertise and skills required to manipulate the drawing process and understand the behaviour of GLS based glasses, an initial test was performed in an extruded GLS (60:40) tube following the guidelines presented in the previous section, and further refined as described in the following sections. Considering the calibration offset of 50 °C and the crystallization temperature of 681.2 °C [1] the approach chosen was to use a high temperature (800 °C) and then reduce the temperature after the necking was observed. As seen in Fig. 7.11, the lack of expertise plus the use of an incorrect temperature led to a crystallized surface. Although temperature proved to soften the glass and stretch it while this, it was also seen that crystallization occurs from outside to the centre of the glass (Fig. 7.12). This failed attempt set the initial considerations that high temperatures, shorten the time of the process but if not done correctly there is a high chance of failure, as this approach needs to have the correct temperature and skills so that no mistakes are made.

FIGURE 7.11: Unsuccessful GLS extruded drawing attempt

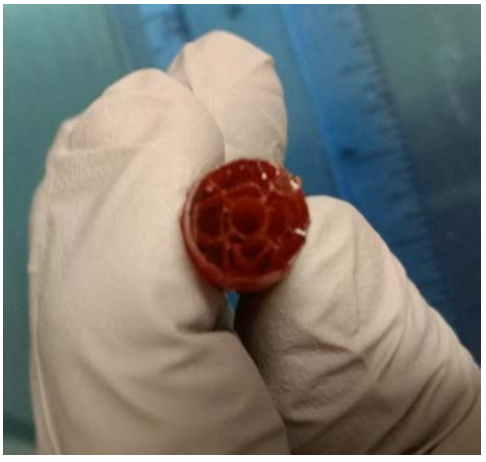

FIGURE 7.12: Transparent glass in the inside, surface crystallized

7.5 Fibre drawing GLS-Se extruded glasses failed attempts

After this initial trial for the next attempts it was decided that in order to obtain the correct temperature and avoid crystallization, accordingly to the DTA and TMA (chapter 6) a low temperature was chosen (530 °C, viscosity $10dPa \cdot s$). This would be the basis to start increasing step by step the temperature until the necking started to show, this approach was slower and crystallization was experienced due to the time consumed, but every new attempt was set to a gradual higher temperature that got closer to the optimum temperature necessary for a continuous process with no crystallization. The first temperature that showed a necking was at 660 °C (viscosity $5dPa \cdot s$) for a GLS-Se 35 mol%. The glass started to flow naturally, but once the tip was outside the furnace, no further elongation was produced. In an attempt to promote the stretching of the glass the feed was started at a speed of 0.5 mm/min and some force was applied manually downwards, trying to stretch the glass and with this reduce the diameter of the rod, so that the temperature applied would be enough for a smaller volume of glass [237]. At this point no fibre drawing was obtained but caning was achieved, although with some surface crystallization. On a trial to avoid further crystallization the feed speed was increased, as this would also improve the cooling rate. The problem is that by increasing the feeding speed at a wrong temperature, there is no sufficient time to allow the glass to soften and it suffers from a heavy tension that could crack the glass rod, also it was seen that a fast change in temperature results in thermal shock [238] (Figs. 7.13 - 7.17).

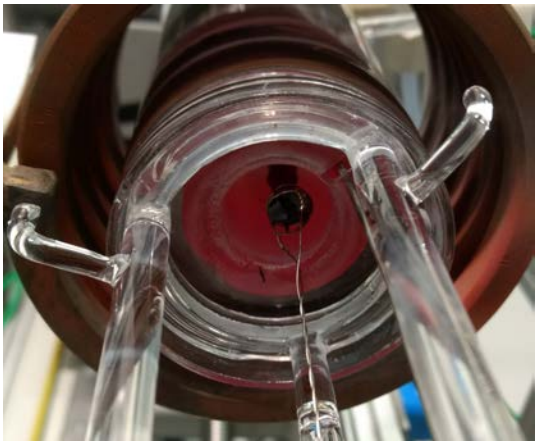

FIGURE 7.13: Glass rod necking naturally after being held at 660 °C for more than 30 minutes

FIGURE 7.14: Glass rod coming out the furnace showing the necking and before any crystallization occurred

FIGURE 7.15: GLS-Se cane after cracking due to a high tension as the temperature was too low for fibre drawing

FIGURE 7.16: GLS-Se glass rod showing an amorphous phase and transparency proving that the furnace does not affect directly the glass in the temperature is low and it is not exposed to heat for a long time

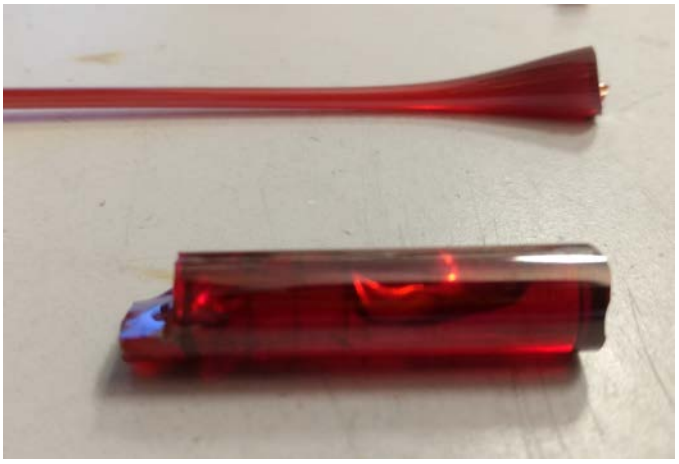

FIGURE 7.17: Broken GLS-Se glass rod showing thermal shock after suddenly taken out of the furnace

Every new trial showed new challenges to be addressed but as explained in chapters 5 and 6, the most detrimental was the quality of the glass rods and structured preforms produced by external contamination that was added during the extrusion process, such as carbon particles or crystallization from the scratched surface. The improvements in the quality of the optical fibre process came along with the improvements of the quality of billets production and the extrusion process itself. To further improve the process and to obtain as much feedback as possible, firstly it was essential to enhance each process step individually to ensure that the material and equipment were exploited to their highest capability. So afterwards it was only a matter of pursuing the skills needed to obtain a reliable process and to fully understand every parameter comprised within this work. In said search for the best available parameters, some steps forward were realized such as several meters (<20 m) of continuous drawn fibre, even with heavy crystallization (Fig. 7.18). Any imperfection on the surface or inside the glass (i.e. carbon particles or crystals) acted as a mechanical weakness [239], and complete glass rods and structured preforms, as well as optical fibre were brittle, broke and impossible to handle (Fig. 7.19).

Further studies and experiments had to be carried to understand this mismatch between theoretical and practical previous works [53, 54, 173] and the initial impossibility to obtain fibre from GLS-Se rods and structured preforms.

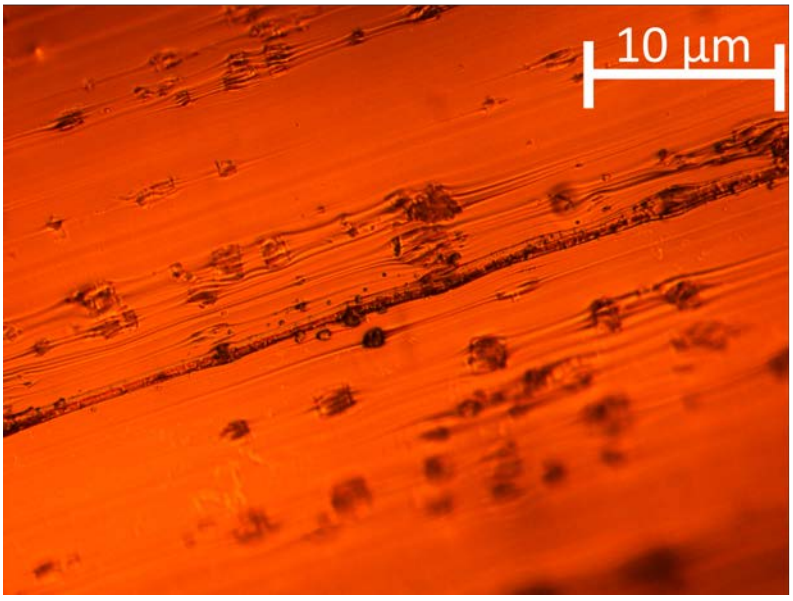

FIGURE 7.18: Heavily crystallized surface after fibre drawing

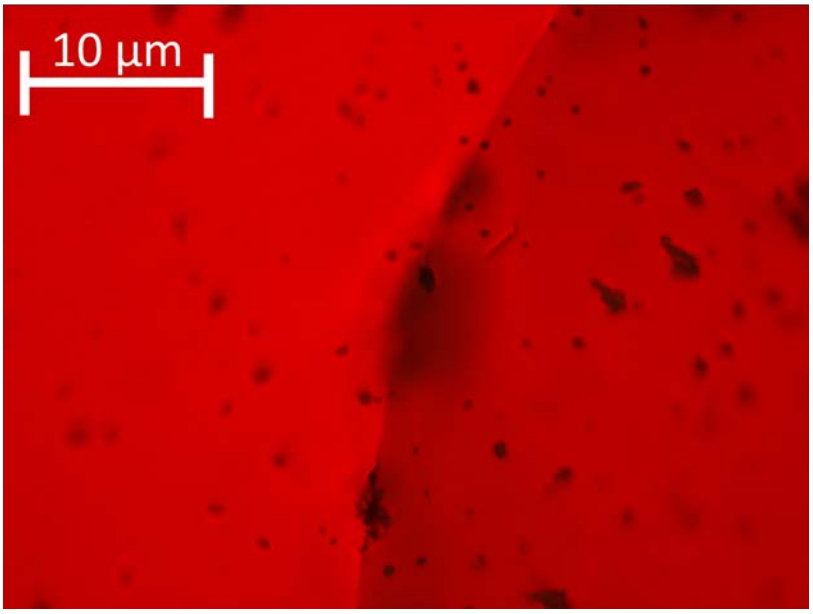

FIGURE 7.19: Structured fibre where crystals and carbon particles are clearly seen

7.6 Thermal studies to understand the behaviour of GLS-Se glasses during fibre drawing

As commented previously, the full scope of this work comprises several processes and steps that are interlinked. Understanding the parameters that belong to

each one and how every action affects the further processing or manufacture is essential. To further understand whether the steps were correctly executed and to discard any possible non-dependent variables, extra thermal studies (DTA and TMA) were carried for extruded GLS-Se samples for which the quality was already proved to be the best at that time. These studies comprise of the same procedures described in previous chapters but using different heating ramping rates to have a better picture about the thermal and mechanical behaviour of the glass and check if these parameters remain consistent or there was a different behaviour as a function of the heating rate..

As seen in Fig. 7.20, if the heating rate is increased the crystallization peak is displaced to the right, this variation is due to the nature of the activation energy of the glass [240]. This is of importance as it shows that the possible displacement of crystallization peak relies fundamentally upon the heating rate, as the glass relaxes isothermally towards a new enthalpy equilibrium that is temperature dependant [241].

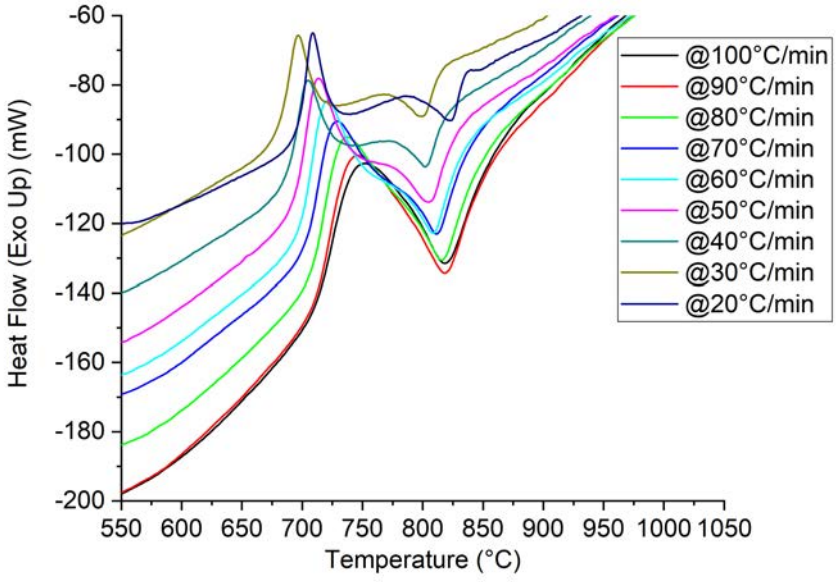

FIGURE 7.20: DTA for an extruded structured preform for different heat rates

Another aspect to consider in the fibre drawing process is the viscosity, as it is temperature dependant. To understand if there is a change in viscosity related to the ramping rate of the fibre drawing furnace (100 °C/min), a TMA was performed with different heating rates. As seen in Fig. 7.21, a slow heat rate is preferred

as it ensures all the volume of the glass is heated uniformly compared to a higher heat rate where the viscosity curve is steeper. The explanation behind this can be described by using the equation 2.4, as the ramp rate is increased so does the difference in position (Δf), which is inversely proportional to the viscosity (η). This results in a situation where the surface of the glass presents a temperature difference compared to the inside [167], producing with this an undesired effect where the surface is ready to be drawn while the inside remains at a higher viscosity.

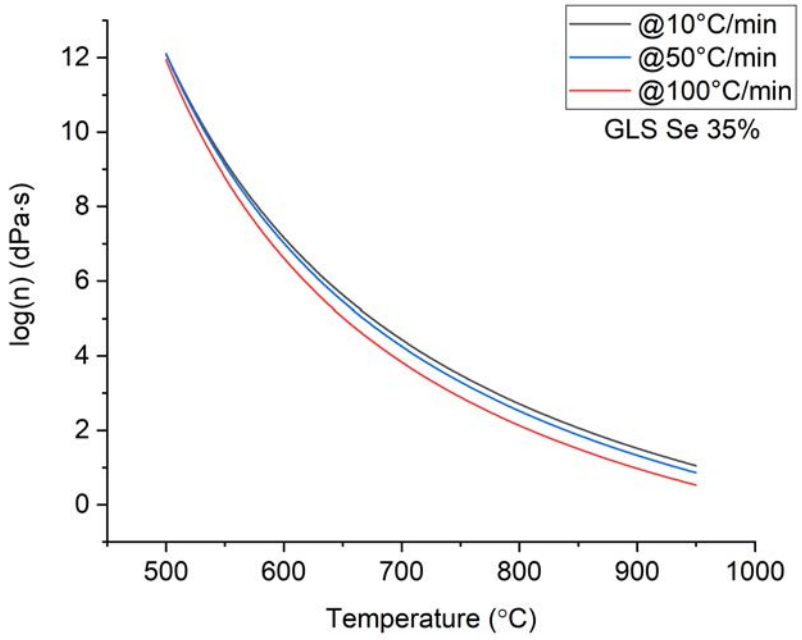

FIGURE 7.21: TMA for an extruded glass rod for different heat rates

These extra thermal and mechanical studies in extruded glass had the objective to simulate the behaviour of the glass in the drawing tower. The value of this information is more theoretical as the skills to obtain reliable optical fibre remain practical, but these extra studies helped understand that the ramping rate can be used in favour of avoiding crystallization in the same way as using lower temperatures, as the viscosity and crystallization peak values are displaced.

7.7 GLS-Se optical fibre drawing from glass rods of a single composition

Thermal and mechanical studies (chapter 5 and 6) in conjunction with previous fibre drawing attempts, including several failures, demonstrated that each composition requires specific parameters (i.e. temperature) and expertise. The biggest challenge with this family of chalcogenide glasses is that there is no previous literature that could explain in depth the behaviour of the glass when they are thermally treated during processing (i.e. optical fibre drawing). One of the problems encountered is that once the temperature is adequate, and set in the furnace, the process needs to go as fast as possible to avoid crystallization while working with a viscosity suitable for optical fibre to be obtained. Therefore, there must be an extra compromise between the feed and drum speeds while controlling the tension of the fibre. This means that high tensions can be used if viscosity is in a value low enough to avoid mechanical stresses that could break the glass rod or fibre, during the optical fibre diameter control. After considering all these aspects, it is good to finally point out that the fibre drawing process does not occur in the actual hot zone (forming region), but it occurs in the already heated and viscous glass (draw-down region) [242], so at this point the cooling rate for the fibre becomes essential to avoid crystals and breakage from thermal shock (Fig. 7.22 and 7.23).

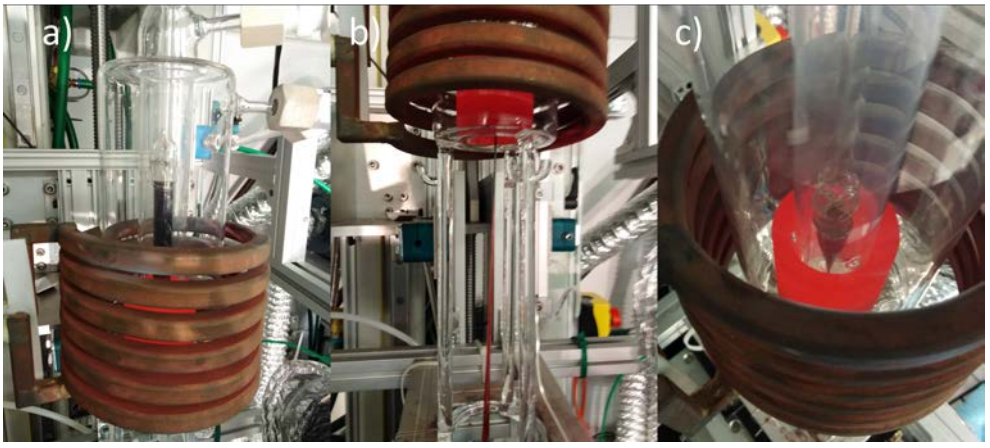

FIGURE 7.22: Fibre drawing process for GLS-Se glass rods where a) is the rod inside the furnace being heated, b) is the beginning of the fibre obtention, and c) the neck profile is clearly seen inside the furnace

FIGURE 7.23: First and last part of the extruded rod after fibre drawing, where the neck presents some surface crystallization due to the time consumed in the whole process

Before being able to draw structured preforms, the goal was to obtain optical fibre from single rod compositions, to verify the steps required and to address any challenge that might arise from the complexity of the process itself. As shown in chapter 6, three compositions of GLS-Se with 20 mol%, 30 mol% and 35 mol% of Ga_2Se_3 were produced in extruded rods and these were drawn into fibre. Temperatures between 780 °C and 800 °C (viscosity $2 - 4dPa \cdot s$) were used during the processes, and optical fibre with diameters between 200 μm and 250 μm and lengths (up to 50 m) where obtained (Fig. 7.24). To measure the losses and characterize the fibre (Figs. 7.25 - 7.28) the cut back method was used along with an optical spectrum analyser (OSA) and an ARCoptix®portable FTIR. Losses vary through compositions, and further research must be carried to determine if the process itself increases the losses or the raw materials have a direct relation with them, however, it is demonstrated that extruded GLS-Se glass rods can be drawn into optical fibre.

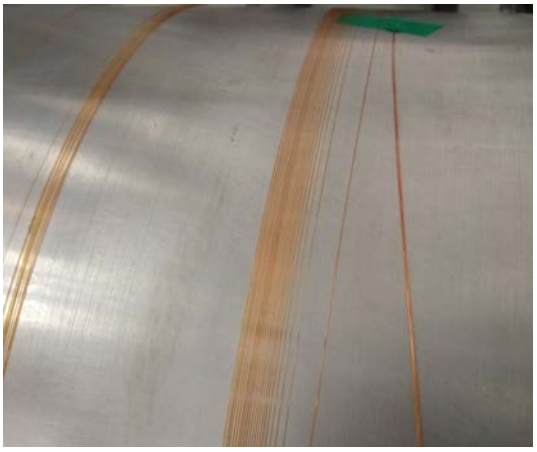

FIGURE 7.24: GLS-Se optical fibre collected in the drum after the fibre drawing process

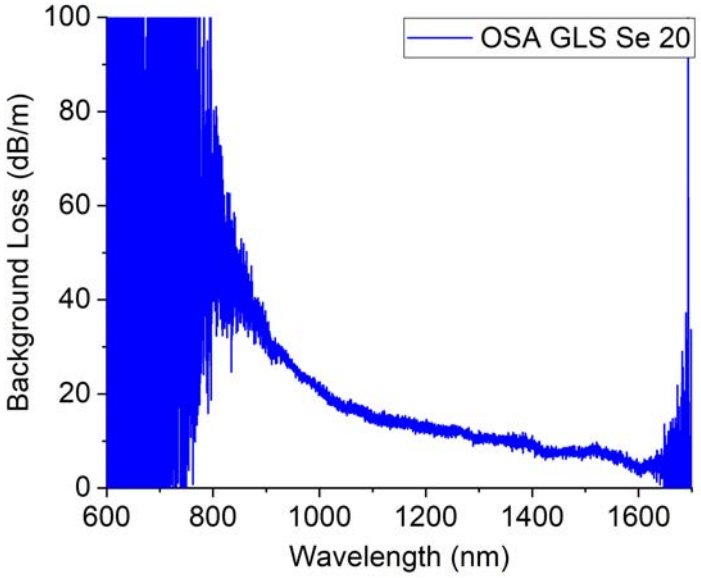

FIGURE 7.25: GLS-Se with Ga_2Se_3 20 mol% optical fibre losses (600 nm-1.7 μm)

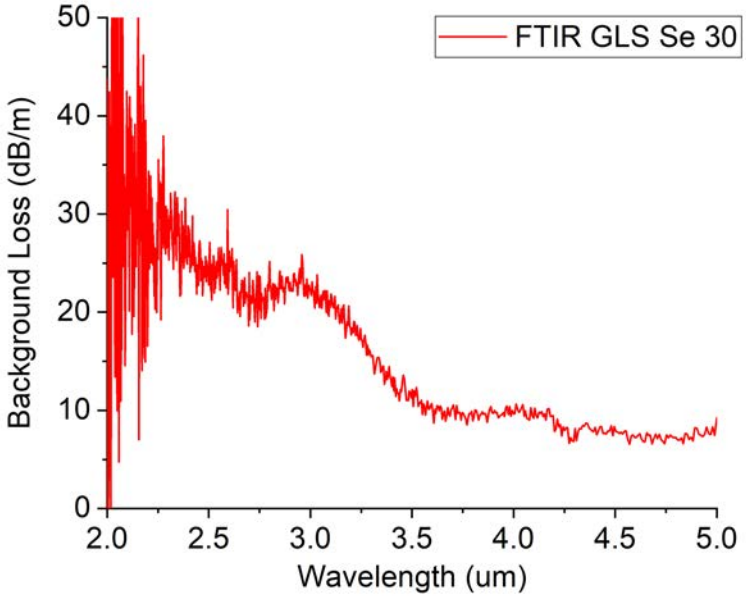

FIGURE 7.26: GLS-Se with Ga2Se3 30 mol% optical fibre losses (2-5 μm)

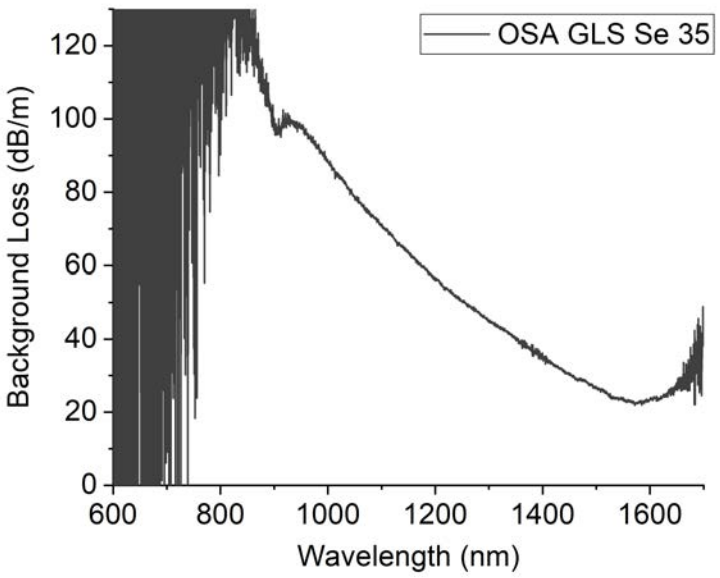

FIGURE 7.27: GLS-Se with Ga_2Se_3 35 mol% optical fibre losses (600 nm-1.7 μm)

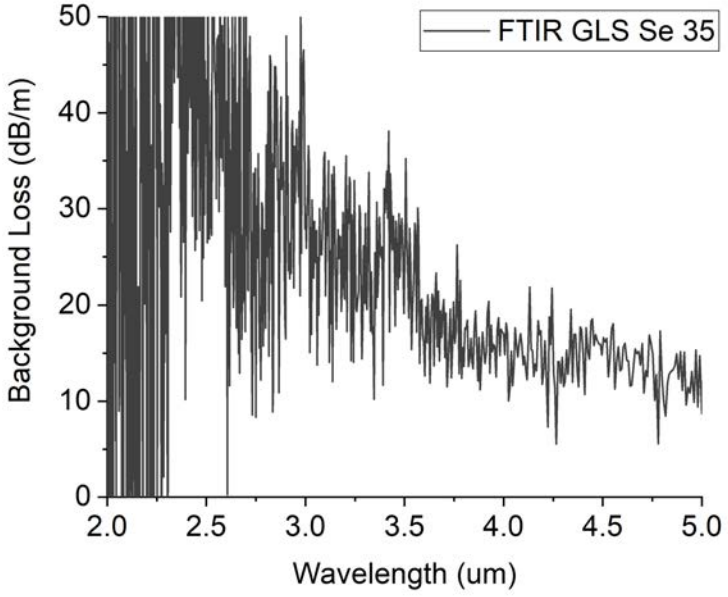

FIGURE 7.28: GLS-Se with Ga2Se3 35 mol% optical fibre losses (2-5 μm)

7.8 GLS-Se optical fibre from structured preforms

Structured preforms were fabricated (chapter 6) using GLS-Se glasses with Ga_2Se_3 concentrations of 35 mol% and 30 mol%, for the core and cladding respectively. As these compositions are thermally and mechanically similar the decision was made to establish a middle ground and use a maximum temperature of 710 °C and a minimum of 690 °C (viscosity $4 - 4.5 dPa \cdot s$). These are the lowest temperatures ever used, and the approach taken was to wait until the neck was produced and then to start decreasing the temperature by 2 °C until the fibre was attached to the drum (Fig. 7.29). Temperature was only decreased, and drum speed modified to adjust tension. The last three structured preforms fabricated included every single polishing and cleaning step available to increase the chances of success. Being meticulous paid off as the success rate for fibre drawing was of 100%, this means that from when the fibre was attached to the drum for collection the process was never stopped, and no breakage was produced at any moment until the glass was finished. For the first time continuous and uninterrupted long lengths (up to 220 m) of GLS-Se optical fibre were produced, with the best surface quality to date (Figs. 7.30, 7.31 and 7.32).

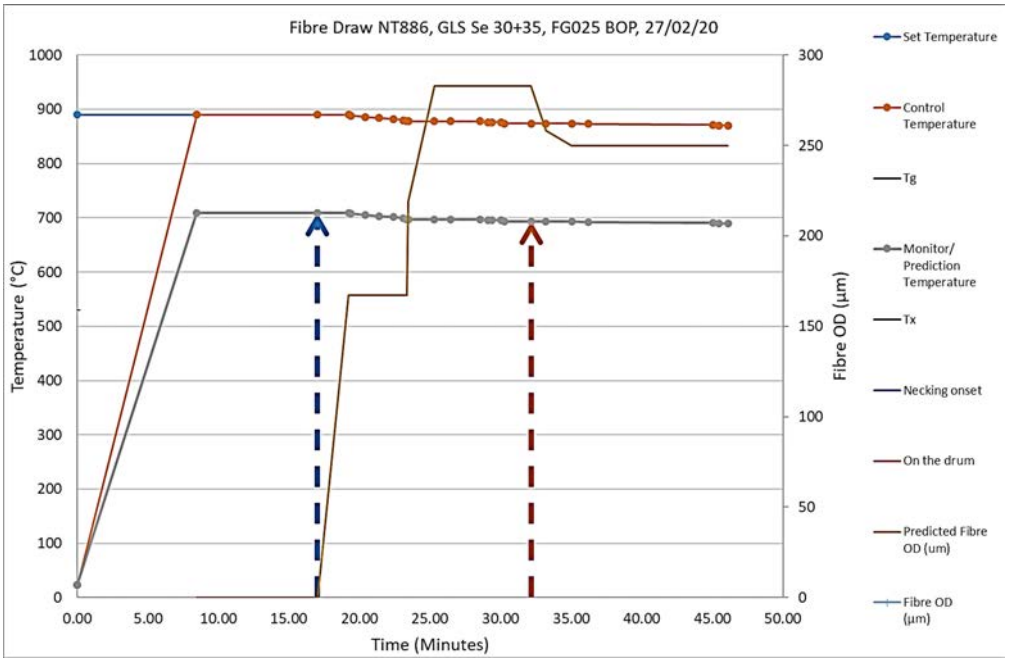

FIGURE 7.29: Example of a fibre drawing timeline to observe the behaviour of the process (figure designed by Bruno Moog for the Novel Glass Group) *Note: image quality is a result of the spreadsheet it was extracted from*

FIGURE 7.30: GLS-Se structured optical fibre being transferred from the drum to a bobbin

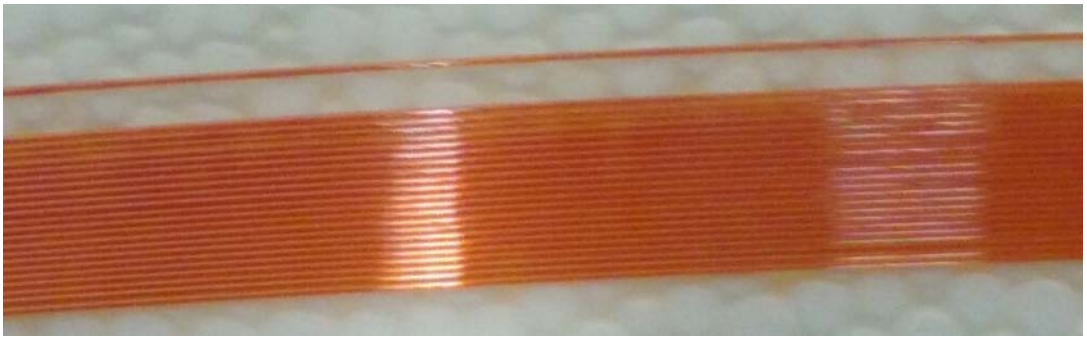

FIGURE 7.31: Close up of GLS-Se structure optical fibre

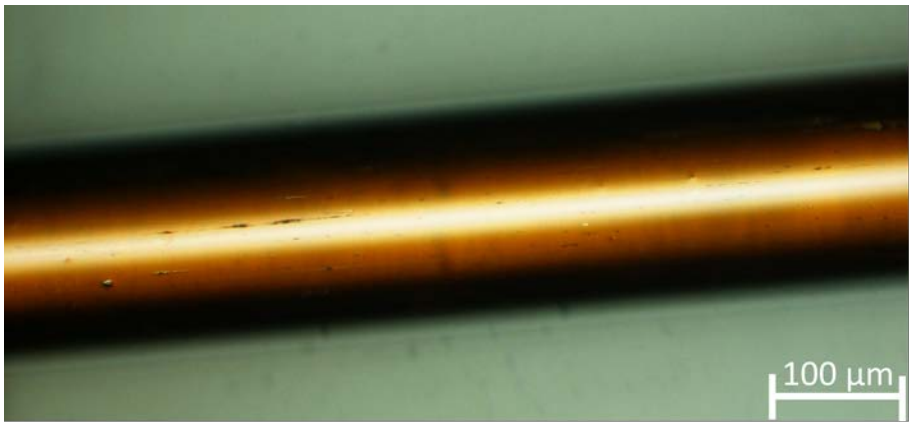

FIGURE 7.32: GLS-Se optical fibre of 210 μm in diameter, with the lowest surface defects ever achieved

In previous chapters it was explained that one future goal to achieve is the control in the core diameter for GLS-Se structured optical preforms. Therefore, the same applies for GLS-Se structured optical fibre where the core diameter varies depending the section of the preform that is drawn into a fibre (Figs. 7.33). Same as with single composition glass rods, the obtained fibre diameters are between 190-250 μm. These proof of principle results can lead to the obtention of thinner fibre and to achieve smaller diameters. This can establish a possibility of decreasing the losses in the fibre [141]. Characterization of the fibres used the cutback method and an ARCoptix®portable FTIR, for clarity only the lowest values obtained are shown (Fig. 7.34). The losses shown in this graph portray an increasing loss tendency with increasing wavelengths, this could be an effect of the non-constant core diameter over long lengths of fibre used to measure the loss by the cut-back method. For further studies and research that include the fabrication of optical fibre with a constant core diameter this effect could be affirmed or denied.

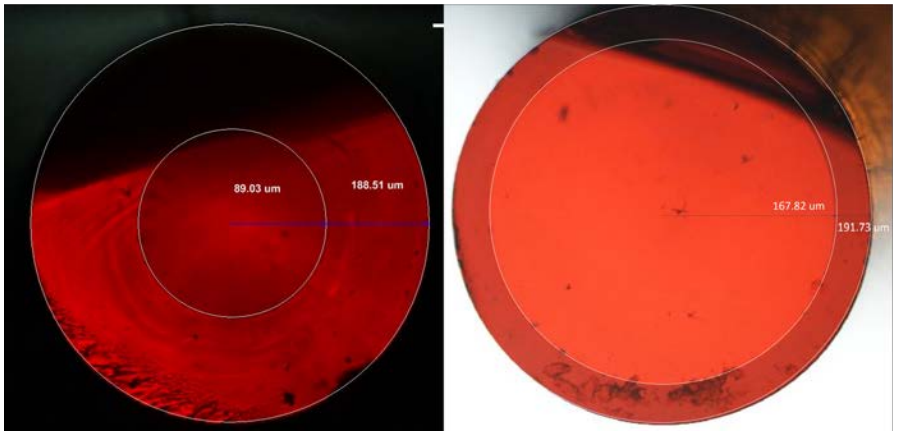

FIGURE 7.33: Structured GLS-Se optical fibre showing different core diameters

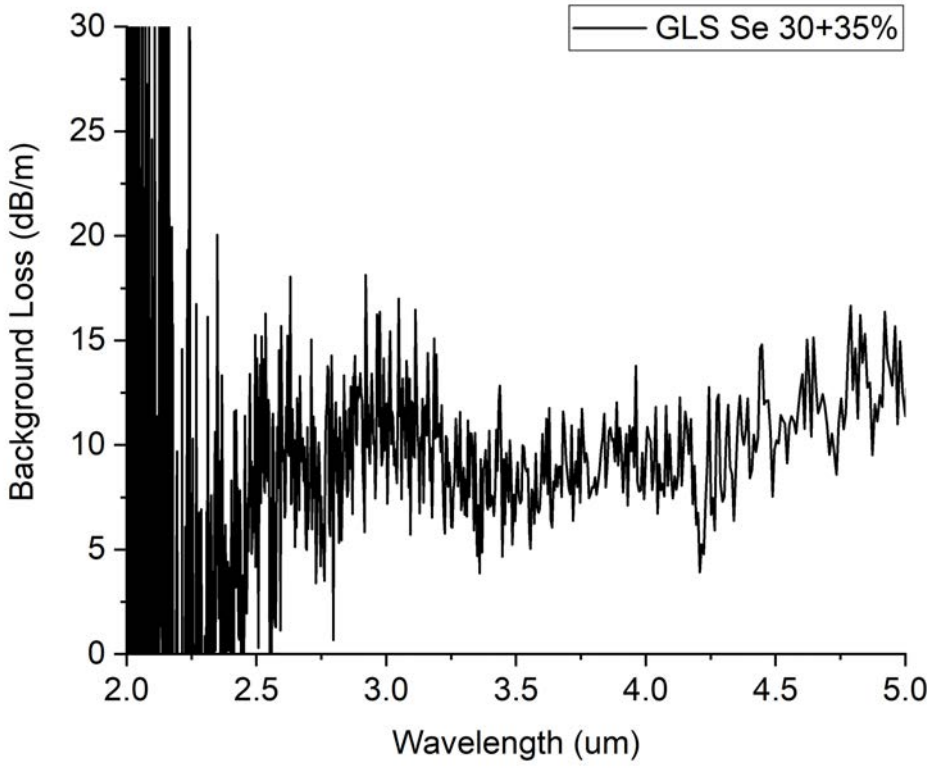

FIGURE 7.34: Structured GLS-Se optical fibre losses

7.9 Conclusions

GLS-Se glass rods and structured preforms have been drawn into optical fibres for the first time with losses of 10-15 dB/m. This achievement required a solid practical expertise of the thermal and mechanical characteristics of these chalcogenide glasses. The main challenge to draw GLS-Se glasses into an optical fibre is to maintain their original bulk properties, as additional thermal processing could modify their structure and processing steps might add contaminant particles. However, the results shown in this work prove that GLS-Se optical fibres are now an option to continue exploring applications in the optics industry, such as high-power fibre lasers, IR light confinement, and leaves space for improving the transmission at longer wavelengths to exploit in full the properties of GLS-Se glasses as optical fibres.

Chapter 8

Final remarks and future work

GLS-Se based glasses are a desirable optical material to be exploited in several applications, some of which require an optical fibre geometry. This interest has led the research to decide which approach is the most suitable to transform bulk glass into a rod or preform, while maintaining its optical, thermal and mechanical properties. These properties are crucial as any change in them means that the glass will not be reliable for optical fibre applications and would mean that the process itself is not ideal.

GLS-Se glass thermal characteristics have opened the possibility of using extrusion to modify its geometry, as they require lower temperatures compared to silica-based glass. Temperature is a significant parameter, temperatures above the crystallization point must be avoided but still suitable for structure modification, i.e. Extrusion or drawing as a fabrication process, it is therefore necessary to develop a practical expertise by understanding the thermal and mechanical behaviour of the glass along with the previous analysis to delimit the useful range of temperatures for extrusion.

For a reliable process, a complete methodology must be developed, including steps that do not detriment the quality of the glass. For GLS-Se glass billets it was proved that after the melt-quenching technique and annealing process, the billets need to undergo a polishing step. During this work it was seen that polishing provides extra surface cleaning, as it can remove any possible carbon particle adhered to the surface during the glass fabrication. Particles of any kind are detrimental during the extrusion process as they can act as a nucleus and promote crystallization, even if temperatures are low enough and should not modify the

glass phase. Moreover, polishing provides the billets with an optical finish that is useful for refractive index measurements to verify their conditions and to establish a difference between compositions for a structured preform. It is to be noted that part of the future work regarding the elimination of carbon particles includes further research to investigate if the 24 hours melt-quenching process does not assist in delivering inclusions of carbon within the bulk glass that could promote crystallization during the extrusion or fibre drawing processes.

As polishing was set as a step of the process, cleaning the lubricant used for this purpose was needed. Manual cleaning of the billets seemed impractical as there is no guarantee that the process is repeatable, therefore with the help of an ultrasonic bath and isopropanol any ethanediol residual was removed. This cleaning step also provided the glass billets with dust removal.

Extrusion can be as simple as setting a temperature and a load, but the goal of this project was to obtain the optimal conditions for a successful process. GLS-Se thermal and mechanical analysis provide a range of working temperatures useful for extrusion but do not show the effects of each temperature or point out the best one. Therefore, a set of experiments were carried out to identify any temperature that would be detrimental for the billets. It was proved that viscosity curves are only an aid for the process as they do not take into account the whole volume and thermal behaviour of the glass, so the best approach to define an extrusion temperature is practical. Low temperature and high viscosity turned out to be the ideal conditions for non-crystallized and transparent glass rods and preforms. These conditions, in addition to the polishing and cleaning steps, improved the process quality and defined the minimum parameters needed for the future of GLS-Se extrusions.

Optical, thermal and mechanical parameters for extruded GLS-Se rods and preforms, showed that there was a maximum of 5% loss in transmission, for one composition, and an absorption peak between 10 to 12 μm, which means that during extrusion there might be some mass loss resulting in a reduction in Se content due to the unpurged extrusion apparatus. Refractive index, Raman spectroscopy and XRD measurements were carried out to corroborate the maintenance of the amorphous phase and whether the different compositions tested were in accordance with pre-extrusion and previous GLS-Se glass studies. All measurements and analyses showed that extrusion does not affect the glass structure and that different concentrations of Ga_2Se_3 present their expected characteristics as stated

in previous research, with the difference that the more Se content in the glass billets, the higher the loss in transmission for the extruded samples.

The fibre drawing process also requires the use of thermal and mechanical analysis as an aid to obtaining a reliable process, but at each different composition, new practical skills need to be developed. For GLS-Se extruded rods and preforms, the lower the content in Ga_2Se_3 the easier it is to obtain optical fibre and the lower the losses that are presented. This might mean that the higher the selenium content, the more it interacts with the environment and could produce oxidation and therefore inclusions and crystals that increases the scattering. On the other hand, the more cleaning and polishing steps taken during the extrusion process and prior fibre drawing, the higher the quality of the glass rods and preforms obtained. This latter completely modifies the procedure and the possibility to obtain a successful fibre drawing process. During the necking region and the last section of the glass rod, heavy crystallization is presented as these sections are exposed to heat a longer time.

This works presents a complete study and methodology to successfully extrude and obtain optical fibre based on GLS-Se glass compositions. Future work needs to be directed toward obtaining lower losses and a complete crystal free optical fibre. Some ideas include the use of modified glass compositions or combining GLS-Se glasses with GLSO for structured preforms, to have a more thermal stable cladding to protect the GLS-Se core. The volume of the extruded rod plays a role in how much temperature and time is required to start and continue with the fibre drawing process. This means that reducing the diameter might allow the use of a lower temperature and less time, thus facilitating obtaining a completely transparent optical fibre.

Another future goal is the fabrication of single mode fibres, where the diameter of the preforms and fibres is controllable. Future work also includes modifying the extrusion apparatus to produce different type of core diameters and isolating it with a purged environment to verify whether the oxide absorption peak between 10 and 12 μm disappears. Finally, this work also opens the possibility for the fabrication of structured RE doped preforms and fibres, to further explore the characteristics and applications of the GLS-Se glass family.

Appendix A

Cast analysis of the stainless steel used for the billet container.

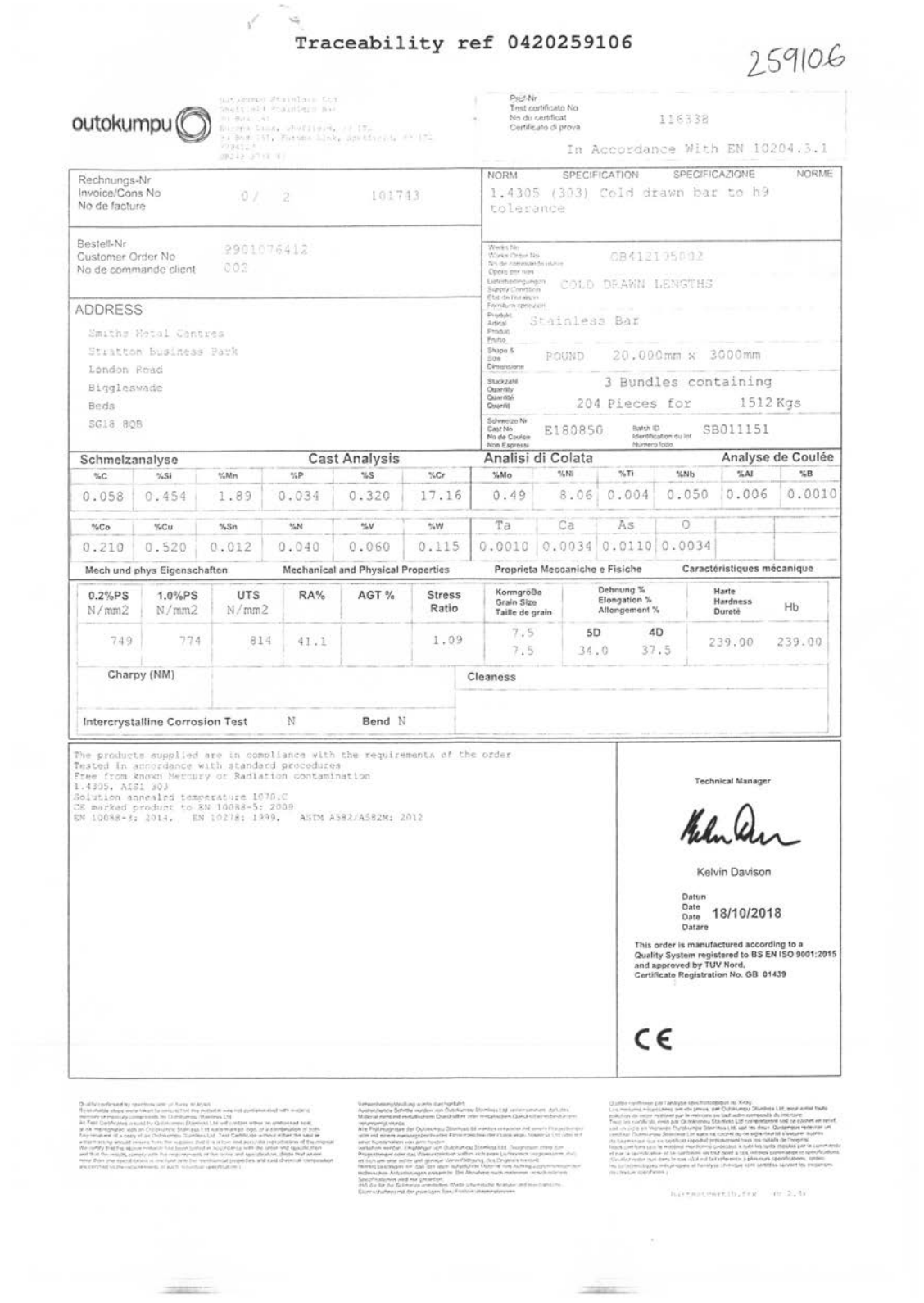

Traceability ref 0420259106

259106

outokumpu

Prod Nr
Test certificate No
No du certificat
Certificato di prova 116338

In Accordance With EN 10204.3.1

Rechnungs-Nr / Invoice/Cons No / No de facture	0/ 2 101743
Bestell-Nr / Customer Order No / No de commande client	2901076412 002
ADDRESS	Smiths Metal Centres Stratton Business Park London Road Biggleswade Beds SG18 8QB
NORM SPECIFICATION SPECIFICAZIONE NORME	1.4305 (303) Cold drawn bar to h9 tolerance
Works No / Work Order No / No de commande usine / Opera per non	OB4121050002
Lieferbedingungen / Supply Condition / Etat de livraison / Fornitura richiesta	COLD DRAWN LENGTHS
Produkt / Article / Produit / Frutto	Stainless Bar
Shape & Size / Dimensione	ROUND 20.000mm x 3000mm
Stückzahl / Quantity / Quantité / Quantità	3 Bundles containing 204 Pieces for 1512 Kgs
Schmelze Nr / Cast No / No de Coulee / Nre Espressi	E180850
Batch ID / Identification du lot / Numero lotto	SB011151

Schmelzanalyse / Cast Analysis / Analisi di Colata / Analyse de Coulée

%C	%Si	%Mn	%P	%S	%Cr	%Mo	%Ni	%Ti	%Nb	%Al	%B
0.058	0.454	1.89	0.034	0.320	17.16	0.49	8.06	0.004	0.050	0.006	0.0010

%Co	%Cu	%Sn	%N	%V	%W	Ta	Ca	As	O		
0.210	0.520	0.012	0.040	0.060	0.115	0.0010	0.0034	0.0110	0.0034		

Mech und phys Eigenschaften / Mechanical and Physical Properties / Proprieta Meccaniche e Fisiche / Caractéristiques mécanique

0.2%PS N/mm2	1.0%PS N/mm2	UTS N/mm2	RA%	AGT %	Stress Ratio	Korngröße Grain Size Taille de grain	Dehnung % Elongation % Allongement %		Harte Hardness Dureté	Hb
749	774	814	41.1		1.09	7.5 7.5	5D 34.0	4D 37.5	239.00	239.00

Charpy (NM)		Cleaness
Intercrystalline Corrosion Test	N	Bend N

The products supplied are in compliance with the requirements of the order
Tested in accordance with standard procedures
Free from known Mercury or Radiation contamination
1.4305, AISI 303
Solution annealed temperature 1070.C
CE marked product to EN 10088-5: 2009
EN 10088-3: 2014, EN 10278: 1998, ASTM A582/A582M: 2012

Technical Manager

Kelvin Davison

Datun / Date / Date / Datare 18/10/2018

This order is manufactured according to a Quality System registered to BS EN ISO 9001:2015 and approved by TUV Nord, Certificate Registration No. GB 01439

CE

Appendix B

List of all the extrusions performed: type of glass, parameters and notes.

Extrusion Summary

Extrusion temp. is the MAX temp. set in the controller, and load is the MAX load before stopping the extrusion

Preform Number	Date	Clad	Core	Clad #	Core #	Extrusion Temp (oC)	Load (kN)	Extrusion Time (min)	Length (cm)	Diameter (mm)	Fibre Drawn	Notes
FG001	06/12/2017		GLS 65:35		LD1876	670	8.04	~360	N/A			Sample cut in rectangles to fit the sleeve.
FG002	13/12/2017		GLS 65:35		LD1867	695	43.67	~360	N/A			Sample cut in rectangles to fit the sleeve. Tg=562°C
FG003	20/12/2017		GLS 60:40		---	670	24.29	~210	14.04	~10	NT679	Sample cut in rectangles to fit the sleeve. Tg=555°C
FG004	16/03/2018		GLS Se 35%		LD1928-LD1932	610	15.23	175	<15	~10	NT684-3	Use of 5 small billets, polished optical finish both ends. Tg=510 C
FG005	23/03/2018	GLS Se 30%		LD1933-1937		620	18.64	156	<15	~10	NT698	Use of 5 small billets, polished optical finish both ends. Tg=518 C
FG006	06/04/2018		GLS Se 35%		LD1953	610	7.53	87	<15	~10	NT690	repeat FG004 recipe
FG007	21/06/2018		GLS Se 35%		LD1965-1969	610	16	179	<15	~10	NT712	Samples were not polished.
FG008	22/08/2018	GLS Se 30%	GLS Se 35%	LD1960-1961	LD1962, LD1964	610	5.16	87	---	---		First attempt for core clad structure, use of 4 billets, 2 for each composition.
FG009	24/08/2018	GLS Se 30%	GLS Se 35%	LD1963	LD1964	610	21.5	100	~19	~10	NT737, NT748	Second trial for co extrusion, initial values 600 and 610 C.
FG010	11/08/2018	GLS Se 30%	GLS Se 35%	LD1963	LD1964	625	11.77	113	~16.5	~10	NT802, NT804	Repeat steps from FG009
FG011	06/09/2018	GLS Se 30%	GLS Se 35%	LD1963	LD1964	625	2.5	76	~14.6	~10	NT749	Use temperature parameters from FG010
FG012	07/09/2018	GLS Se 30%	GLS Se 35%	LD1963	LD1964	620	---	87	~14	~10	NT754, NT755	Use 5 degrees less in each section as initial temperature.
FG013	15/10.2018		GLS Se 35%		LD1987	630	43.91	116	~41	~10	---	Use od a 1 mm diameter die
FG014	10/11/2018	GLS Se 30%	GLS Se 35%	LD1969	LD1990	615	17.28	100	~18	~10	NT805, NT806	Use less temperature than in FG012
FG015	11/11/2018	GLS Se 30%	GLS Se 35%	LD1969	LD1990	615	17	105	~19.5	~10	NT776, NT800, NT801	Same recipe as FG014
FG016	31/01/2019	GLS Se 30%	GLS Se 35%	LD1987	LD1990	615	41	101	~20.5	~10	NT832, NT833	Same recipe as FG014, but billets were etched with HF, repolished and cleaned with ultrasonic bath.
FG017	04/02/2019	GLS Se 30%	GLS Se 35%	LD1969	LD1990	615	15	97	~16	~10	NT852, NT853	Same recipe as FG016, and same procedure and initial material.
FG018	07/03/2019	GLS Se 30%	GLS Se 35%	LD1987	LD1988	615	27	107	~22	~10	NT854, NT855	Same recipe as FG017, double step cleaning did not changed IPA between steps. Die cleaned for 30 mins.
FG019	08/03/2019	GLS Se 30%	GLS Se 35%	LD1987	LD1988	612	34	105	~19	~10	NT867, NT868	Try to use 10 degrees less for extrusion, double step cleaning with new Ipa in each step, die cleaned with clean Ipa for 1 hour.
FG020	12/03/2019	GLS Se 30%	GLS Se 35%	LD1987	LD1988	612	26	103	~25.5	~10	NT869, NT870	Same recipe as FG019, same cleaning steps. These where the thickest billets ever used.
FG021	27/03/2019		GLS Se30%		LD1989	612	16.4	94	~19	~10	NT845, NT848	Same recipe as FG020. Unpolished samples, 1 step cleaning, die cleaned 1 hour with clean IPA.
FG022	29/03/2019		GLS Se 35%	LD2030	LD2031	612	41	95	~16	~10	NT849, NT851	Same recipe as FG021, billets done by dobble melting and stacking, samples had some cermics on the bottom part of each
FG023	18/04/2019		GLS Se 20%		LD2038	612	24.7	106	~21.8	~10	NT838, NT839	initially 2 degrees less than recipe for FG022 but in the end again same recipe, use of three billets, made by double melt as first melt didn't work, broken by hand, no clean before remelt, billets only 12 hours, cloud, polished.
FG024	23/08/2019	GLS Se 20%	GLS Se 20+Nd 0.05%	LD2037	LD2040, LD2042	610	32.9	103	~21	~10	NT875, NT884	Used same steps as FG023 with the only difference initial temperatures were maintained through all the process (2 degress less), billets polished in both faces, not polished on the sides, acetone cleaning to remove ethanediol. 2 steps cleaning, Die was cleaned in acetone too.
FG025	17/11/2019	GLS Se 30%	GLS Se 35%	LD1991	LD1989	610	43	105	~21	~10	NT886, NT887	Preform came well no apparent crystal on the surface, no crystals on surface and surface came smoother thn previos, probably the polishing.
FG026	24/01/2019	GLS Se 20%	GLS Se 35%	LD2038	LD2029	620	42	160	---	---	---	The glass was too viscous it deformed the die, so only the middle part of
FG027	27/01/2019	GLS Se 30%	GLS Se 35%	LD1992	LD2028	610	---	106	---	---	---	Normal Steps require a waiting of minimum 5 min after controller
FG028	28/01/2019	GLS Se 20%	GLS Se 20+Nd 0.05%	LD2037	LD2041, LD2043	615	42	111	---	---	---	There was a misfunctioning in the extruder, making one side of the die being colder and making a twisted structure.

Appendix C

List of all the fibre drawing attempts.

Preform	Fibre drawing #	Successful	Performed by	Date
FG001	---	---	---	---
FG002	---	---	---	---
FG003	NT679	No	FG, AR, BM	09/04/2018
FG004	NT684-3	No	FG, BM	11/05/2018
FG005	NT698	No	FG, BM	06/06/2018
FG006	NT690	No	FG, BM	29/05/2018
FG007	NT712	No	FG, BM	25/06/2018
FG008	---	---	---	---
FG009	NT737, NT748	No	FG, AR, BM, CC	30/08/2018, 28/09/2018
FG010	NT802, NT804	Yes (partially)	FG, BM, CC	16/01/2019, 21/01/2019
FG011	NT749	Yes (partially)	FG, BM, CC	27/09/2018
FG012	NT754, NT755	Yes(cane)	FG, BM, CC	02/10/2018
FG013	---	---	---	---
FG014	NT805, NT806	Yes (partially)	FG, BM, CC	21/01/2019
FG015	NT776, NT800, NT801	Yes (partially)	FG, BM, CC	15/11/2018, 16/01/2019
FG016	NT832, NT833	No	FG, BM, CC	14/03/2019
FG017	NT852, NT853	Yes (partially)	FG, BM, CC, ZF	27/06/2019, 28/06/2019
FG018	NT854, NT855	Yes (partially)	FG, CC, ZF, AV	08/07/2019, 09/07/2019
FG019	NT867, NT868	Yes	FG, BM, CC	29/08/2019, 30/08/2019

FG020	NT869, NT870	Yes	FG, AV	02/09/2019, 06/09/2019
FG021	NT845, NT847	Yes (partially)	FG, BM, CC	22/05/2019, 04/06/2019
FG022	NT849, NT851	Yes (partially)	FG, BM, CC	18/06/2019, 26/06/2019
FG023	NT838, NT839	Yes (partially)	FG, BM, CC	08/05/2019
FG024	NT875, NT884	Yes	FG, BM, EA	21/11/2019, 20/02/2020
FG025	NT886, NT887	Yes	FG, BM, EA	27/02/2020, 28/02/2020
FG026	---	---	---	---
FG027	---	---	---	---
FG028	---	---	---	---

Bibliography

[1] P. Bastock, C. Craig, K. Khan, E. Weatherby, J. Yao, and D. W. Hewak, "Properties of gallium lanthanum sulphide glass," in *2015 Conference on Lasers and Electro-Optics (CLEO)*, pp. 1–2.

[2] J. S. Sanghera, L. B. Shaw, L. E. Busse, V. Q. Nguyen, P. C. Pureza, B. C. Cole, B. B. Harrison, I. D. Aggarwal, R. Mossadegh, F. Kung, D. Talley, D. Roselle, and R. Miklos, "Development and infrared applications of chalcogenide glass optical fibers," *Fiber and Integrated Optics*, vol. 19, no. 3, pp. 251–274, 2000.

[3] J. A. Harrington, *Infrared fibers and their applications.* SPIE Press monograph: PM135, Bellingham, Wash. : SPIE, c2004., 2004.

[4] A. Ravagli, C. Craig, K. A. Morgan, I. Zeimpekis, A. Aghajani, E. C. Weatherby, and D. W. Hewak, "Structural modification of ga-la-s glass for a new family of chalcogenides," in *SPIE Defense + Security*, vol. 10181, p. 8, SPIE.

[5] A. Ravagli, C. Craig, G. A. Alzaidy, P. Bastock, and D. W. Hewak, "Optical, thermal, and mechanical characterization of ga2se3-added gls glass," *Advanced Materials*, vol. 29, no. 27, p. 1606329, 2017.

[6] A. Ravagli, N. G. Boetti, F. A. Guzman Cruz, G. A. Alzaidy, D. Pugliese, D. Milanese, and D. W. Hewak, "Structural and spectral characterisation of er3+ and nd3+ doped ga-la-s-se glasses," *RSC Advances*, vol. 8, no. 48, pp. 27556–27564, 2018.

[7] H. G. Pfaender, *Schott guide to glass.* London: Chapman & Hall, 1996.

[8] C. R. Kurkjian and W. R. Prindle, "Perspectives on the history of glass composition," *Journal of the American Ceramic Society*, vol. 81, no. 4, pp. 795–813, 1998.

[9] A. Winkelmann and O. Schott, "Ueber thermische widerstandscoefficienten verschiedener gläser in ihrer abhängigkeit von der chemischen zusammensetzung," *Annalen der Physik*, vol. 287, no. 4, pp. 730–746, 1894.

[10] A. Winkelmann, "Ueber die specifischen wärmen verschieden zusammengesetzter gläser," *Annalen der Physik*, vol. 285, no. 7, pp. 401–420, 1893.

[11] H. Hovestadt, J. D. Everett, and A. Everett, *Jena glass and its scientific and industrial applications*. London; New York: Macmillan, 1902.

[12] O. Schott, "Glass," 1915.

[13] J. Steiner, "Otto schott und die erfindung des borosilicatglases," *Glastech. Ber.*, 2000.

[14] Corning, "Pyrex," *Journal of Chemical Education*, vol. 2, no. 12, p. 1158, 1925.

[15] G. W. Morey, "The properties of glass. pp, 561. new york; reinhold publishing corp.; london: Chapman & hall, ltd., 1938. 62s. 6d," *Journal of the Society of Chemical Industry*, vol. 58, no. 18, pp. 422–422, 1939.

[16] E. Sullivan and W. C. Taylor, "Glass," 1919.

[17] S. Sudo, *Optical fiber amplifiers : materials, devices, and applications*. Boston, Mass.: Artech House, 1997.

[18] H. Bach and N. Neuroth, *The properties of optical glass*. Springer Science & Business Media, 1998.

[19] N. Kapany, "Fiber optics. principles and applications," *New York: Academic Press, 1967*, 1967.

[20] H. Lamm, "Biegsame optische gerate," *Zeitschrift fur Instrumeten Kunde*, vol. 50, pp. 579–581, 1930.

[21] B. O'Brien, "Optical image forming devices," 1958.

[22] L. E. Curtiss, "Glass fiber optical devices," 1971.

[23] J. Hecht, *City of light: the story of fiber optics*. Oxford University Press on Demand, 1999.

[24] K. C. Kao and G. A. Hockham, "Dielectric-fibre surface waveguides for optical frequencies," *Proceedings of the Institution of Electrical Engineers*, vol. 113, no. 7, pp. 1151–1158, 1966.

[25] A. de Panafieu, *Fabrication of Optical Fibers*, pp. 25–42. Springer, 1979.

[26] J. R. Simpson and J. B. Macchesney, "Optical fibres with an al2o3-doped silicate core composition," *Electronics Letters*, vol. 19, no. 7, pp. 261–262, 1983.

[27] R. M. Nor, S. N. Mohd Halim, M. Taib, A.-B. Ibrahim, and A.-R. M. Kamil, "First principles study on phonon energy in sio2 glass with the incorporation of al2o3," *Solid State Phenomena*, vol. 268, pp. 160–164, 2017.

[28] H. J. Eichler, J. Eichler, and O. Lux, *Lasers: basics, advances and applications*, vol. 220. Springer, 2018.

[29] R. P. Tumminelli, B. C. McCollum, and E. Snitzer, "Fabrication of high-concentration rare-earth doped optical fibers using chelates," *Journal of Lightwave Technology*, vol. 8, no. 11, pp. 1680–1683, 1990.

[30] R. Frerichs, "New optical glasses with good transparency in the infrared," *Journal of the Optical Society of America*, vol. 43, no. 12, pp. 1153–1157, 1953.

[31] R. R. Standel and R. E. Hendrickson, "Infrared fiber optics techniques," *Infrared Physics*, vol. 3, no. 4, pp. 223–227, 1963.

[32] J.-L. Adam and X. Zhang, *Chalcogenide glasses: preparation, properties and applications*. Woodhead publishing, 2014.

[33] L. B. Shaw, B. Cole, P. A. Thielen, J. S. Sanghera, and I. D. Aggarwal, "Mid-wave ir and long-wave ir laser potential of rare-earth doped chalcogenide glass fiber," *IEEE Journal of Quantum Electronics*, vol. 37, no. 9, pp. 1127–1137, 2001.

[34] A. Ravagli, C. Craig, J. Lincoln, and W. Hewak Daniel, "Ga-la-s-se glass for visible and thermal imaging," *Advanced Optical Technologies*, vol. 6, no. 2, p. 131, 2017.

[35] N. S. Kapany and R. J. Simms, "Recent developments in infrared fiber optics," *Infrared Physics*, vol. 5, no. 2, pp. 69–80, 1965.

[36] T. Li, *Optical fiber communications: fiber fabrication*. Elsevier, 2012.

[37] J. Nishii, S. Morimoto, I. Inagawa, R. Iizuka, T. Yamashita, and T. Yamagishi, "Recent advances and trends in chalcogenide glass fiber technology: a review," *Journal of Non-Crystalline Solids*, vol. 140, pp. 199–208, 1992.

[38] P. Klocek, M. Roth, and R. Rock, "Chalcogenide glass optical fibers and image bundles: Properties and applications," *Optical Engineering*, vol. 26, no. 2, p. 260288, 1987.

[39] T. Kanamori, Y. Terunuma, S. Takahashi, and T. Miyashita, "Chalcogenide glass fibers for mid-infrared transmission," *Journal of Lightwave Technology*, vol. 2, no. 5, pp. 607–613, 1984.

[40] J. Nishii, T. Yamashita, and T. Yamagishi, "Low-loss chalcogenide glass fiber with core-cladding structure," *Applied Physics Letters*, vol. 53, no. 7, pp. 553–554, 1988.

[41] A. B. Seddon, D. Furniss, and D. J. Sims, *Gallium-lanthanum-sulphide glasses: extrusion of fiber optic preforms and relevant physical properties*, vol. 3849 of *Photonics East '99*. SPIE, 1999.

[42] S. D. Savage, C. A. Miller, D. Furniss, and A. B. Seddon, "Extrusion of chalcogenide glass preforms and drawing to multimode optical fibers," *Journal of Non-Crystalline Solids*, vol. 354, no. 29, pp. 3418–3427, 2008.

[43] D. J. Brady, T. Schweizer, J. Wang, and D. W. Hewak, "Minimum loss predictions and measurements in gallium lanthanum sulphide based glasses and fibre," *Journal of Non-Crystalline Solids*, vol. 242, no. 2, pp. 92–98, 1998.

[44] W. B. Jensen, "A note on the term chalcogen," *Journal of Chemical Education*, vol. 74, no. 9, p. 1063, 1997.

[45] P. Taylor, M. Theye, J. Orenstein, S. Elliott, B. Golding, and D. Fox, *Optical properties of the chalcogenide glasses*, pp. 281–320. Springer, 1984.

[46] B. J. Eggleton, B. Luther-Davies, and K. Richardson, "Chalcogenide photonics," *Nature Photonics*, vol. 5, p. 141, 2011.

[47] A. Zakery and S. R. Elliott, "Optical properties and applications of chalcogenide glasses: a review," *Journal of Non-Crystalline Solids*, vol. 330, no. 1, pp. 1–12, 2003.

[48] A. Zakery and S. R. Elliott, "Optical nonlinearities in chalcogenide glasses and their applications," 2007.

[49] D. B. Ostrowsky, *Fiber and integrated optics*, vol. 41. Springer Science & Business Media, 2012.

[50] L. Calvez, "Chalcogenide glasses and glass-ceramics: Transparent materials in the infrared for dual applications," *Comptes Rendus Physique*, vol. 18, no. 5, pp. 314–322, 2017.

[51] C.-C. Huang, *Development of germanium based sulphide glass by chemical vapour deposition (CVD)*. Thesis, 2005.

[52] D. W. Hewak, D. Brady, R. J. Curry, G. Elliott, C.-C. Huang, M. Hughes, K. Knight, A. Mairaj, M. Petrovich, and R. Simpson, "Chalcogenide glasses for photonics device applications," *Photonic glasses and glass-ceramics*, pp. 29–102, 2010.

[53] D. J. Brady, *Gallium lanthanum sulphide based glasses for mid-infrared optical fibres*. Thesis, 1999.

[54] A. Ravagli, *Development of Visible-to-LWIR multispectral chalcogenide glasses*. Thesis, 2018.

[55] D. Furniss and A. B. Seddon, *Thermal Analysis of Inorganic Compound Glasses and Glass-Ceramics*, pp. 410–449. 2008.

[56] P. W. France, *Fluoride glass optical fibres*. Springer Science & Business Media, 2012.

[57] J. Sanghera and I. D. Aggarwal, *Infrared fiber optics*. CRC Press, 1998.

[58] L. Mattos Jr and A. G. Clare, "The crystallisation and optical properties of gallium cerium lanthanum sulphide glass," *Physics and chemistry of glasses*, vol. 34, no. 6, pp. 244–250, 1993.

[59] H. Rawson, *Inorganic glass-forming systems*. London; New York: Academic Press, 1967.

[60] M. B. Myers and J. S. Berkes, "Phase separation in amorphous chalcogenides," *Journal of Non-Crystalline Solids*, vol. 8, pp. 804–815, 1972.

[61] P. Gabbott, *Principles and applications of thermal analysis*. John Wiley & Sons, 2008.

[62] J. B. Clarke, J. W. Hastie, L. H. E. Kihlborg, R. Metselaar, and M. M. Thackeray, "Definitions of terms relating to phase transitions of the solid state (iupac recommendations 1994)," 1994.

[63] M. M. A. Imran, D. Bhandari, and N. S. Saxena, "Enthalpy recovery during structural relaxation of se96in4 chalcogenide glass," *Physica B: Condensed Matter*, vol. 293, no. 3, pp. 394–401, 2001.

[64] J.-H. Kim, J. S. Park, E. S. Park, W. T. Kim, and D. H. Kim, "Estimation of critical cooling rates for glass formation in bulk metallic glasses through non-isothermal thermal analysis," *Metals and Materials International*, vol. 11, no. 1, pp. 1–9, 2005.

[65] M. F. Churbanov, "High-purity chalcogenide glasses as materials for fiber optics," *Journal of non-crystalline solids*, vol. 184, pp. 25–29, 1995.

[66] M. D. Mikhailov and A. S. Tverjanovich, "Critical cooling rates of some chalcogenide glass-forming melts," *Fiz. Khim. Stekla*, vol. 12, no. 3, pp. 274–284, 1986.

[67] G. Riontino and M. Baricco, "Structural relaxation in metallic glasses," *Philosophical Magazine B*, vol. 56, no. 2, pp. 177–183, 1987.

[68] L. H. Adams and E. D. Williamson, "A note on the annealing of optical glass," *JOSA*, vol. 4, no. 4, pp. 213–223, 1920.

[69] P. Badrinarayanan, W. Zheng, Q. Li, and S. L. Simon, "The glass transition temperature versus the fictive temperature," *Journal of Non-Crystalline Solids*, vol. 353, no. 26, pp. 2603–2612, 2007.

[70] J. C. Mauro, R. J. Loucks, and P. K. Gupta, "Fictive temperature and the glassy state," *Journal of the American Ceramic Society*, vol. 92, no. 1, pp. 75–86, 2009.

[71] A. Zakery and S. Elliott, "An introduction to chalcogenide glasses," *Optical Nonlinearities in Chalcogenide Glasses and Their Applications*, pp. 1–28, 2007.

[72] W. H. Zachariasen, "The atomic arrangement in glass," *Journal of the American Chemical Society*, vol. 54, no. 10, pp. 3841–3851, 1932.

[73] A. M. Loireau-Lozac'h, M. Guittard, and J. Flahaut, "Verres formes par les sulfures l2s3 des terres rares avec le sulfure de gallium ga2s3," *Materials Research Bulletin*, vol. 11, no. 12, pp. 1489–1496, 1976.

[74] J. Flahaut and A. M. Loireau Lozac'h, "Rare earth sulphide and oxysulphide glasses," 1983.

[75] M. N. Petrovich, A. Favre, D. W. Hewak, H. N. Rutt, A. C. Grippo, J. F. Gubeli, K. C. Jordan, G. R. Neil, and M. D. Shinn, "Near-ir absorption of ga:la:s and ga:la:s:o glasses by free-electron laser-based laser calorimetry," *Journal of Non-Crystalline Solids*, vol. 326-327, pp. 93–97, 2003.

[76] A. F. Kozmidis-Petrović, "Theoretical analysis of relative changes of the hruby, weinberg, and lu–liu glass stability parameters with application on some oxide and chalcogenide glasses," *Thermochimica Acta*, vol. 499, no. 1, pp. 54–60, 2010.

[77] A. Mairaj, *Optical waveguides and lasers in improved gallium lanthanum sulphide glass*. Thesis, 2003.

[78] A. N. Gent, "Theory of the parallel plate viscometer," *British Journal of Applied Physics*, vol. 11, no. 2, pp. 85–87, 1960.

[79] P. Koštál, J. Shánělová, and J. Málek, "Viscosity of chalcogenide glass-formers," *International Materials Reviews*, vol. 65, no. 2, pp. 63–101, 2020.

[80] "Glass viscosity and viscometric fixed points," 1987.

[81] J. Lucas, J. Troles, X. H. Zhang, C. Boussard-Pledel, M. Poulain, and B. Bureau, "Glasses to see beyond visible," *Comptes Rendus Chimie*, vol. 21, no. 10, pp. 916–922, 2018.

[82] A. K. Vijh, "Chemical approaches to the approximate prediction of band gaps of binary semiconductors and insulators," *Journal of The Electrochemical Society*, vol. 117, no. 5, p. 173C, 1970.

[83] F. Di Quarto, C. Sunseri, S. Piazza, and M. C. Romano, "Semiempirical correlation between optical band gap values of oxides and the difference of electronegativity of the elements. its importance for a quantitative use of photocurrent spectroscopy in corrosion studies," *The Journal of Physical Chemistry B*, vol. 101, no. 14, pp. 2519–2525, 1997.

[84] "The nature of vibrational spectroscopy." https://www2.chemistry.msu.edu.

[85] "Bond vibrations, ir spectroscopy, and the ball and spring model." https://www.masterorganicchemistry.com/2016/11/11/bond-vibrations-ir-spectroscopy/.

[86] B. H. Stuart, *Infrared spectroscopy : fundamentals and applications*. Chichester, West Sussex: Wiley, 2005.

[87] E. Holden Norman, B. Coplen Tyler, K. Böhlke John, V. Tarbox Lauren, J. Benefield, R. de Laeter John, G. Mahaffy Peter, G. O'Connor, E. Roth, H. Tepper Dorothy, T. Walczyk, E. Wieser Michael, and S. Yoneda, "Iupac periodic table of the elements and isotopes (iptei) for the education community (iupac technical report)," 2018.

[88] G. Ghosh, "Sellmeier coefficients and dispersion of thermo-optic coefficients for some optical glasses," *Applied Optics*, vol. 36, no. 7, pp. 1540–1546, 1997.

[89] M. 2010/M. http://www.metricon.com/model-2010-m-overview/, 2015.

[90] H. Onodera, I. Awai, and J.-i. Ikenoue, "Refractive-index measurement of bulk materials: prism coupling method," *Applied optics*, vol. 22, no. 8, pp. 1194–1197, 1983.

[91] C. E. Pearson and R. N. Parkins, *The Extrusion of Metals. (Second edition.)*. Pp. ix. 336. Chapman & Hall: London, 1960.

[92] E. Roeder, "Extrusion of glass," *Journal of Non-Crystalline Solids*, vol. 5, no. 5, pp. 377–388, 1971.

[93] W. A. Weyl and E. C. Marboe, *The Constitution of Glasses: Fundamentals of the structure of inorganic liquids and solids*, vol. 1. Interscience Publishers, 1962.

[94] A. K. Singh, "A short over view on advantage of chalcogenide glassy alloys," *Journal of Non-Oxide Glasses*, vol. 3, pp. 1–4, 2012.

[95] E. Roeder, "Flow behaviour of glass during extrusion," *Journal of Non-Crystalline Solids*, vol. 7, no. 2, pp. 203–220, 1972.

[96] B. G. Aitken, S. C. Currie, B. C. Monahan, L.-m. Wu, and E. W. Coonan, "Chalcogenide glass for low viscosity extrusion and injection molding," 2006.

[97] J. C. Knight, T. A. Birks, P. S. J. Russell, and D. M. Atkin, "All-silica single-mode optical fiber with photonic crystal cladding," *Optics Letters*, vol. 21, no. 19, pp. 1547–1549, 1996.

[98] T. M. Monro, K. M. Kiang, J. H. Lee, K. Frampton, Z. Yusoff, R. Moore, J. Tucknott, D. W. Hewak, H. N. Rutt, and D. J. Richardson, "High nonlinearity extruded single-mode holey optical fibers," in *Optical Fiber Communications Conference*, vol. 70 of *OSA Trends in Optics and Photonics*, p. FA1, Optical Society of America.

[99] V. V. Ravi Kanth Kumar, A. K. George, W. H. Reeves, J. C. Knight, P. S. J. Russell, F. G. Omenetto, and A. J. Taylor, "Extruded soft glass photonic crystal fiber for ultrabroad supercontinuum generation," *Optics Express*, vol. 10, no. 25, pp. 1520–1525, 2002.

[100] A. Bornstein, N. Croitoru, and E. Marom, *Chalcogenide Infrared Glass Fibers*, vol. 0320 of *1982 Los Angeles Technical Symposium*. SPIE, 1982.

[101] X. Feng, A. Mairaj, D. Hewak, and T. Monro, "Nonsilica glasses for holey fibers," *Lightwave Technology, Journal of*, vol. 23, pp. 2046–2054, 2005.

[102] M. Vlček, L. Tichý, J. Klikorka, and A. Tříska, "Influence of oxygen traces on physical properties of glassy gese2," *Journal of Materials Science*, vol. 22, no. 6, pp. 2119–2123, 1987.

[103] P. K. Saha, *Aluminum extrusion technology*. Asm International, 2000.

[104] H. Farzad and R. Ebrahimi, "Die profile optimization of rectangular cross section extrusion in plane strain condition using upper bound analysis method and simulated annealing algorithm," *Journal of Manufacturing Science and Engineering*, vol. 139, no. 2, 2017.

[105] A. H. Shabaik, "Differential pressure extrusion through double reduction dies," *Journal of Engineering for Industry*, vol. 95, no. 3, pp. 890–894, 1973.

[106] C. Jiang, X. Wang, M. Zhu, H. Xu, Q. Nie, S. Dai, G. Tao, X. Shen, C. Cheng, Q. Zhu, F. Liao, P. Zhang, P. Zhang, Z. Liu, and X.-H. Zhang, "Preparation of chalcogenide glass fiber using an improved extrusion method," *Optical Engineering*, vol. 55, no. 5, p. 056114, 2016.

[107] A. Belwalkar, H. Xiao, W. Z. Misiolek, and J. Toulouse, "Extruded tellurite glass optical fiber preforms," *Journal of Materials Processing Technology*, vol. 210, no. 14, pp. 2016–2022, 2010.

[108] Z. Xue, S. Liu, Z. Zhao, N. Mi, B. Wu, X. Li, P. Zhang, and X. Wang, "Infrared suspended-core fiber fabrication based on stacked chalcogenide glass extrusion," *Journal of Lightwave Technology*, vol. 36, no. 12, pp. 2416–2421, 2018.

[109] G. Tao, S. Shabahang, E.-H. Banaei, J. J. Kaufman, and A. F. Abouraddy, "Multimaterial preform coextrusion for robust chalcogenide optical fibers and tapers," *Optics Letters*, vol. 37, no. 13, pp. 2751–2753, 2012.

[110] K. Laue and H. Stenger, "Extrusion: processes, machinery, tooling," *American Society for Metals, 1981*, p. 457, 1981.

[111] S. Ramachandran and S. G. Bishop, "Low loss photoinduced waveguides in rapid thermally annealed films of chalcogenide glasses," *Applied Physics Letters*, vol. 74, no. 1, pp. 13–15, 1999.

[112] M. Bakhshi-Jooybari, "A theoretical and experimental study of friction in metal forming by the use of the forward extrusion process," *Journal of Materials Processing Technology*, vol. 125-126, pp. 369–374, 2002.

[113] I. Flitta and T. Sheppard, "Nature of friction in extrusion process and its effect on material flow," *Materials Science and Technology*, vol. 19, no. 7, pp. 837–846, 2003.

[114] A. F. Castle and T. Sheppard, "Pressure required to initiate extrusion in some aluminium alloys," *Metals Technology*, vol. 3, no. 1, pp. 465–475, 1976.

[115] "Technical data," *Stainless steel*, vol. 1.4305 - 303, 2016.

[116] H. Ebendorff-Heidepriem and T. M. Monro, "Analysis of glass flow during extrusion of optical fiber preforms," *Optical Materials Express*, vol. 2, no. 3, pp. 304–320, 2012.

[117] H. Ebendorff-Heidepriem and T. M. Monro, "Extrusion of complex preforms for microstructured optical fibers," *Optics Express*, vol. 15, no. 23, pp. 15086–15092, 2007.

[118] J. Pfitzner, "Poiseuille and his law," *Anaesthesia*, vol. 31, no. 2, pp. 273–275, 1976.

[119] G. Cox and E. Roeder, "Power requirements and exit velocities in the extrusion of alkali-lime-silica glass part 1. flows in the orifice channel with the use of different materials for construction," *Glastech. Ber.*, vol. 57, no. 7, pp. 182–187, 1984.

[120] R. P. Bauman and R. Schwaneberg, "Interpretation of bernoulli's equation," *The Physics Teacher*, vol. 32, no. 8, pp. 478–488, 1994.

[121] V. E. Bean, *NIST pressure calibration service*. US Department of Commerce, Technology Administration, National Institute of Standards and Technology, 1994.

[122] H. Ebendorff-Heidepriem, T. M. Monro, M. A. van Eijkelenborg, and M. C. J. Large, "Extruded high-na microstructured polymer optical fibre," *Optics Communications*, vol. 273, no. 1, pp. 133–137, 2007.

[123] R. J. Crowson, A. J. Scott, and D. W. Saunders, "Rheology of short glass fiber-reinforced thermoplastics and its application to injection molding. iii. use of a high shear rate capillary rheometer in the injection molding shear rate range," *Polymer Engineering & Science*, vol. 21, no. 12, pp. 748–754, 1981.

[124] A. K. Mairaj, X. Feng, and D. W. Hewak, "Extruded channel waveguides in a neodymium-doped lead–silicate glass for integrated optic applications," *Applied Physics Letters*, vol. 83, no. 17, pp. 3450–3452, 2003.

[125] D. I. H. Atkinson and P. W. McMillan, "Glass-ceramics with random and oriented microstructures," *Journal of Materials Science*, vol. 12, no. 3, pp. 443–450, 1977.

[126] P. M. Gresho, "Incompressible fluid dynamics: some fundamental formulation issues," *Annual review of fluid mechanics*, vol. 23, no. 1, pp. 413–453, 1991.

[127] C. Riff, "Computational fluid dynamics (cfd) modeling," *Laboratory for Product and Process Design*, 2004.

[128] D. Gross, W. Ehlers, P. Wriggers, J. Schröder, and R. Müller, *Hydrodynamics*, pp. 227–246. Berlin, Heidelberg: Springer Berlin Heidelberg, 2017.

[129] A. A. Kamal, *Fluid Dynamics*, pp. 391–408. Berlin, Heidelberg: Springer Berlin Heidelberg, 2011.

[130] W. B. Fulks, R. B. Guenther, and E. L. Roetman, "Equations of motion and continuity for fluid flow in a porous medium," *Acta Mechanica*, vol. 12, no. 1, pp. 121–129, 1971.

[131] K. Bhowmick, H. P. Morvan, D. Furniss, A. B. Seddon, and T. M. Benson, "Co-extrusion of multilayer glass fiber-optic preforms: Prediction of layer dimensions in the extrudate," *Journal of the American Ceramic Society*, vol. 96, no. 1, pp. 118–124, 2013.

[132] S. Richardson, "The die swell phenomenon," *Rheologica Acta*, vol. 9, no. 2, pp. 193–199, 1970.

[133] H. M. Chiu, G. Kumar, J. Blawzdziewicz, and J. Schroers, "Thermoplastic extrusion of bulk metallic glass," *Scripta Materialia*, vol. 61, no. 1, pp. 28–31, 2009.

[134] H. R. Lillie, "Viscosity of glass between the strain point and melting temperature," *Journal of the American Ceramic Society*, vol. 14, no. 7, pp. 502–512, 1931.

[135] D. W. Hewak, R. C. Moore, T. Schweizer, J. Wang, B. Samson, W. S. Brocklesby, D. N. Payne, and E. J. Tarbox, "Gallium lanthanum sulphide optical fibre for active and passive applications," *Electronics Letters*, vol. 32, no. 4, p. 384, 1996.

[136] N. K. Goel, G. Pickrell, and R. Stolen, "An optical amplifier having 5cm long silica-clad erbium doped phosphate glass fiber fabricated by "core-suction" technique," *Optical Fiber Technology*, vol. 20, no. 4, pp. 325–327, 2014.

[137] D. Furniss and A. B. Seddon, "Towards monomode proportioned fibreoptic preforms by extrusion," *Journal of Non-Crystalline Solids*, vol. 256-257, pp. 232–236, 1999.

[138] A. B. Seddon, D. Furniss, and A. Motesharei, *Extrusion method for making fiber optic preforms of special glasses*, vol. 3416 of *Lasers and Materials in Industry and Opto-Contact Workshop*. SPIE, 1998.

[139] E. T. Y. Lee and E. R. M. Taylor, "Two-die assembly for the extrusion of glasses with dissimilar thermal properties for fibre optic preforms," *Journal of Materials Processing Technology*, vol. 184, no. 1, pp. 325–329, 2007.

[140] C. Gouveia, J. M. Baptista, and P. Jorge, *Refractometric Optical Fiber Platforms for Label Free Sensing*, pp. 345–372. 2013.

[141] G. R. Newns, P. Pantelis, J. L. Wilson, R. W. J. Uffen, and R. Worthington, "Absorption losses in glasses and glass fibre waveguides," *Opto-electronics*, vol. 5, no. 4, pp. 289–296, 1973.

[142] B. J. Eggleton, "Chalcogenide photonics: fabrication, devices and applications introduction," *Optics Express*, vol. 18, no. 25, pp. 26632–26634, 2010.

[143] Y. D. West, T. Schweizer, D. J. Brady, and D. W. Hewak, "Gallium lanthanum sulphide fibers for infrared transmission," *Fiber and Integrated Optics*, vol. 19, no. 3, pp. 229–250, 2000.

[144] X. Gai, T. Han, A. Prasad, S. Madden, D.-Y. Choi, R. Wang, D. Bulla, and B. Luther-Davies, "Progress in optical waveguides fabricated from chalcogenide glasses," *Optics Express*, vol. 18, no. 25, pp. 26635–26646, 2010.

[145] J. Troles, Q. Coulombier, G. Canat, M. Duhant, W. Renard, P. Toupin, L. Calvez, G. Renversez, F. Smektala, M. El Amraoui, J. L. Adam, T. Chartier, D. Mechin, and L. Brilland, "Low loss microstructured chalcogenide fibers for large non linear effects at 1995 nm," *Optics Express*, vol. 18, no. 25, pp. 26647–26654, 2010.

[146] R. J. Weiblen, A. Docherty, J. Hu, and C. R. Menyuk, "Calculation of the expected bandwidth for a mid-infrared supercontinuum source based on as2s3 chalcogenide photonic crystal fibers," *Optics Express*, vol. 18, no. 25, pp. 26666–26674, 2010.

[147] K. Suzuki and T. Baba, "Nonlinear light propagation in chalcogenide photonic crystal slow light waveguides," *Optics Express*, vol. 18, no. 25, pp. 26675–26685, 2010.

[148] M. W. Lee, C. Grillet, C. Monat, E. Mägi, S. Tomljenovic-Hanic, X. Gai, S. Madden, D.-Y. Choi, D. Bulla, B. Luther-Davies, and B. J. Eggleton, "Photosensitive and thermal nonlinear effects in chalcogenide photonic crystal cavities," *Optics Express*, vol. 18, no. 25, pp. 26695–26703, 2010.

[149] A. B. Seddon, Z. Tang, D. Furniss, S. Sujecki, and T. M. Benson, "Progress in rare-earth-doped mid-infrared fiber lasers," *Optics Express*, vol. 18, no. 25, pp. 26704–26719, 2010.

[150] T. Schweizer, D. W. Hewak, D. N. Payne, T. Jensen, and G. Huber, "Rare-earth doped chalcogenide glass laser," *Electronics Letters*, vol. 32, no. 7, pp. 666–667, 1996.

[151] T. Schweizer, B. N. Samson, R. C. Moore, D. W. Hewak, and D. N. Payne, "Rare-earth doped chalcogenide glass fibre laser," *Electronics Letters*, vol. 33, no. 5, pp. 414–416, 1997.

[152] A. Vasilev, G. Devyatykh, E. Dianov, A. Guryanov, A. Laptev, V. Plotnichenko, Y. Pyrkov, G. Snopatin, I. Skripachev, M. Churbanov, and V. Shipunov, "Two-layer chalcogenide-glass optical fibers with optical losses below 30 db/km," *Quantum Electronics - QUANTUM ELECTRON*, vol. 23, pp. 89–90, 1993.

[153] C. Conseil, Q. Coulombier, C. Boussard-Plédel, J. Troles, L. Brilland, G. Renversez, D. Mechin, B. Bureau, J. L. Adam, and J. Lucas, "Chalcogenide step index and microstructured single mode fibers," *Journal of Non-Crystalline Solids*, vol. 357, no. 11, pp. 2480–2483, 2011.

[154] J. Nishii, T. Yamashita, and T. Yamagishi, "Chalcogenide glass fiber with a core–cladding structure," *Applied Optics*, vol. 28, no. 23, pp. 5122–5127, 1989.

[155] Z. Tang, V. S. Shiryaev, D. Furniss, L. Sojka, S. Sujecki, T. M. Benson, A. B. Seddon, and M. F. Churbanov, "Low loss ge-as-se chalcogenide glass fiber, fabricated using extruded preform, for mid-infrared photonics," *Optical Materials Express*, vol. 5, no. 8, pp. 1722–1737, 2015.

[156] N. Anscombe, "The promise of chalcogenides," *Nat. Photonics*, vol. 5, p. 474, 2011.

[157] H. Parnell, D. Furniss, Z. Tang, N. C. Neate, T. M. Benson, and A. B. Seddon, "Compositional dependence of crystallization in ge–sb–se glasses relevant to optical fiber making," *Journal of the American Ceramic Society*, vol. 101, no. 1, pp. 208–219, 2018.

[158] U. C. Paek, "Laser drawing of optical fibers," *Applied Optics*, vol. 13, no. 6, pp. 1383–1386, 1974.

[159] R. E. Jaeger, *Fiber Drawing Process: Characterization and Control*, pp. 33–53. Boston, MA: Springer US, 1979.

[160] D. S. Vaidya and G. D. Mihalacopoulos, "Characterization of meltdown profile during fiber draw," in *Int. Wire Cable Symp. Proc*, vol. 48, pp. 73–80.

[161] X. Cheng and Y. Jaluria, "Effect of furnace thermal configuration on optical fiber heating and drawing," *Numerical Heat Transfer, Part A: Applications*, vol. 48, no. 6, pp. 507–528, 2005.

[162] S. Xue, G. Barton, S. Fleming, and A. Argyros, "Heat transfer modeling of the capillary fiber drawing process," *Journal of Heat Transfer*, vol. 139, no. 7, pp. 072001–072001–12, 2017.

[163] G. E. Snopatin, V. S. Shiryaev, V. G. Plotnichenko, E. M. Dianov, and M. F. Churbanov, "High-purity chalcogenide glasses for fiber optics," *Inorganic materials*, vol. 45, no. 13, p. 1439, 2009.

[164] U. C. Paek, "Free drawing and polymer coating of silica glass optical fibers," *Journal of Heat Transfer*, vol. 121, no. 4, pp. 774–788, 1999.

[165] U. C. Paek and R. B. Runk, "Physical behavior of the neck-down region during furnace drawing of silica fibers," *Journal of Applied Physics*, vol. 49, no. 8, pp. 4417–4422, 1978.

[166] K. Kim, D. Kim, and H. S. Kwak, "The role of helium/argon gas flow in a glass fiber drawing furnace," *Computational Thermal Sciences*, vol. 4, pp. 263–270, 2012.

[167] X. Cheng and Y. Jaluria, "Optimization of a thermal manufacturing process: Drawing of optical fibers," *International Journal of Heat and Mass Transfer*, vol. 48, no. 17, pp. 3560–3573, 2005.

[168] R. E. Loehman and A. J. Armstrong, "Crystallization of as2se3-as2te3 glasses," *Journal of the American Ceramic Society*, vol. 60, no. 1-2, pp. 71–75, 1977.

[169] L. Yu and S. M. Reutzel-Edens, *CRYSTALLIZATION Basic Principles*, pp. 1697–1702. Oxford: Academic Press, 2003.

[170] M. Churbanov and V. Shiryaev, "Crystallization of chalcogenide glasses," *Vysokochistye Veshchestva*, pp. 21–33, 1994.

[171] M. Poulain, "Overview of crystallization in fluoride glasses," *Journal of Non-Crystalline Solids*, vol. 140, pp. 1–9, 1992.

[172] M. Poulain, "Fluoride glasses: properties, technology and applications," 2010.

[173] P. Bastock, *Manufacturing novel fibre*. Thesis, 2015.

[174] P. Checcacci, A. M. Sheggi, and M. Brenci, "R.f. induction furnace for silica-fibre drawing," 1976.

[175] Q. Coulombier, L. Brilland, P. Houizot, T. N. Nguyen, T. Chartier, G. Renversez, A. Monteville, J. Fatome, F. Smektala, T. Pain, H. Orain, J.-C. Sangleboeuf, and J. Trolès, *Fabrication of low losses chalcogenide photonic crystal fibers by molding process*, vol. 7598 of *SPIE OPTO*. SPIE, 2010.

[176] Z. Yin and Y. Jaluria, "Neck down and thermally induced defects in high-speed optical fiber drawing," *Journal of Heat Transfer*, vol. 122, no. 2, pp. 351–362, 1999.

[177] J. M. Senior, *Optical fiber communications : principles and practice*. Englewood Cliffs, NJ : Prentice-Hall International, 1984., 1984.

[178] I. P. Kaminow, T. Li, and A. E. Willner, *Optical fiber telecommunications V*. Amsterdam ; London : Elsevier/Academic Press, 2008., 2008.

[179] M. A. Laughton and D. F. Warne, "Electrical engineer's reference book," *Burlington, MA: Elsevier Science*, 2013.

[180] C. K. Eastman, "Fiber-optic array of limited acceptance angle," 1994.

[181] R. Hui, *Introduction to Fiber-Optic Communications*. Academic Press, 2019.

[182] S. I. Najafi, *Introduction to glass integrated optics*. Artech House, 1992.

[183] S. K. Sheem, "Single mode operation with non-single mode optical fiber transmission cable," 1987.

[184] E.-G. Neumann, *Single-mode fibers: fundamentals*, vol. 57. Springer, 2013.

[185] S. Kasap, K. Koughia, G. Soundararajan, and M. G. Brik, "Optical and photoluminescence properties of erbium-doped chalcogenide glasses (gegas:er)," *IEEE Journal of Selected Topics in Quantum Electronics*, vol. 14, no. 5, pp. 1353–1360, 2008.

[186] F. Chen, T. Wei, X. Jing, Y. Tian, J. Zhang, and S. Xu, "Investigation of mid-infrared emission characteristics and energy transfer dynamics in er3+ doped oxyfluoride tellurite glass," *Scientific Reports*, vol. 5, p. 10676, 2015.

[187] R. Wang, X. Meng, F. Yin, Y. Feng, G. Qin, and W. Qin, "Heavily erbium-doped low-hydroxyl fluorotellurite glasses for 2.7 μm laser applications," *Optical Materials Express*, vol. 3, no. 8, pp. 1127–1136, 2013.

[188] M. Hughes, D. W. Hewak, and R. J. Curry, "Concentration dependence of the fluorescence decay profile in transition metal doped chalcogenide glass," in *Integrated Optoelectronic Devices 2007*, vol. 6469, p. 9, SPIE.

[189] A. Belykh, L. Glebov, C. Lerminiaux, S. Lunter, M. Mikhailov, A. Plyukhin, M. Prassas, and A. Przhevuskii, "Spectral and luminescence properties of neodymium in chalcogenide glasses," *Journal of Non-Crystalline Solids*, vol. 213-214, pp. 238–244, 1997.

[190] A. K. Mairaj, M. N. Petrovich, Y. D. West, A. Fu, D. W. J. Harwood, L. Ng, T. M. Monro, N. G. Broderick, and D. W. Hewak, "Advances in gallium lanthanum sulphide glass for optical fiber and devices," in *Environmental and Industrial Sensing*, vol. 4204, p. 9, SPIE.

[191] P. Lucas, M. R. Riley, C. Boussard-Plédel, and B. Bureau, "Advances in chalcogenide fiber evanescent wave biochemical sensing," *Analytical Biochemistry*, vol. 351, no. 1, pp. 1–10, 2006.

[192] J. S. Sanghera, I. D. Aggarwal, L. E. Busse, P. C. Pureza, V. Q. Nguyen, R. E. Miklos, F. H. Kung, and R. Mossadegh, "Development of low-loss ir transmitting chalcogenide glass fibers," in *Photonics West '95*, vol. 2396, p. 7, SPIE.

[193] J. S. Sanghera, L. B. Shaw, and I. D. Aggarwal, "Chalcogenide glass-fiber-based mid-ir sources and applications," *IEEE Journal of Selected Topics in Quantum Electronics*, vol. 15, no. 1, pp. 114–119, 2009.

[194] A. K. Mairaj, A. M. Chardon, D. P. Shepherd, and D. W. Hewak, "Laser performance and spectroscopic analysis of optically written channel waveguides in neodymium-doped gallium lanthanum sulphide glass," *IEEE Journal of Selected Topics in Quantum Electronics*, vol. 8, no. 6, pp. 1381–1388, 2002.

[195] D. L. Perry, *Handbook of inorganic compounds*. CRC press, 2016.

[196] J. A. Duffy and M. D. Ingram, "Solvent properties of glass melts: resemblance to aqueous solutions," *Comptes Rendus Chimie*, vol. 5, no. 11, pp. 797–804, 2002.

[197] C. A. Faick, A. E. Williams, and G. F. Rynders, "Effect of convection currents on the distribution of striae in pots of optical glass," *Journal of research of the National Bureau of Standards*, vol. 42, no. 2, pp. 153–169, 1949.

[198] D. Hewak, P. Bastock, C. Craig, C.-C. Huang, K. Khan, A. Ravagli, and E. Weatherby, "Next generation chalcogenide glasses for visible and ir imaging," 2016.

[199] D. Xue, P. Wang, L. Jiao, W. Li, and Y. Ji, "Experimental study on chemical mechanical polishing of chalcogenide glasses," *Applied optics*, vol. 58, no. 8, pp. 1950–1954, 2019.

[200] R. B. McIntosh and R. A. Paquin, "Chemical–mechanical polishing of low-scatter optical surfaces," *Applied Optics*, vol. 19, no. 14, pp. 2329–2331, 1980.

[201] J. M. Bennett, J. J. Shaffer, Y. Shibano, and Y. Namba, "Float polishing of optical materials," *Applied Optics*, vol. 26, no. 4, pp. 696–703, 1987.

[202] J. R. Hird and J. E. Field, "Diamond polishing," *Proceedings of the Royal Society of London. Series A: Mathematical, Physical and Engineering Sciences*, vol. 460, no. 2052, pp. 3547–3568, 2004.

[203] C. Vitale-Brovarone, G. Novajra, J. Lousteau, D. Milanese, S. Raimondo, and M. Fornaro, "Phosphate glass fibres and their role in neuronal polarization and axonal growth direction," *Acta Biomaterialia*, vol. 8, no. 3, pp. 1125–1136, 2012.

[204] R. F. Bartholomew and A. L. Sadd, "Solution doping of porous preforms," 1992.

[205] J. E. Townsend, S. B. Poole, and D. N. Payne, "Solution-doping technique for fabrication of rare-earth-doped optical fibres," *Electronics Letters*, vol. 23, no. 7, pp. 329–331, 1987.

[206] R. Mossadegh, J. S. Sanghera, D. Schaafsma, B. J. Cole, V. Q. Nguyen, R. E. Miklos, and I. D. Aggarwal, "Fabrication of single-mode chalcogenide optical fiber," *Journal of Lightwave Technology*, vol. 16, no. 2, pp. 214–217, 1998.

[207] M. Zhu, X. Wang, Z. Pan, C. Cheng, Q. Zhu, C. Jiang, Q. Nie, P. Zhang, Y. Wu, and S. Dai, "Fabrication of an ir hollow-core bragg fiber based on chalcogenide glass extrusion," *Applied Physics A*, vol. 119, no. 2, pp. 455–460, 2015.

[208] J. Bamberg, L. Steinhauser, E. Bayer, and P. Adam, "Ceramic, heat insulation layer on metal structural part and process for its manufacture," 1996.

[209] D. Furniss and A. B. Seddon, "Extrusion of gallium lanthanum sulfide glasses for fiber-optic preforms," *Journal of Materials Science Letters*, vol. 17, no. 18, pp. 1541–1542, 1998.

[210] S. K. Lee, D. C. Ko, and B. M. Kim, "Optimal die profile design for uniform microstructure in hot extruded product," *International Journal of Machine Tools and Manufacture*, vol. 40, no. 10, pp. 1457–1478, 2000.

[211] J. Brnic, G. Turkalj, M. Canadija, D. Lanc, and S. Krscanski, "Responses of austenitic stainless steel american iron and steel institute (aisi) 303 (1.4305) subjected to different environmental conditions," *Journal of Testing and Evaluation*, vol. 40, no. 2, pp. 319–328, 2012.

[212] M. Y. Anastas, *A visual study of the dynamics of polymer extrusion*. Thesis, 1973.

[213] A. Bornstein, N. Croitoru, and E. Marom, "Chalcogenide infrared as2 - xse3 + x glass fibers," *Journal of non-crystalline solids*, vol. 74, no. 1, pp. 57–65, 1985.

[214] C. R. Quick, J. E. K. Schawe, P. J. Uggowitzer, and S. Pogatscher, "Measurement of specific heat capacity via fast scanning calorimetry—accuracy and loss corrections," *Thermochimica Acta*, vol. 677, pp. 12–20, 2019.

[215] J. D. Shephard, R. I. Kangley, R. J. Hand, D. Furniss, M. O'Donnell, C. A. Miller, and A. B. Seddon, "The effect of gase on ga–la–s glasses," *Journal of Non-Crystalline Solids*, vol. 326-327, pp. 439–445, 2003.

[216] H. Suzuki and R. Mori, "Phase study on binary system ga-se," *Japanese Journal of Applied Physics*, vol. 13, no. 3, pp. 417–423, 1974.

[217] X. Jiang and A. Jha, "Engineering of a ge–te–se glass fibre evanescent wave spectroscopic (fews) mid-ir chemical sensor for the analysis of food and pharmaceutical products," *Sensors and Actuators B: Chemical*, vol. 206, pp. 159–169, 2015.

[218] G. L. Roberts and F. H. Field, "The absorption spectra of certain nickel(ii) and cobalt(ii) complex ions," *Journal of the American Chemical Society*, vol. 72, no. 9, pp. 4232–4235, 1950.

[219] F. Smektala, C. Quemard, V. Couderc, and A. Barthélémy, "Non-linear optical properties of chalcogenide glasses measured by z-scan," *Journal of Non-Crystalline Solids*, vol. 274, no. 1, pp. 232–237, 2000.

[220] C. Julien, S. Barnier, M. Massot, N. Chbani, X. Cai, A. M. Loireau-Lozac'h, and M. Guittard, "Raman and infrared spectroscopic studies of gegaag sulphide glasses," *Materials Science and Engineering: B*, vol. 22, no. 2, pp. 191–200, 1994.

[221] M. Dunleavy, G. C. Allen, and M. Paul, "Characterization of lanthanum sulphides," *Advanced Materials*, vol. 4, no. 6, pp. 424–427, 1992.

[222] B. Jariwala, D. Voiry, A. Jindal, B. A. Chalke, R. Bapat, A. Thamizhavel, M. Chhowalla, M. Deshmukh, and A. Bhattacharya, "Synthesis and characterization of res2 and rese2 layered chalcogenide single crystals," *Chemistry of Materials*, vol. 28, no. 10, pp. 3352–3359, 2016.

[223] X. Zhang, H. Ma, and J. Lucas, "Applications of chalcogenide glass bulks and fibres," *J. Optoelectron. Adv. Mater*, vol. 5, no. 5, pp. 1327–1333, 2003.

[224] J. Le Person, F. Smektala, T. Chartier, L. Brilland, T. Jouan, J. Troles, and D. Bosc, "Light guidance in new chalcogenide holey fibres from gegasbs glass," *Materials Research Bulletin*, vol. 41, no. 7, pp. 1303–1309, 2006.

[225] D. Lezal, "Chalcogenide glasses-survey and progress," *Journal of Optoelectronics and Advanced Materials*, vol. 5, no. 1, pp. 23–34, 2003.

[226] D. W. Hewak, A. K. Mairaj, M. N. Petrovich, and Y. D. West, "Application of novel glass for the next generation of optical fibre devices," 2000.

[227] J. W. Mullin, *Crystallization*. Butterworths, 1961., 1961.

[228] R. Hand, R. Kangley, J. Shephard, D. Furniss, and A. Seddon, *GaLaS optical fibers: thermo-optical properties and fiber drawing*, vol. 4215 of *Information Technologies 2000*. SPIE, 2001.

[229] N. G. R. Broderick, D. W. Hewak, T. M. Monro, D. J. Richardson, and Y. D. West, "Holey optical fibres of non-silica based glass," 2006.

[230] J. S. Sanghera, L. B. Shaw, and I. D. Aggarwal, "Rare earth doped infrared-transmitting glass fibers," *OPTICAL ENGINEERING-NEW YORK-MARCEL DEKKER INCORPORATED*, vol. 71, pp. 449–530, 2001.

[231] R. J. Curry, A. K. Mairaj, C. C. Huang, R. W. Eason, C. Grivas, D. W. Hewak, and J. V. Badding, "Chalcogenide glass thin films and planar waveguides," *Journal of the American Ceramic Society*, vol. 88, no. 9, pp. 2451–2455, 2005.

[232] T. Schweizer, D. J. Brady, and D. W. Hewak, "Fabrication and spectroscopy of erbium doped gallium lanthanum sulphide glass fibres for mid-infrared laser applications," *Optics Express*, vol. 1, no. 4, pp. 102–107, 1997.

[233] R. Müller, E. D. Zanotto, and V. M. Fokin, "Surface crystallization of silicate glasses: nucleation sites and kinetics," *Journal of Non-Crystalline Solids*, vol. 274, no. 1, pp. 208–231, 2000.

[234] G. W. Fynn, G. Fynn, and W. J. A. Powell, *Cutting and polishing optical and electronic materials*. CRC Press, 1988.

[235] G. K. Chui and R. Gardon, "Interaction of radiation and conduction in glass," *Journal of the American Ceramic Society*, vol. 52, no. 10, pp. 548–553, 1969.

[236] D. W. Hewak, Y. D. West, N. G. R. Broderick, T. M. Monro, and D. J. Richardson, "The fabrication and modelling of non-silica microstructured optical fibres," in *OFC 2001. Optical Fiber Communication Conference and Exhibit. Technical Digest Postconference Edition (IEEE Cat. 01CH37171)*, vol. 2.

[237] A. Mawardi and R. Pitchumani, "Optical fiber drawing process model using an analytical neck-down profile," *IEEE Photonics Journal*, vol. 2, no. 4, pp. 620–629, 2010.

[238] C. Lin, C. Rüssel, and S. Dai, "Chalcogenide glass-ceramics: Functional design and crystallization mechanism," *Progress in Materials Science*, vol. 93, pp. 1–44, 2018.

[239] P.-X. Jiang, Z. Wang, Z.-P. Ren, and B.-X. Wang, "Experimental research of fluid flow and convection heat transfer in plate channels filled with glass or metallic particles," *Experimental Thermal and Fluid Science*, vol. 20, no. 1, pp. 45–54, 1999.

[240] H. E. Kissinger, "Variation of peak temperature with heating rate in differential thermal analysis," *Journal of research of the National Bureau of Standards*, vol. 57, p. 217, 1956.

[241] O. A. Lafi, M. M. A. Imran, and M. K. Abdullah, "Glass transition activation energy, glass-forming ability and thermal stability of se90in10-xsnx (x=2, 4, 6 and 8) chalcogenide glasses," *Physica B: Condensed Matter*, vol. 395, no. 1, pp. 69–75, 2007.

[242] B. P. Huynh and R. I. Tanner, "Study of the non-isothermal glass fibre drawing process," *Rheologica acta*, vol. 22, no. 5, pp. 482–499, 1983.